Functional characterization of Oligoadenylate Synthetase (OAS) by dual polymerase-endoribonuclease assay

by

Nikhat Lubna

A Thesis submitted to Faculty of Graduate studies of

The University of Manitoba

In partial fulfillment of the requirements for the degree of

MASTER OF SCIENCE

Department of Chemistry

Faculty of Science

University of Manitoba

Winnipeg, Manitoba, Canada

Abstract

The innate immune system includes a class of viral double stranded RNA (dsRNA) binding enzymes known as 2'-5'-oligoadenylate synthetases (OAS). The OAS family detects viral dsRNA and initiates downstream processes. The binding of viral dsRNA by OAS enables catalysis of substrate ATP into 2′-5′-linked oligoadenylate chains (2-5A). 2-5A chains longer than 3 nucleotides then activate an RNA degrading enzyme named RNase L, which in turn non-specifically degrades cellular and viral RNA causing host cell death. My research group has been investigating the interaction between the smallest OAS family member, OAS1 (42 kDa), with a double-stranded region of the West Nile virus (WNV) RNA genome. This region of the genome is conserved amongst the *Flaviviridae* family of viruses, of which WNV is a member. Therefore, the goal of my work is to see whether similar RNA regions in other *Flaviviridae* members using Zika Virus, Japanese Encephalitis Virus, WNV and Dengue Virus as model systems for studying this interaction. The approach will be to produce viral RNA from the conserved regions and determine the minimal RNA required for binding of OAS1 and catalytic activation of OAS1. We have previously investigated the role of WNV in activation of OAS using an enzyme kinetics assay that measures pyrophosphates production (from ATP) as an indirect indicator of OAS activity. However, this assay does not measure whether 2-5A chains are of sufficient length to activate RNase L downstream. The OAS enzymes depend largely on the endonuclease activity of RNase L to mediate its antiviral activity. Therefore, any OAS activity assay that does not take into account RNase L activation is fundamentally incomplete. Although the established colorimetric assay demonstrates OAS activity quite well, whether RNase L is being activated downstream remains unanswered. With this in

mind, I have produced a dual OAS-RNase L activity assay which provides data in shorter time intervals, measures OAS activity and RNase L activity simultaneously, and requires very low concentrations of reactants. The data obtained from this assay will be used to assess activation of OAS enzyme by *flavivirus* RNA and help paint a more complete picture of OAS mechanism of action.

Acknowledgements

I take this opportunity to convey my gratitude to all the individuals who have supported me during my time as researcher. I want to start by expressing heartfelt gratitude to my MSc supervisor Dr. Sean A. McKenna, without whom my research would not have been possible. As an international student from a third world country, I lacked specific knowledge and skills pertaining to this project when I first joined the McKenna lab. However, Dr. McKenna has always had faith in my aptitude and competency in research. Throughout my time as a newcomer in a foreign country, I have faced numerous hardships. However, throughout all the difficulties, Dr. McKenna has always been extremely patient and supportive. I have always considered myself extremely lucky to have been part of the McKenna group due to the compassionate nature of all of its members.

I would also like to thank the members of the McKenna lab including Dr. Evan P. Booy, Daniel Gussakovsky, Mira Brown as well as past members Dr. Amit Koul, Taegi Choi, Nicole Neudorf and Steven Dupas. My lab members have helped me troubleshoot difficulties at numerous points of my research and also provided the occasional comedic relief during frustrating moments. Without them, my research would not have been possible.

And finally I would like to express my gratitude toward Dr. Mazdak Khajehpour and Dr. Stéphanie Portet for the advice and guidance they provided over the years of my graduate program. I appreciate the time and effort they have spent in order to review my thesis and give me helpful feedback.

My research work has been possible due to the support of Natural Sciences and Engineering Research Council of Canada (NSERC). The Faculty of Graduate Studies, U of Manitoba (University of Manitoba Graduate Fellowship), and the Department of Chemistry (Hugh J. Anderson scholarship) have also provided their support in the form of funding for my research.

Dedication

I want to dedicate this thesis to my mother, Lily Jasmin and my brother Ibrahim Naser who have taught me how to find my inner strength during hardships. They were always there for me when I lost my bearings even though we were miles apart. I would also like to sincerely thank my dear friends Cheneé Merchant and Larissa Adams on hard days when I needed emotional support. They are my family away from home and they have taught me about integrity and what it means to be a supportive friend. I am very lucky to have them in my life.

Table of contents

List of figures

List of abbreviations

3’TR	3’ untranslated regions
5’TR	5’untranslated regions
A	adenylate
ADARs	adenosine deaminases acting on RNAs
ADP	adenosine diphosphate
ANK	ankyrin repeat
AP-1	activator protein 1
ATP	adenosine triphosphate
BHQ 1	black hole quencher 1
BSA	bovine serum albumin
CAFAKA	mutation of cysteine, phenyl alanine and lysine to alanine
CARD	two N-terminal caspase recruiting domains
cGAS	cyclic GMP-AMP synthase
CS	conserved sequences
CTD	dsRNA binding C-terminal domain
CV	column volume
DB	dumbbell
DENV	aengue virus
DMEM	Dulbecco’s Modified Eagle’s Medium
dsRBD	dsRNA binding domain
dsRBMs	double stranded RNA binding motifs
DTT	dithiothreitol
EDTA	ethylenediaminetetraacetic acid
FAM	fluorescein phosphoramidite
FBS	fetal bovine serum
FPLC	fast protein liquid chromatography
GST	glutathione S-transferases
HCV	hepatitis C virus
HEPES	4-2-hydroxyethyl-1-piperazineethanesulfonic acid
HIV	human immunodeficiency virus
IFIT	IFN-induced proteins with tetratricopeptide repeats
IFN	interferon
IFNAR	IFN-α/β cell surface receptor
IGEPAL	octylphenoxy polyethyleneoxy ethanol
IL	interleukin
IPTG	isopropyl-β-D-thio-galactopyranoside
IRF3	interferon regulatory factor 3
IRF9	interferon regulatory factor 9
ISG	stimulating transcription of interferon stimulated genes

ISRE	IFN-stimulated response elements
JAK/STAT	janus kinase/signal transducers and activators of transcription
JEV	japanese encephalitis
LB	lysogeny Broth
LGP2	laboratory of genetics and physiology 2
LPS	lipopolysaccharides
LRR	leucine-rich repeats
MAVS	mitochondrial antiviral signaling
MD	molecular dynamics
MDA5	melanoma differentiation-associated gene 5
NACHT	N-terminal effector domain, a central NTPase domain
NFkB	nuclear factor kappa-light-chain-enhancer of activated B cells
Ni-NTA	nickel- nitrilotriacetic acid
NK	natural killer
NLRs	NOD like receptors
NOD	nucleotide-binding oligomerization domain
NOD	nucleotide-binding oligomerization domain
NSP3	non-structural protein 3
OAS	2’-5’-oligoadenylate synthetases
OAS	2'-5' -oligoadenylate synthetase
OAS 1	2'-5' -oligoadenylate synthetase 1
OAS 2	2'-5' -oligoadenylate synthetase 2
OAS 3	2'-5' -oligoadenylate synthetase 3
OASL	OAS-Like
OD	optical density
PACT	protein activator of PKR
PAMP	pathogen-associated molecular patterns
PAP	polyadenosine polymerase
PK	pseudo Kinase
PKR	dsRNA-dependent protein kinase
PMSF	phenylmethylsulfonyl fluoride
pol β	DNA polymerase β
PPi	pyrophosphate
PRRs	pathogen-or pattern-recognition receptors
qPCR	quantitative real- time PCR
RCS	repeated conserved sequences
RD	helicase/repressor domains and
RFU	relative fluorescence units
RIG-I	retinoic acid-inducible gene 1
RLR	RIG-I like receptors
SARS-CoV2	Severe acute respiratory syndrome coronavirus 2.

SDS-PAGE	sodium dodecyl-sulfate polyacrylamide gel electrophoresis
SEC	size exclusion chromatography
SL	stem loop
SLA	stem loops A
SLB	stem loops B
SNP	single nucleotide polymorphism
ssRNA	single stranded RNA ssRNA
ssRNA	single stranded ribonucleic acid
TBE	tris-Borate-EDTA
TBEV	tick-borne encephalitis virus
TEV	tobacco etch virus
TIR	Toll/interleukin-1 receptor
TLRs	Toll-like receptors
TNF- α	tumor necrosis factor α
UAR	upstream AUG region
VAI	adenovirus genome
WNV	west nile virus
YFV	yellow fever virus
ZBD	Z-DNA-binding domain
ZIKV	zika virus

CHAPTER 1: INTRODUCTION

In this thesis, I present my work on investigating 2'-5' oligoadenylate synthetase (OAS) activity by utilizing a newly developed dual enzyme assay. The OAS family of polymerases plays an important role in preventing double-stranded RNA (dsRNA) virus replication in the cell and its subsequent dissemination in the host. Despite its significant role in the immune system, the catalytic mechanism and substrate specificity of this polymerase family is largely unknown. Moreover, the current methods of investigation lack the ability to analyze the consequence of OAS activation on downstream RNase L enzymatic activity. The purpose of this thesis is to describe a new method to study OAS activity which will be preceded by a general introduction to the innate immune system and its relationship with the OAS family of proteins.

1.1 INNATE IMMUNE SYSTEM

Living organisms have evolved sophisticated mechanisms to fight off threats from their immediate environment. This mechanism is divided into two branches: innate and acquired immunity (Paul, 2012). In vertebrates, the innate immune system functions as the body's first line of defense while the acquired immune system is involved in long-term protection by generating immunological memory (Akira, Uematsu, & Takeuchi, 2006). One of the defense strategies involved in innate immune system are a set of receptors referred to as pathogen-or pattern-recognition receptors (PRRs) that detect foreign

particles of microbial origin. Foreign particles or molecules that illicit an immune response are known as pathogen-associated molecular patterns (PAMP) (Akira et al., 2006). PAMPs are essential for microbial survival and therefore are often conserved. Different PRRs recognize specific PAMPs and initiate distinct signaling pathways, express specific genes, and lead to antipathogen responses that are specific to the invading pathogens. PAMPs can have incredible molecular diversity for targets such as double stranded RNA (dsRNA), peptidoglycan from bacterial cell wall, lipopolysaccharide from gram-negative bacterial cell wall, and fungi glucans (Janeway Jr, Travers, Walport, & Shlomchik, 2001). A diverse range of PRRs are activated by such molecules such as Toll-like receptors (TLRs), retinoic acid-inducible gene 1 (RIG-I) like receptors (RLRs), nucleotide-binding oligomerization domain (NOD) like receptors (NLRs), the dsRNA-dependent protein kinase (PKR), 2'-5'-oligoadenylate synthetases (OAS) and interferon (IFN)-induced proteins with tetratricopeptide repeats (IFITs) (Akira et al., 2006; Schoggins & Rice, 2011).

1.2. INTERFERONS AND THEIR ROLE IN ANTIVIRAL INNATE IMMUNITY

IFN works by way of several systems interacting with the IFN-α/β cell surface receptor (IFNAR), stimulating transcription of interferon stimulated genes (ISGs) that contain IFN-stimulated response elements (ISRE) within their sequence (Sadler & Williams, 2008). There are two main types of IFNs: type I and type II. Type I IFNs are divided into 2 subclasses; IFN α which is a multigene family, predominantly

synthesized by leukocytes and IFN β which are common to most cells but characteristic of fibroblasts.

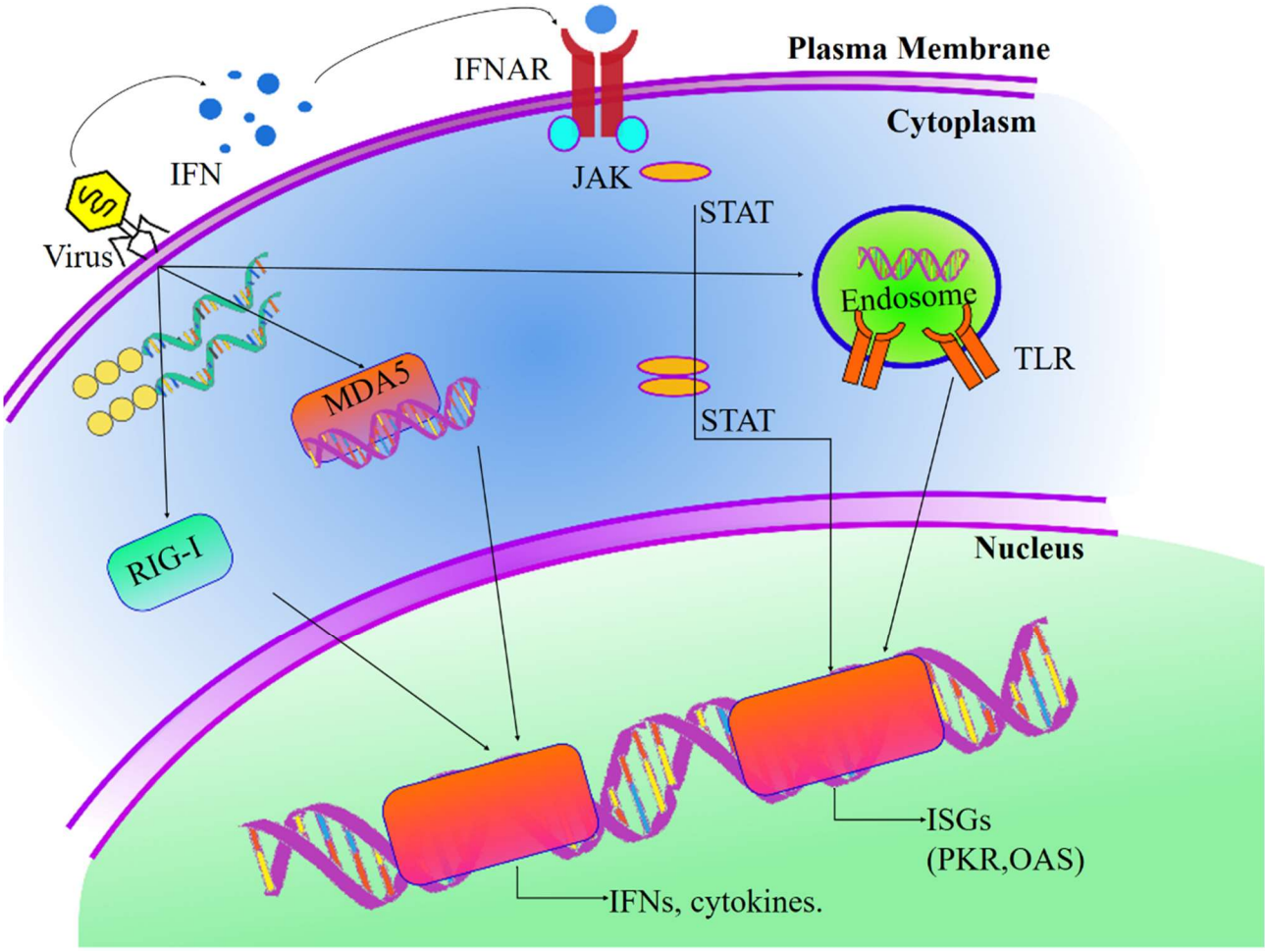

Figure 1.1 Innate immune response to viral infection

Schematic of innate immune response showing several signaling pathways activated by viral particles and genetic material. Presence of virus activates release of interferon molecules that bind to interferon alpha receptor subunit (IFNAR) in the plasma membrane. This initiates JAK/STAT pathway whereby a cascade of messenger molecules inside the cell relays information to activate transcription of various immune regulatory proteins. Viral genomic material such as single stranded RNA (ssRNA) and

double stranded RNA (dsRNA) activate separate signal pathways. For instance, viral ssRNA with 5'triphosphate binds to RIG-I while dsRNA binds to MDA-5. Both these receptors initiate downstream responses that initiate transcription of various immune enzymes such as OAS and PKR.

When T lymphocytes and natural killer (NK) cells are exposed to viruses, they activate IFN-γ gene which in turn synthesize IFN II (Vilcek & Sen, 1996). Although there are no structural similarities between IFN I and IFN II, there are broad similarities between the genes that they induce (Stark, Kerr, Williams, Silverman, & Schreiber, 1998).

IFN I can be divided into four subtypes: IFN-α, IFN-β, IFN-ω, and IFN-τ. Among them several IFN-α and IFN-β intronless gene families are present in mammals and are often coordinated together due to sequence homology within their gene clusters. When confronted by viral genetic material both IFN-α and IFN-β secretory proteins bind to the same cellular receptors and induce production of several MHC class I molecules, making it easy to target infected cells by cytotoxic T lymphocytes (Grandvaux et al., 2002; Wang et al., 2009).

The sole member of type II IFN family is IFN-γ, and unlike IFN-α and IFN-β, is a secreted glycoprotein containing introns. IFN- γ is produced in NK cells and T-lymphocytes where they increase expression of MHC class II antigen presentation on infected cells. NK cells and T lymphocytes receive signal from monocytes/macrophages via interleukin-12 (IL-12) produced as a result of PRRs

activated by PAMPs (Der, Zhou, Williams, & Silverman, 1998; Sadler & Williams, 2008; Stetson & Medzhitov, 2006).

PRR activation initiates a cascade of proteins involved in gene regulation to mount an IFN-mediated innate immune response. One such pathway involves the phosphorylation, dimerization and nuclear localization of interferon regulatory factor 3 (IRF3) (Grandvaux et al., 2002). IRF3 starts a chain reaction involving nuclear factor kappa-light-chain-enhancer of activated B cells (NFkB) and activator protein 1 (AP-1) thereby recruiting several transcriptional factors resulting in upregulation of IFN-β genes. Interleukins, and various PRRs such as TLRs, tumor necrosis factor α (TNF- α), reactive oxygen species and bacterial lipopolysaccharides activates NFkB (Fitzgerald et al., 2007; Qin, Wilson, Lee, Zhao, & Benveniste, 2005). In addition to being activated by viral infection and other signaling factors, IFN-α is also influenced by IFN-β as part of a feedback mechanism (Marié, Durbin, & Levy, 1998; Sen, 2001). IFN-β release can be in the form of a paracrine (act on cells producing it) or autocrine (act on neighboring cells) manner (Darnell Jr, 1997; Darnell Jr, Kerr, & Stark, 1994). IFN-β binds to IFNAR, inducing transcription of several ISGs through activation of Janus kinase/signal transducers and activators of transcription (JAK/STAT) pathway (Shuai & Liu, 2003). JAK/STAT phosphorylate STAT1 and STAT2 which results in them binding to interferon regulatory factor 9 (IRF9) to form an important ISG regulatory factor known as ISGF3 (Leonard & O'Shea, 1998; Lin, Génin, Mamane, & Hiscott, 2000) (Figure 1.1).

1.2.1 VIRAL RNA SENSING BY RNA-DEPENDENT PRRS

Part of the viral life cycle in a cell is the replication of its genomic material. When viral RNA is exposed in the cytosol, the host cell can detect this foreign genetic material through its various PAMPs such as RLR, RIG-I, melanoma differentiation-associated gene 5 (MDA5) and laboratory of genetics and physiology 2 (LGP2). In endosomes (Figure 1.1), TLRs act as RNA sensors and can distinguish between viral double stranded and single stranded nucleic acids (Pichlmair et al., 2011). Cellular PAMPs can distinguish between self and non-self-nucleic acid based on specific molecular patterns. These patterns include chemical modifications of RNA, specific secondary/tertiary structure, particular sequence, or annealed dsRNA intermediates occurring during viral propagation (Rehwinkel & Reis e Sousa, 2010). For example, some studies show a correlation between modifications at the 5'-end of an RNA and its recognition by cellular PAMPs (Hyde & Diamond, 2015; Pichlmair et al., 2011). To date more than 140 post translational cellular RNA modifications has been characterized (Nachtergaele & He, 2018). Interestingly, some of these modifications trigger the innate immune system intentionally.

1.2.2. TOLL-LIKE RECEPTORS

TLRs are a large group of PRRs that detect a variety of PAMPs and are important instigators of IFN cascade response (Michel, Reichhart, Hoffmann, & Royet, 2001; Takeda, Kaisho, & Akira, 2003). There are 10 structurally different

TLRs located primarily on the cell membrane and endosomal compartments. TLRs detect various PAMPs such as viral nucleic acids, viral structural components and non-structural proteins and lipopolysaccharides (LPS) which are a large component of Gram-negative bacteria (Kawai & Akira, 2011). Different TLRs contain extracellular regions, such as leucine-rich repeat motifs and a cytoplasmic tail containing Toll/interleukin-1 (IL-1) receptor (TIR) domain that helps them recognize different surface and intracellular components. This interaction initiates several signaling pathways that triggers the activation of innate immune system (Takeda et al., 2003).

1.2.3 RETINOIC ACID

Similar to TLRs, RLRs also recognize nucleic acid PAMPs and trigger interferon mediated innate immune responses. There are three types of RLRs in humans; RIG-I, MDA5, and LGP2 (Yoneyama et al., 2005). RIG-I activates ATP-dependent downstream signaling by recognizing viral RNAs that contain a panhandle double stranded structure and either a 5’- triphosphate or 5’-diphosphate moiety (Figure 1.1).

RIG-I is comprised of an ATP binding helicase domain, dsRNA binding C-terminal domain (CTD) and two N-terminal caspase recruiting domains (CARD). The central helicase domain is known as a DExD/H-box helicase with an ATP binding motif. Upon binding with PAMP RNA ATP is hydrolyzed, which leads to conformational change and release of the CARD domain from the CTD. CARD then

seeks out and interacts with other CARD-containing proteins in the cell, such as mitochondrial antiviral signaling (MAVS) (Hiscott, Lin, Nakhaei, & Paz, 2006). MAVS initiates a signaling cascade which leads transcription or activation of several innate immune factors (Burghaus & Holder, 1994). Similarly, MDA5 is composed of CARD, CTD, and helicase domains. Unlike RIG-I, which recognizes chemical groups on the 5' end and shorter lengths, MDA5 discriminates dsRNA based on molecular length and is activated by longer structured dsRNA molecules (Kato et al., 2006; Loo et al., 2008). Both, however, recognize RNase L RNA cleavage products which is crucial for enhancing IFN-B production (Malathi, Dong, Gale, & Silverman, 2007; Rosenbaum, 1986). Another member of the RLR family, LGP2, has been implicated in both negative and positive regulation of RIG-I/MDA5-mdiated signaling through *in vitro* studies (Komuro & Horvath, 2006; Rothenfusser et al., 2005; Yoneyama et al., 2005). Therefore, apart from the physiological significance of LGP2 in interferon mediated response, its mechanism of action is still unclear due to contradictory results. One study shows LGP2 knockout negatively regulates MDA5 and RIG-I while another study shows it to be a positive regulator (Satoh et al., 2010; Venkataraman et al., 2007). However, research has established that both MDA5 and LGP2 bind to dsRNA and similar to RIG-I, work synergistically to control viral infection by signaling interferon production (Ablasser & Hur, 2020; Broggi et al., 2020; Lucas et al., 2020; Schneider, Chevillotte, & Rice, 2014; Z. Zhou et al., 2020).

1.2.4 ADENOSINE DEAMINASES ACTING ON RNAS

Adenosine deaminases acting on RNAs (ADARs) are a class of enzymes that modify adenosine (A) residues of dsRNAs to inosines (I). There are three human ADAR proteins, all comprised of RNA-binding domains containing tandem repeats (Z-DNA-binding domain (ZBD), dsRNA binding domain (dsRBD), and/or arginine-rich domain (R-domains)) and a deaminase domain (Pedersen, Henrichsen, & Schiffman, 1982). ADAR1 is ubiquitously expressed, recognizing ~300bp transposable introns and 3'-TRs whilst ADAR2 is expressed only in the central nervous system, modifying hair-pins in coding regions (Hundley & Bass, 2010; Tan et al., 2017). Although ADAR3 contains catalytic residues, it cannot carry out enzymatic activity and is believed to function as an inhibitor of ADAR2 (Oakes, Anderson, Cohen-Gadol, & Hundley, 2017).

Depending on the type of host cells and virus, ADARs can act for or against an invading pathogen. Against single stranded RNA (ssRNA) viruses (eg. Influenza virus, measles virus, Hepatitis C virus (HCV), Human immunodeficiency virus (HIV) etc) and dsRNA viruses (polyoma virus and Kaposis sarcoma virus) ADARs play an antiviral role (Cattaneo & Billeter, 1992; Gandy et al., 2007; Kumar & Carmichael, 1997; Suspène et al., 2011). However, ADARs' suppressive action on PKR, OAS, and IRF3 exemplifies its proviral capabilities (Clerzius et al., 2009; George, Gan, Liu, & Samuel, 2011; Samuel, 2001; Schoggins et al., 2011). Deletion of ADAR1 causes accumulation of self dsRNA which causes activation of the OAS-RNase L pathway (discussed below), leading to apoptosis (Y. Li et al., 2017). Suppression

of interferon stimulated enzymes might have been an evolutionary mechanism designed to avoid unnecessary initiation of the innate immune system.

1.2.5 NUCLEOTIDE-BINDING AND OLIGOMERIZATION DOMAIN LIKE RECEPTORS (NLRS)

NLRs are a large family of cytosolic proteins that play a several different roles from the inflammatory response to the antibacterial or antiviral immune response. In humans, NLRs are composed of twenty-two members that share a similar N-terminal effector domain, a central NTPase domain (known as the NACHT domain), and leucine-rich repeats (LRR) at the C-terminus. The LRR recognizes dsRNA while the central NACHT domain binds to nucleic acid-based PAMPs (Broz & Dixit, 2016; Kanneganti & Lamkanfi, 2007; Koonin & Aravind, 2000). Once PAMPs are detected, signal transduction is carried out by the N-terminal domain or in some cases the CARD domain. NOD-1 and NOD-2 in particular are involved in antiviral response and belong to the group NLRC that have CARD domains for signal transduction. NOD-2 and other subgroups called NLRP1 and NLRP3 have shown to be antiviral effectors against Sendai virus, influenza virus and respiratory syncytial virus (Allen et al., 2009; Sabbah et al., 2009). Several studies have shown that both NLRP1 and NLRP3 are direct sensors for dsRNA while NOD-2 has been shown to respond to ssRNA.

1.2.6 RNA DEPENDENT PROTEIN KINASE (PKR)

Antiviral responses are also mediated through kinases such as PKR, which is a dsRNA binding enzyme. Upon activation via PAMPs, PKR causes global translational shutdown (Balachandran et al., 2000). Although dsRNAs are its primary activators, there are others such as protein activators of the interferon-induced protein kinase (PACT) and heparin (an anticoagulant) (Chong et al., 1992; Garcia et al., 2006). PKR comprised of a single N-terminal dsRBD and a C-terminal catalytic domain that carries out phosphorylation. The phosphate and ribose backbone of dsRNA interact with the dsRBD of PKR in a sequence dependent manner (Bevilacqua & Cech, 1996). PKR belongs to a class of enzymes known as Serine/Threonine kinases because of important amino acid residues in its catalytic domain. Under normal conditions, PKR is an inactive monomer that dimerizes with itself upon binding to a 20 – 80 bp long dsRNA or other activators. Once activated, PKR undergoes autophosphorylation at Thr446 in the C-terminal domain, and then phosphorylates its target substate, eIF2α, at Ser51 (Dar, Dever, & Sicheri, 2005; F. Li et al., 2013; Manivannan, Siddiqui, & Malathi, 2020). eIF2 α is a translation initiation factor in eukaryotes and its phosphorylation results in blocked translation initiation and accumulation of stalled ribosomal pre-initiation complexes. Importantly, viral protein synthesis often depends on eIF2α and so inactivation of this protein not only lead to apoptosis but also halts viral replication (Balachandran et al., 2000; Garcia et al., 2006). Therefore, it is not surprising that certain viruses have developed mechanisms to avoid PKR activation. Some viruses have intrinsic

proteins that bind to dsRNA to block its binding to PKR or prevent nucleic acid recognition by PKR such as the non-structural protein 3 (NSP3) of rotaviruses (Langland, Pettiford, Jiang, & Jacobs, 1994) and NSP1 of influenza viruses (Schierhorn et al., 2017).

1.2.7 OLIGOADENYLATE SYNTHETASE (OAS)

Another class of interferon inducible enzymes capable of detecting nucleic acid-based PAMPs are the family of 2' -5' oligoadenylate synthetases (OAS). OAS enzymes contain a polymerase beta (pol-β) nucleotidyl transferase domain, placing them as part of a larger nucleotidyl transferase superfamily consisting of other immune sensors such as cytoplasmic double stranded DNA synthase and the cyclic GMP-AMP synthase (cGAS) (Hornung, Hartmann, Ablasser, & Hopfner, 2014; Kranzusch, Lee, Berger, & Doudna, 2013). OAS enzymes are template-dependent RNA polymerase enzymes similar to other enzymes such as polyadenosine polymerase (PAP) and tRNA class I CCA adding enzymes (CCA) (Torralba, Sojat, & Hartmann, 2008). Unlike PAP and CCA, the OAS enzymes produce polyadenine chain containing a rare 2'-5' phosphodiester linkage (2-5A) instead of the more common 3'-5' bond, and does not require an RNA primer. The OAS family of proteins are part of the template independent nucleotide polymerase family with their own nucleotidyl transferases domain (Kristiansen, Gad, Eskildsen-Larsen, Despres, & Hartmann, 2011)

Some researchers propose that a 2'-5' linked RNAs were essential for early life to develop as this linkage requires less energy to denature and therefore could have been used to store genetic information (Giannaris & Damha, 1993; Wasner et al., 1998). In the prebiotic world, non-enzymatic nucleic acid synthesis might have generated RNA/DNA molecules with heterogeneous 2'-5' and 3'-5' linked backbones (Gilbert, 1986). Moreover, Engelhart *et al.* demonstrated that RNAs with 2'-5' phosphodiester linkages retain the ability to fold, recognize ligands, and catalyze reactions (Engelhart, Powner, & Szostak, 2013). Since three-dimensional interaction with protein would require RNA or DNA to be flexible, it is then reasonable to assume that heterogeneous RNAs played an important role in primitive life.

In humans, 2-5A synthesized catalytically by OAS enzymes from ATP act as a second messenger to activate a latent endonuclease RNase L. RNase L indiscriminately cleaves both foreign and host cell RNAs with minimal sequence specificity, ranging from tRNAs, rRNAs, mRNAs and other non-coding RNAs. Similar to PKR action, RNase L activation ceases global translation suppression, cell growth arrest, cell death and most importantly attenuates production of virus particles (Hovanessian & Justesen, 2007; Kristiansen et al., 2011)

OAS were among the first interferon-stimulated proteins purified in 1975, and were initially thought to lack catalytic activity (Hovanessian, Brown, & Kerr, 1977). However, further studies demonstrated enzymatic activity upon dsRNA induction (Justesen, Hartmann, & Kjeldgaard, 2000; Minks, 1979). There are four isoforms of OAS in humans. OAS1, OAS2, and OAS3 are enzymatically active isoforms while

OASL (OAS-Like) is not. OAS1, OAS2, and OAS3 have one, two, and three nucleotidyl transferases domains respectively and this domain is encoded by five shared exons. Although OASL possesses a catalytic domain, mutations at specific residues render it ineffective. With the exception of OASL, all of the three OAS genes are located in chromosome 12 located at the region 12q24.1 and give rise to multiple splice variants in humans (Hovnanian et al., 1998).

OAS1 and OAS2 are further divided into multiple isoforms while OAS3 (isoform p100) and OASL (isoform p59) only have one each (Justesen et al., 2000). Although OASL possesses a catalytic domain, mutations at specific residues render it ineffective. With the exception of OASL, all of the three OAS genes are located in chromosome 12 located at the region 12q24.1 and give rise to multiple splice variants in humans (Hovnanian et al., 1998). OAS1 consists of five isoforms; p42, p44, p46, p48 and p52 while OAS2 have two; p69 and p71 (Justesen et al., 2000; Vagn et al., 2005). These isoforms arise from splice-site-polymorphism variations (i.e. splice site contains an single nucleotide polymorphism (SNP) with specific alleles corresponding to each isoform). Among the numerous polymorphisms, the A/G substitution at a splice acceptor site of exon 6 determines the generation of p46 isoform alone or p48 and p52 isoforms. Bonnevie–Nielsen *et al.* have reported that only the G allele is able to produce the p46 isoform of OAS1 while the A allele produces the other two mentioned previously. This A/G single nucleotide polymorphism either confers resistance to a variety of diseases or increases associated risk. For instance, individuals with the G variant express the p46 isoform of OAS1 and have high 2-5A activity. Whereas, individuals expressing one or both

alleles with A variant express isoforms p42, p44, p48, and p52 with a significantly lower OAS activity (Carey et al., 2019; Megyeri et al., 1995) (Figure 1.2).

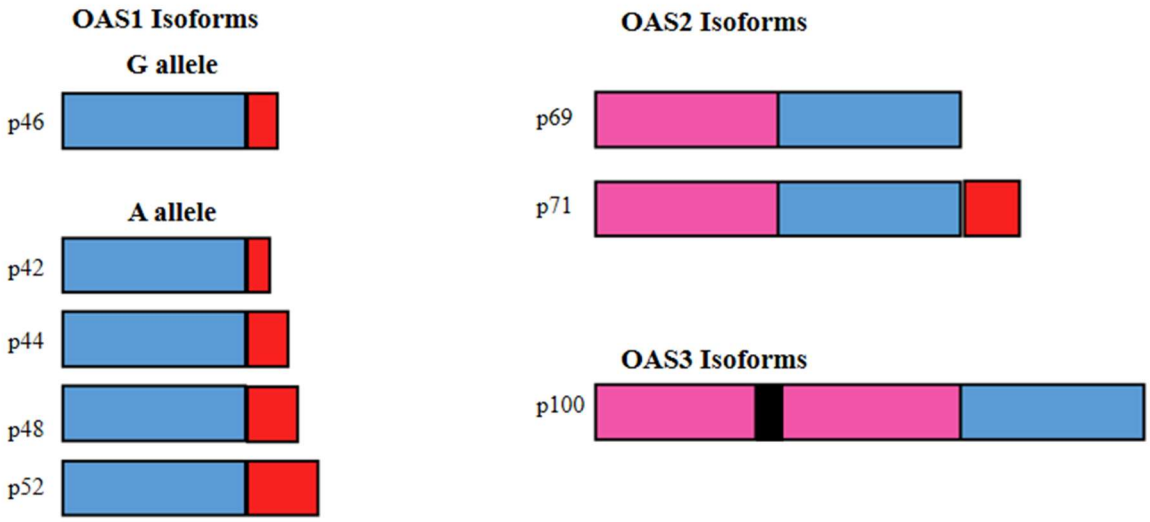

Figure 1.2. Organization of OAS

Schematic of OAS1, OAS2 and OAS3 isoforms. Different coding sequences are indicated by different colors. Red color indicate variable regions at the C terminus of OAS proteins. Regions that code for catalytically active domains are indicated with blue while pink regions code for catalytically inactive domain. OAS1 isoforms are further distinguished by whether they are expressed by A or G allele at splice acceptor site.

Due to this isoform variability, OAS1 can differ significantly in terms of synthetase activity, protein stability, protein folding, protein intracellular localization and post-translational modification (Di, Elbahesh, & Brinton, 2020). For instance, Di *et al.* show that OAS1 p42 binds to F-actin binding protein Supervillin (SVIL) whereas p44 binds to Fibrillin 1 (FBN1). SVIL is an important cytoskeletal protein that is implicated in cellular localization of signal proteins, however its exact function with OAS1 is unknown (Khurana & George, 2008). FBN1 is an extracellular matrix glycoprotein protein that is capable of downregulating TGF-β signaling (Wipff, Allanore, & Boileau, 2009). Although it is unclear how FBN1 relates to OAS1 but it is suggested that it might help localize OAS1 from extracellular matrix into the intracellular matrix (Di et al., 2020).

A study performed in yeast suggests that alteration in the C-terminal region of OAS1 results in isoform-specific function through different protein-protein interactions. In fact, p46 possesses a prenylation motif that localizes this isoform to mitochondria, while p42 lacks the motif and is cytosolic (Kjær et al., 2014; Skrivergaard et al., 2019). Studies have shown that mitochondrial OAS is predominantly of the G variant while cytoplasmic variant is predominantly that of A variant (Skrivergaard et al., 2019). Therefore, it is speculated that the prenylation motif plays a major role in determining which variant of OAS exists in the cells. This difference in cellular localization may be the reason for their differential antiviral activity (Skrivergaard et al., 2019).

A key feature of this polymerase family is the presence of a very important aspartic acid triad on the beta sheet and two arginine residues on the alpha helix of

the NTase catalytic domain (Sarkar, Ghosh, Wang, Sung, & Sen, 1999). The aspartic acid residues coordinate two Mg^{2+} ions and the arginine residues recruit ATP molecules to facilitate the catalysis of 2-5A formation (Rune Hartmann, Justesen, Sarkar, Sen, & Yee, 2003). Additionally, OAS enzymes also contain several arginine and lysine residues at the dsRNA binding site that help dsRNA binding and subsequent activation of enzyme. Binding of dsRNA is largely mediated through 2'-hydroxyl groups of the dsRNA interacting with basic amino acids of the nucleic acid binding site (Donovan, Dufner, & Korennykh, 2013; Rune Hartmann et al., 2003). A study performed on OAS from ancient to modern animals clearly demonstrates a pattern that correlates to assimilation of more basic amino acids into the binding site as OAS evolved (Hu et al., 2018). This makes sense because basic amino acids would be able to attract the negatively charged OH groups of dsRNA. This property is unique to the OAS family as other IFN induced proteins such as RIG-I and PKR require additional nucleic acid binding domains such as helicase/repressor domains (RD) and double stranded RNA binding motifs (dsRBMs) respectively(Jiang et al., 2011; McKenna et al., 2007).

1.2.8 OAS1 STRUCTURAL INFORMATION

The crystal structure of porcine OAS1 published by Hartmann *et al.* two decades ago, in combination with the more recent human OAS1 structure bound to dsRNA by Donovan *et al.,* helps us further understand the mechanism of 2-5A formation (Donovan et al., 2013). OAS1 is the smallest OAS isoform and contains

only a single catalytically active domain. The presence of the catalytic domain was first discovered when comparing the structures of OAS1 and DNA polymerase β (pol β) (Sarkar, Ghosh, et al., 1999), which hinted at a conserved catalytic region in the OAS family.

The importance of structural organization and the function of key amino acid residues in porcine OAS1 was elucidated later in 2003 by Hartmann et al. (Rune Hartmann et al., 2003). From this structure, it was determined that OAS1 is a bilobal protein comprising of a short N-terminal extension linking to a large C-terminal domain through a helix-loop-helix linker (Figure 1.3). Both the N-terminal chain and linkers stabilize the OAS1 structure. The active site resides in the cleft between the N and C lobes. Additionally, the crystal structure also revealed several important residues that are involved in the NTPase activity and the dsRNA binding capabilities, which was later confirmed through mutational studies. Investigating the crystal structures of other nucleotidyl transferases such as pol β and PAP, it is apparent the orientation of specific residues within the catalytic site determines substrate specificity. Therefore, the 2’ specificity of OAS1 arises from the orientation of aspartic acids (D74, D76, & D146) that orients the ribose 2’-OH group as an acceptor in the catalytic site (Koonin & Aravind, 2000). In addition, several studies suggest that mutating a few key lysine and arginine residues on the opposite face of the active site greatly hinders binding of dsRNA activator.

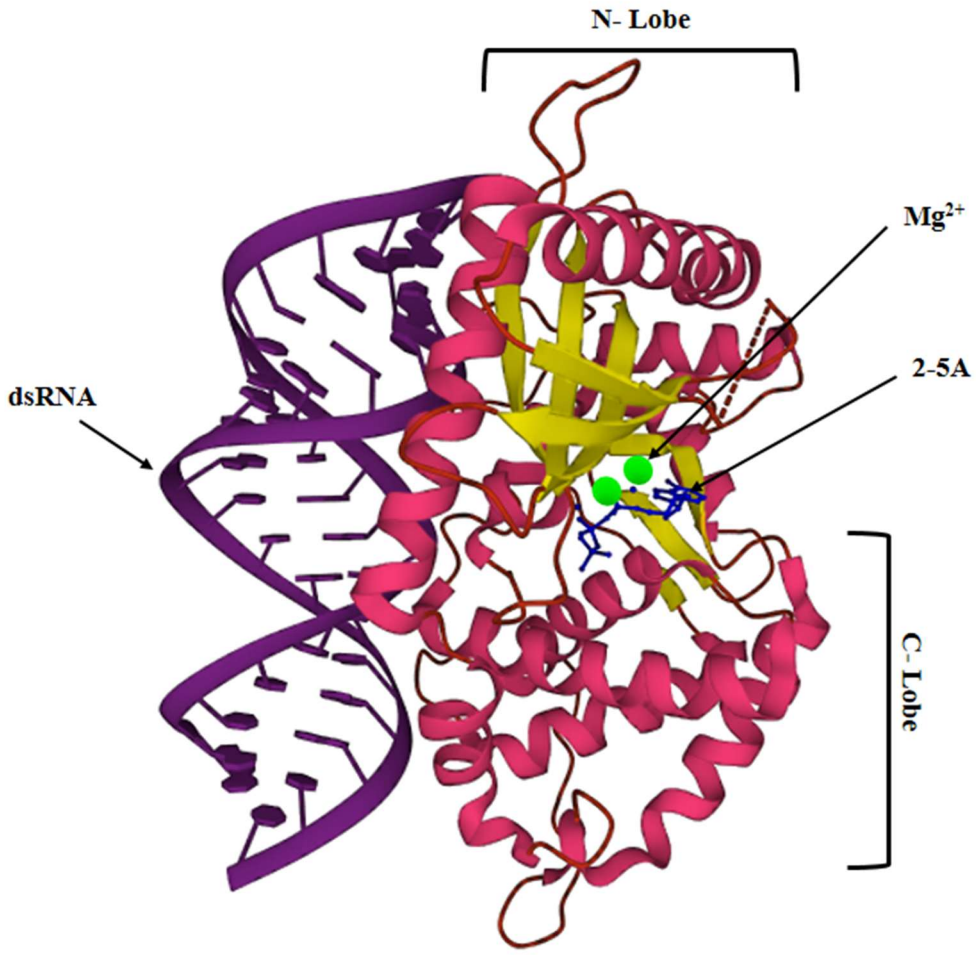

Figure 1.3. Ribbon diagram of OAS1

Structural diagram of OAS1 structure with dsRNA (purple), Mg^{2+} (green) and an elongating 2-5 polyadenine (2-5A) chain (PDB4IG8). The dsRNA sits in the junction between N- and C- lobe (indicated in the image) which brings about a conformational change. Rearrangements of secondary structures within each lobes allow the synthesis of 2-5A chains.

Despite not having a classical nucleic acid binding domain, it was hypothesized from the OAS1 crystal structure that the dsRNA binding is mediated through negatively charged basic amino acids such as Arg38, Lys41, Lys59, Arg194, Arg198 & Lys203 (Rune Hartmann et al., 2003). Although the possibility of conformational change upon activator binding was hypothesized, it wasn't until a decade later that this was confirmed through a new OAS1 crystal structure bound to dsRNA substrate (Donovan et al., 2013). This structure revealed that binding of dsRNA of sufficient length narrowed the active site cleft. Structural analysis revealed that the dsRNA binding motif comprised two binding sites parallel to each other with a gap of 30Å between them that is just large enough to accommodate a dsRNA. The two sites make contact with both strands of the RNA and show some sequence specificity. The binding sites can accommodate a maximum of two RNA minor grooves which explains why the minimum length of dsRNA must be at least 17bp in order to activate OAS1 catalytic activity. This minimum length also ensures that shorter cellular RNAs do not trigger an IFN response. Upon activator binding, the dsRNA is bent out of its A-form shape by strong hydrogen binding and electrostatic interactions by the lysine and arginine residues situated at the binding site. In order for dsRNA to be successful, the 2'-OH groups are extremely necessary as substitution of these groups with 2'-*O*-methylated completely prevented OAS1 from activation. Some researchers have also shown that OAS1 not only detects dsRNA by hydrogen bonding and electrostatic interactions but also discriminates based on the residues present (Kodym, Kodym, & Story, 2009; Vachon, Calderon, & Conn, 2015). The mechanism of binding dsRNA PAMPs through electrostatic and

hydrogen bonding also observed in other PRRs such as RIG-I and TLR3 (Jiang et al., 2011; Liu et al., 2008). However, these interactions can be disrupted by modified nucleotides such as conversion of uridine to pseudouridine (Anderson et al., 2011) and o-methylation of the 2' –OH group. This may be explained by the fact that pseudouridine bends A-form RNA out of shape so it might not be able to fit correctly in the DNA binding groove (Schwartz & Conn, 2019). Fortunately, only a few viruses have been reported to have a pseudouridine substitution such as turnip mosaic virus (Becker, Motorin, Florentz, Giegé, & Grosjean, 1998), brome mosaic virus(Baumstark & Ahlquist, 2001; Marceau et al., 2016), HCV and DENV (Marceau et al., 2016).

A number of viruses including *flaviviruses* also have 2′-O-methylation in their RNA genome (Netzband & Pager, 2020). RNA modification may be an evolutionary mechanism for cellular mRNAs to avoid detection by host immune system and prevent development of autoimmune disorder. Examples of cellular mRNA modifications include N6-methyladenosine, 5-methylcytidine, and pseudouridine (Boo & Kim, 2020).

The OAS1-dsRNA crystal structure also revealed that following dsRNA binding on the back side of the enzyme, the interlobe cleft becomes narrower; the conformational change is brought on by rearrangements of a few α-helices and a beta sheet in the N terminal region. This change includes shifting of the N3 helix to a position that no longer blocks the dsRNA binding site. Additionally, the C-terminal portion of the N5 helix also moves by 11Å to accommodate the dsRNA. Finally, the β-strand floor slides more towards the N5 helix in order to expose the aspartic acid

catalytic triad. Notable among these changes is the formation of a new alpha helix (N4 helix) brought on by the positional exchange of several amino acids. In particular, two basic amino acids, K66 and R195, move position next to a glutamate residue E233 that puts R195 at the protein/RNA interface, bringing about the formation of the new helix. This new helix is important because it brings the aspartic acid triad (D75, D77, D148) to a position where they can use Mg^{2+} and ATP to form 2-5A (Donovan et al., 2013). Donovan *et al.* refers to this catalytically important part as RICS (RNA-induced catalytic structure) which comprises of strands β1, β2, helix N4 and the connecting loops. Interestingly, other nucleotidyl transferase enzymes such as PAP1 and CCA don't go through such a complex activation process and instead their RICS-like structures stay constitutively active.

Although the role of dsRNA in the activation of OAS1 is somewhat elucidated, the formation of 2-5A polymers remains more elusive. Some researchers have attempted to define the mechanism using a combination of chemically-modified ATP substrates and mutational studies (Lohöfener et al., 2015). The authors observed that binding of acceptor AMP molecule after activation shifts the N-terminal β-sheet towards the dsRNA while several amino acid side chains rearrange their orientation. The Mg^{2+} ions bind triphosphate while the 2'-hydroxyl group of the donor AMP interacts directly with the active site. The crystal structure of dsRNA bound OAS1 with both donor and acceptor AMPs in the active site reveals mechanism of 2-5A formation. In this state, the AMP acceptor ring is oriented at an ~90 degree angle relative to the donor. This position ensures that the 2'-OH group of the accepter is in close proximity to the alpha phosphate of the donor AMP. This

arrangement puts the molecules in prime position for a nucleophilic attack and subsequent formation of the 2'-5' linkage. It is important not to overlook the significance of the Mg^{2+} molecules in this reaction which work to coordinate the two AMPs into the correct positions (Lohöfener et al., 2015).

Alteration of vital active site residues or basic amino acids important for dsRNA binding are not the only ways OAS1 can be inactivated. Several studies have found that residues involved in OAS1 domain oligomerization also nullify its ability to function (Ghosh, Sarkar, Rowe, & Sen, 2001; Sarkar, Pal, & Sen, 2002). Through analysis of mutant enzymes isolated from transgenic mice researchers have shown that if Cys31, Phe332, Lys333 (CFK motif) residues are mutated, it disrupts OAS1's ability to oligomerize thereby rendering the enzyme completely inactive (Ghosh et al., 2001). These results were consistent across different expression systems such as *E. coli*, rabbit reticulocyte or insect cells. However, subsequent studies show that an OAS1 isoform that exists as a tetramer in nature can still be active as a monomer in insect cells (Justesen et al., 2000). These studies prove that our understanding of the protein truly functions in the cell is largely unclear. Further research is needed to fully elucidate the overlapping relationship between isoforms, oligomerization and polymorphisms of this family of proteins.

1.2.9 OAS2 STRUCTURAL FEATURES

Despite there being substantial structural research on OAS1 and OAS3; very little is known about OAS2's structural features and mechanism of action. This is hardly surprising as OAS2 is difficult to produce and purify. OAS2 proteins produced from bacterial cells show reduced yield and specific activity (Bandyopadhyay, Ghosh, Sarkar, & Sen, 1998; Schwartz & Conn, 2019). A possible reason hypothesized by the study was that lack of post translational modifications somehow impacted the enzymatic activity. A similar study performed previously, hypothesized the protein myristoylation might be an important contributor to enzyme activity (R. Hartmann et al., 1998). However, radiolabeled studies provided evidence that this was not the case and instead, a different kind of post translational modification was the culprit. OAS2 protein purified from insect cells contains several *N*-glycosylation sites compared none on the protein purified from bacteria. The importance of glycosylation on OAS2 activity was later revealed when protein purified from insect cells treated with tunicamycin, a known inhibitor of glycosylation process, had no enzymatic activity (Sarkar, Bandyopadhyay, Ghosh, & Sen, 1999). Further, gel filtration of OAS2 reveal it is a dimer since its apparent molecular weight (MW) is 160kDa and calculated MW is 80.8kDa (Koul, Gemmill, et al., 2020).

Furthermore, it has been previously established through *in-vitro* transcription-translation that the two isoforms of OAS2 generates proteins of two different molecular weights (69kDa and 70kDa) and they bind to the same monoclonal antibody (R. Hartmann et al., 1998). Indeed, when truncated versions of N- and C-

terminus domains of the 69kDa and 70kDa proteins are expressed separately, they are found to be enzymatically inactive (Marie, Rebouillat, & Hovanessian, 1999). Taking a closer look at the sequence homology between both domains reveals slight differences. Domain I (DI) contains only partially conserved dsRNA binding sequence and lacks the crucial aspartic acid triad necessary for 2-5A synthesis, while domain II (DII) is similar to the catalytically active domain of OAS1. Moreover, the sequence implicated in dsRNA binding in DI (FEVLAAF) is only partially conserved when compared to OAS1 (FDVLPAF). *In-vitro* expression of individual domains in separate rabbit reticulocyte cells show DI activity to be significantly lower than DII (R. Hartmann et al., 1998). This suggests that DII cannot catalyze 2-5A and is incapable of binding to dsRNA.

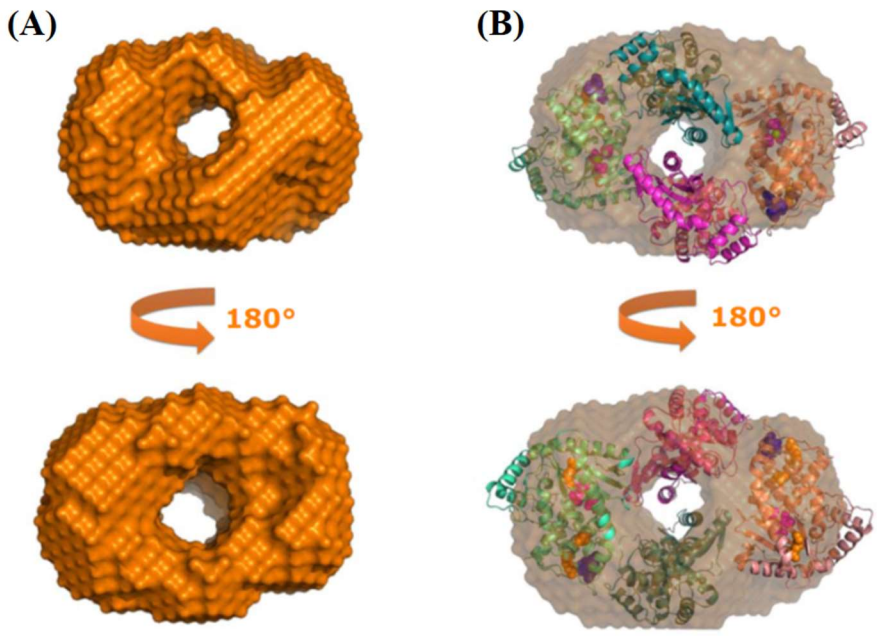

Figure 1.4. *Ab initio* modeling of OAS2.

(A) DAMMIN *ab initio* modeling showing surface of OAS2 in two different orientations rotated at 180°.

(B) *Ab initio* model superimposed on OAS1 high resolution structures (PDB 4RWN) Adapted from (Koul, Gemmill et al. 2020)

How exactly OAS2 synthesizes 2-5A or the purpose of this inactive domain is still not fully understood. However, a few studies have attempted to answer these questions. Recent studies (Calderon & Conn, 2018; Koul, Deo, et al., 2020) have shown a length dependence of OAS2 and OAS3 activation. Unlike OAS1, OAS2 requires a minimum length of 35-40bp dsRNA in order to activate (Koul, Deo, et al., 2020) and has the capacity to produce higher 2-5A oligomers compared to OAS3 (Marie, Blanco, Rebouillat, & Hovanessian, 1997; Sarkar, Ghosh, et al., 1999). The larger dsRNA size requirement could mean that 4 minor grooves are interacting with the cofactor binding site which is double the required number for OAS1. Since DI cannot bind dsRNA, researchers suggest that both DII domains might be used to support longer dsRNA molecules. However, it is hard to prove this hypothesis without a high-resolution structure of OAS2 bound to dsRNA activator.

Recently, the low resolution structure of OAS2 has been published that reveals its hydrodynamic characteristics (Koul, Gemmill, et al., 2020). It was demonstrated through DLS and SV-AUC experiments that OAS2 exists as a dimer, confirming the previous hypothesis (Sarkar, Bandyopadhyay, et al., 1999). Using fractional ratio data from AUC experiments, researchers observed that OAS2 adopts

a globular shape and exists as a dimer in solution. These results are further confirmed using SEC-SAXS which is a method to investigate the structure, dynamics and interactions within biomolecules directly in solution. By analyzing thirteen low resolution structures obtained from SAXS, results suggest that OAS2 may adopt a globular donut shaped structure with a prominent central cavity (Figure 1.4). Homology modeling and rigid-body data show two possible orientations for the four individual OAS2 domains. Atomistic models suggests that the catalytically active domains (DII) are present either side by side or across from each other.

Apart from low resolution structural analysis, mutational studies also revealed important information about OAS2. Amino acids important for dimerization (CAFAKA) and 2-5A synthesis (D481A) established in previous studies were mutated to observe what effects they would have on OAS2 function (Koul, Deo, et al., 2020; Sarkar, Ghosh, et al., 1999). As expected, mutation of any of the three catalytic aspartic acid residues located in the active site rendered OAS2 completely inactive. Interestingly, mutations that prevented OAS2 dimerization (CAFAKA), did show activity albeit lower than wild type enzyme (Koul, Gemmill, et al., 2020). Further, co-immunoprecipitation studies show that OAS2 self-associates in human (HEK293T) cells.

With the lack of crystal structures, researchers have to find indirect ways to identify important residues that are implicated in OAS2 function. By synthesizing ATP analogs for both donor and acceptor sites and mutating residues of interest, important questions can be answered. By creating a donor ATP molecule devoid of 2'OH group and an acceptor ATP molecule with its 5' phosphate group blocked,

researchers provided supporting evidence that 2-5A synthesis might be a two-step process (Sarkar, Pal, et al., 2002). Although modification of ATP does not stop it from binding to either the donor or acceptor sites indiscriminately, the sites have difference in binding affinities towards specific ligands. Moreover, they also carried out pulldown assays by crosslinking the ATP analogs bound to their respective sites in the protein. Peptide analysis of these samples were then carried out and mutation of specific residues such as S420, Y421, T422, S423, Q424, K425 and L539, K540, D541,L542, I543, R544, L545, V546, K547 reveals distinct binding affinities to acceptor or donor ATPs respectively. Among them, mutation of Tyr^{421} and Arg^{544} showed an effect on binding efficiencies of the donor and acceptor ATPs.

In another study, several amino acid residues thought to have significance in the OAS reaction mechanism have been mutated in order to find their specific role (Schwartz & Conn, 2019). By purifying 8-azido-(α-^{32}P)ATP UV crosslinked to OAS fusion protein and then subsequent UV irradiation, 5 amino acids (^{196}DFLKQ^{200}) of interest were identified. Among these residues, Lys199 showed to have direct interaction with ATP and subsequent mutational studies reveal its critical role, as replacing it with either arginine or histidine results in loss of function.

1.2.10 OAS3 STRUCTURAL FEATURES

Among the four members of the OAS family, OAS3 shows the highest 2-5A synthesis activity and binds dsRNA 18-fold stronger than OAS1 based on activity assays (J. Donovan, Whitney, Rath, & Korennykh, 2015; Ibsen et al., 2015).

Although initial studies suggested that OAS3 could only produce dimeric forms of 2-5A, and as a result thought to exert a lower level of RNase L activation (Marie et al., 1997; Dominique Rebouillat, Hovnanian, Marié, & Hovanessian, 1999), more recent studies show otherwise. Recent studies comparing activities between OAS1 and OAS3 show that the latter requires between 1,000 and 10,000 less dsRNA to achieve the same level of enzyme activity (Ibsen et al., 2015). Another experiment involving titration of poly I:C reveals an approximate 18-fold stronger binding affinity of OAS3 relative to OAS1 (J. Donovan et al., 2015). OAS3 is a 121 kDa protein comprised of three domains (DI, DII and DIII) with two catalytically inactive domains (DI, DII) and one catalytically active domain (DIII). Therefore, it is hypothesized that the additional inactive domains may be helping to increase OAS3's sensitivity to dsRNA (J. Donovan et al., 2015).

To study OAS3 closely, researchers purified the three domains individually bound to dsRNA activator and crystalized them (J. Donovan et al., 2015). Comparison of DI of OAS1 with DII of OAS3 reveals marked similarities such as binding of dsRNA to both N- and C- terminal domains and conformational change resulting in αN4 helix. However the differences, including the absence of magnesium ions or nucleotides in the active site cleft and αN5 helix remaining in the inactive state, render OAS3 DI inactive. The difference between OAS3 domain sequences and DI of OAS1 provides an explanation for these similarities and differences. In fact the sequence identities shared between these domains are 42%, 47%, and 60% for DI, DII and DIII respectively (Dominique Rebouillat et al., 1999) with the active-site aspartic acid triad missing for DI and DII (D. Rebouillat,

Hovnanian, David, Hovanessian, & Williams, 2000; Sarkar, Ghosh, et al., 1999) (Sarkar 1999; Rebouillat et al. 2000). Therefore, it is reasonable to assume that DI and DII has some alternative role in 2-5A synthesis.

The crystal structure published in 2015 shed some light into the function of the inactive domains (J. Donovan et al., 2015). This study showed that OAS3 DI binds very tightly to dsRNA thus suggesting the requirement for longer dsRNA activators that span DI to DIII. Moreover, the fact that OAS3 DI remains in an inactive state due to αN5 helix conformation might enhance its ability to bind dsRNA. In fact, the crucial role DI in OAS3 activation is exemplified by the fact that its deletion results in abolition of 2-5A synthesis activity. However, deletion DII does not seem to affect catalytic activity to the same degree. Based on biochemical analyses on dsRNA of different lengths, it was inferred that OAS3 domains might be arranged in a linear fashion in order to detect a long stretch of dsRNA. However ,without a crystal structure of full length OAS3, this conformation remains to be observed experimentally.

1.3 OVERVIEW OF FLAVIVIRUSES

The *Flavivirus* genus include over 50 arboviruses (Gubler, 1998) with most of them having significant impact on human health. Some of the deadliest *Flaviviruses* include dengue virus (DENV), Zika virus (ZIKV), West Nile virus (WNV), yellow fever virus (YFV), tick-borne encephalitis virus (TBEV), and Japanese encephalitis virus (JEV) (Barba-Spaeth et al., 2016; Chambers, Hahn, Galler, &

Rice, 1990; Seo et al., 2013). They are positive sense, single-stranded RNA viruses that not only code for viral proteins but also carry RNA motifs that play crucial roles in viral replication. Usually, having noncoding or untranslated RNA motifs that form secondary structures is not uncommon among viruses and are prone to mutations (Fontana, Konings, Stadler, & Schuster, 1993; Rivas & Eddy, 2000). However, some of these structural RNA elements are highly conserved among *flaviviridae* despite the lack of sequence homology among them (Borisevich, Seregin, Nistler, Mutabazi, & Yamshchikov, 2006; Ivanyi-Nagy & Darlix, 2012; Markoff, 2003; Zhang, Dong, Stein, Iversen, & Shi, 2008).

1.4 SIGNIFICANCE OF FLAVIVIRUS TERMINAL REGIONS

Degradation of the invading viral genome by the host is crucial if its replication is to be stopped. The OAS enzymes partially aid in this process by recognizing dsRNA PAMPs and synthesizing 2-5A that activate downstream effector protein RNase L. Though the characteristics for OAS activation may be varied, such as sequence composition and length, the most important criteria is that the RNA activator must be double-stranded. In this context, the *Flaviviridae* family of viruses share a key similarity in their highly structured terminal regions that lead to their detection by OAS and subsequent degradation by RNase L.

The *flavivirus* genome is flanked by 5'untranslated regions (5'TR) and 3' untranslated regions (3'TR) that base pair with each other to form a double-stranded panhandle structure for replication (Figure 1.5) (Chambers et al., 1990).

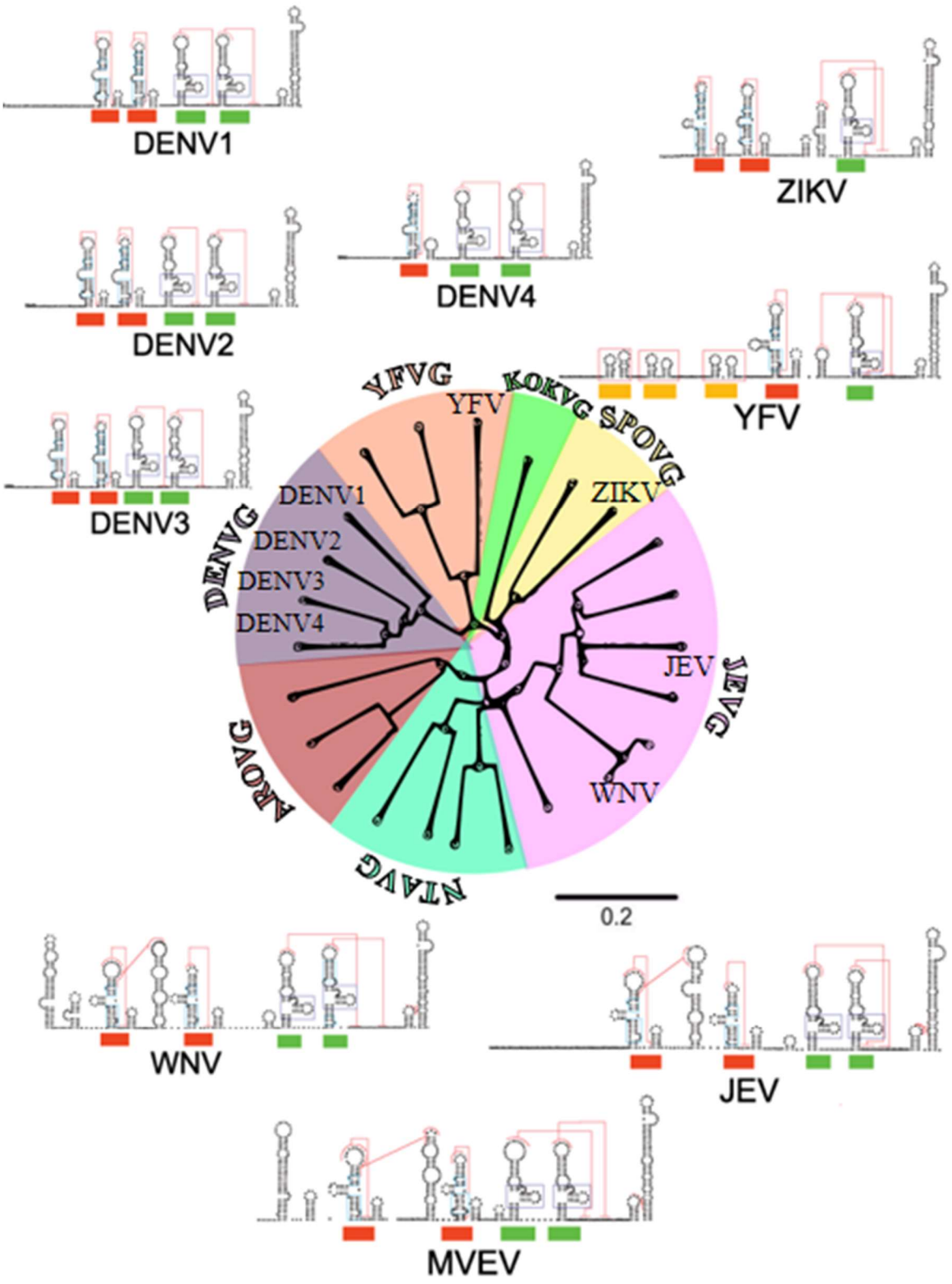
DENV1
ZIKV
DENV4
DENV2
YFV
DENV3
YFVG
YFV
KOKVG
SPOVG
ZIKV
DENVG
DENV1
DENV2
DENV3
DENV4
JEV
JEVG
WNV
NTAVG
0.2
WNV
JEV
MVEV

Figure 1.5. Flaviviral terminal region similarity.

Comparative analysis of *Flaviviral* terminal regions show conserved RNA structures. Same type of RNA structures are color coded with red representing stem loops and green representing dumbbell structure. Pseudoknots are indicated by dashed red line between complimentary regions of RNA. Different *flavivirus* groups are divided into different colors and terminal region examples from a few groups are illustrated. Only mosquito-borne viral groups are shown, which are: the DENV group (DENVG), Japanese encephalitis group (JEVG), YFV group (YFVG), Kokobera virus group (KOKVG), Aroa virus group (AROVG), Ntaya virus group (NTAVG), and Spondweni virus group (SPOVG).

The 5'TR spans approximately 100 nucleotides while the 3'TR ranges from between 400 to 700 bp. A type I cap structure (explained below) is present in the 5'TR sequence while the 3'TR sequence lacks polyadenylation (Brinton & Dispoto, 1988). There can be a wide variety of RNA elements present in the terminal regions that aid in viral replication, translation, and pathogenesis. These include 5′ and 3′ upstream AUG region (UAR), the 5′ stem loops A and B (5′SLA and 5′SLB, respectively), 3′ short hairpin structure (sHP), the 5′ cyclization sequence, and the capsid-coding region hairpin element (cHP) that lies within the ORF and 3′ cyclization sequence, the highly-conserved 3′ stem loop (3'SL) (D. Alvarez et al., 2006; D. E. Alvarez, Lodeiro, Luduena, Pietrasanta, & Gamarnik, 2005; Markoff, 2003).

Although structured elements can vary among different members, there are a few motifs that more or less remain among all *flaviviruses.* These are the small hairpin 3' stem-loop (sHP-3' SL) located at the 3' end of the viral RNA and the Y shape stem-loop A structure (SLA) present at the 5'TR. The 5' cHP element is known to recruit or stabilize initiation factors while the 3' sHP element is responsible for facilitate the cyclization of the genome (Figure 1.6). Although mutations to the 3' sHP disrupts its function in DENV completely, only mutations that disrupt 5' cHP secondary structure effect its function but does not necessarily depend on its function. Base pairing between 3' and 5' TRs hybridize to form a structure called the 5'-3'UAR which together with another hybridized stretch of base pairs known as 5'-3' CS (conserved sequence) forms important elements that are essential for genome cyclization and viral replication (Hahn et al., 1987; Khromykh, Meka, Guyatt, & Westaway, 2001).

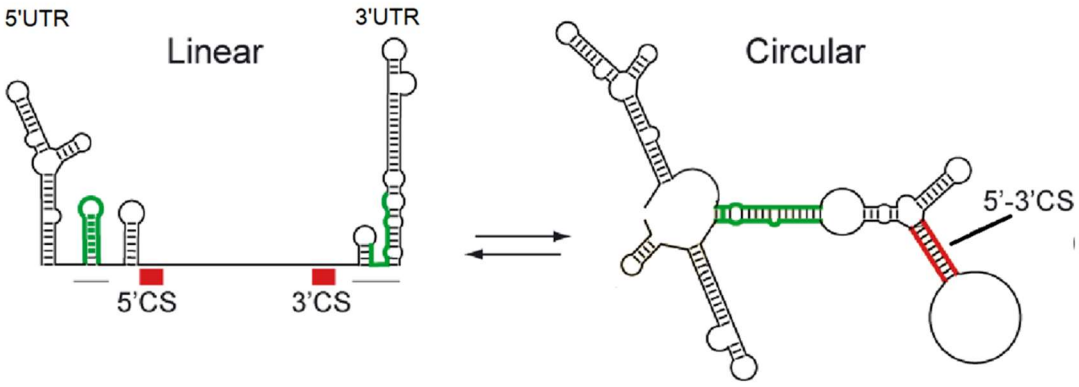

Figure 1.6. Schematic of *flaviviral* genome cyclization

Flaviviral genome exists in either a linear or a circular conformation. The 5' and 3' terminal regions of *flavivirus* contain regions essential for viral replication and modulation of several process in its life cycle. For genome replication, the genome

must adopt a circular conformation whereby 5’ and 3’ terminal regions come together and hybridize within complimentary regions (indicated in red and green). These essential regions include the 5’ and 3’ conserved sequences which is essential for viral replication.

The 5’ TR contains a m7GpppAmpN1 cap structure (7-methyl guanosine triphosphate linked to adenosine 5’-monophosphate followed by any nucleoside residue designated as N) and two conserved stem-loop (SL) regions known as SLA and SLB. *Flavivirus* often rely on this cap structure in order to carry out translation and to protect from 5’-3’ exonucleases. However, there are some exceptions such as DENV which can carry out cap-independent translation through a poorly understood mechanism. The SLA and SLB regions span about 70 and 30 nucleotides in length respectively, with a short span of poly (U) sequence in-between to separate them. SLA is mainly involved in RNA synthesis while SLB contains the crucial 5’ end of the UAR sequence used for genome replication (Brinton & Dispoto, 1988; Filomatori et al., 2006; Lodeiro, Filomatori, & Gamarnik, 2009; Zhang, Dong, Zhou, & Shi, 2008).

The 3’TR is comparatively much longer with lengths ranging from 400 to 600 bases and contains highly conserved structured regions. The most common structural elements include stem-loop (SL) and two dumbbell (DB) structures and within these structures lie conserved sequences (CS) and repeated conserved

sequences (RCS). This region can be divided into 3 domains: domain 1 consisting of one SL structures, domain 2 containing two DB structures and the highly conserved domain 3 consisting one of the CS, one sHP and a large terminal 3'SL structure. The 3'SL structure is conserved among *flaviviruses* and is crucial in the translation and replication process. Contained within domain I of 3'TRs are variable regions of repeat sequences (de Borba et al., 2015; Manzano et al., 2011; Sztuba-Solinska et al., 2013; Villordo, Filomatori, Sánchez-Vargas, Blair, & Gamarnik, 2015). Studies performed on TBEV show deletion of variable sequence region results in elevated virulence, while in DENV2 deletion of specific VR sequences resulted in variable responses in mosquito relative to mammalian cells (Johansson & Ward, 2017). Within the VR there are SL structures that confer resistance against host exoribonuclease. These structures are highly conserved during replication in mammalian cells, suggesting their importance in defense against host immune system. The DB structures play a crucial role in viral translation and RNA replication (Chapman, Moon, Wilusz, & Kieft, 2014; Kieft, Rabe, & Chapman, 2015).

1.5 EFFECT OF FLAVIVIRUS TERMINAL REGION ON OAS ENZYMES

The interaction between the terminal regions of WNV and OAS enzymes have been previously studied. *In vitro* studies with WNV 5' TR showed strong binding affinity for OAS1 (Deo et al., 2015). In this study, a colorimetric assay using ammonium molybdate was used to measure enzyme activity (Koul, Deo, et al., 2020). The assay produced a blue color in the presence of pyrophosphate, which is

a byproduct of 2-5A synthesis. The amount of OAS activity was them measured based on intensity of color produced as a function of time (Deo et al., 2015; Nagul, McKelvie, Worsfold, & Kolev, 2015). To determine specific structures in the 5'TR and 3'TR of WNV and to determine the length required for OAS activation several different truncated RNA TRs were explored. It was observed that simply stem loop 1 and stem loop 2 of 5'TR produced suboptimal levels of enzyme activation while the full length 5'TR was required for full activation of OAS1 (Figure 1.7) (Deo et al., 2015). Moreover, a recent study showed that OAS2 activity increased with increasing length of dsRNA and that OAS2 required at least 35bp long dsRNA to activate (Koul, Deo, et al., 2020; Sarkar, Miyagi, Crabb, & Sen, 2002; Sarkar, Pal, et al., 2002).

In addition, phosphorylation of the 5'TR seems to play a role on OAS1 and OAS2 activation. When compared between phosphorylation states of 5'TR with various levels of phosphorylation, 5' triphosphate group showed that most enhanced activation of OAS1 compared to 5' hydroxyl group (Meng et al., 2012). A recent study looked into the effects of *in vitro* transcribed RNA with 5'-triphosphate group compared to 3' single-stranded pyrimidine overhang and 3' uridine overhang of varying length on OAS2 activation (Vachon et al., 2015). None of RNA tested produced as much of an OAS2 response as 5'-triphosphate group did (J. Donovan et al., 2015). Therefore, it is reasonable to extrapolate that 5' phosphorylation is important but not required for OAS1 and OAS2 activation. On the other hand, 3' overhangs enhances OAS1 and OAS 2 activation (Vachon et al., 2015).

Both 5’ TR and 3’ TR of *flaviviruses* contains conserved sequences that are important for genome cyclization (Figure 1.7). Complimentary regions in the 5’ and 3’ TRs hybridize and form a panhandle like structure to allow genome replication in the host (H. Dong, Zhang, & Shi, 2008; Friebe, Shi, & Harris, 2011; Lo, Tilgner, Bernard, & Shi, 2003; Villordo & Gamarnik, 2009). Whether this conserved panhandle structure plays any role in the activation of OAS1-RNase L pathway remains to be seen. A recent study has shown that stem loops contained within 3’ TR of WNV is capable of activating OAS1 *in vitro*. However, activation of OAS1 by 3’ TR of WNV is shown to be comparatively poorer than poly I:C or 5’ TR of WNV.

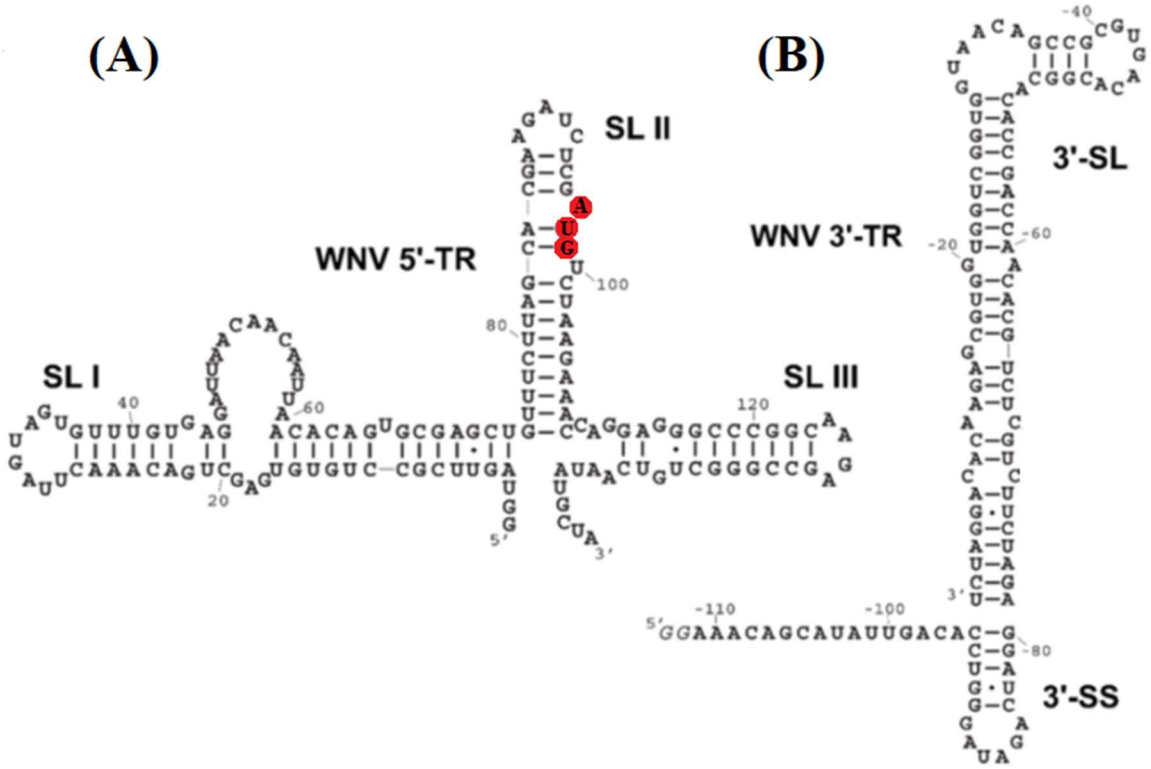

Figure 1.7. Secondary structures and sequence of WNV 5’ and 3’ terminal region.

(A) 5’ terminal region showing three stem loop structures (SL I, II and III). Initiation codons are marked in red circles.

(B) 3’ terminal regions showing a large stem loop (3’-SL) and a small stem loop (3’-SS).

1.6 SEQUENCE SPECIFICITY AND OAS ACTIVATION

Several studies have also explored the effect of dsRNA sequence on OAS activation. One study found that mean a specific non-coding RNA expressed from the adenovirus genome (VAI) with a single stranded pyramidine rich (CUUU) over hang produced a stronger OAS1 activation than one without (Vachon et al., 2015). In the case of OAS2, a study revealed that activation was 2-fold stronger in the presence of a dsRNA containing a 17 nucleotide long single stranded overhang (with alternating uracil residues) versus a monouracil (Koul, Deo, et al., 2020). Several other studies have shown that OAS1 activation is contingent upon the presence of a conserved sequence, WWN9WG, whereby W is either A or U and N is any nucleotide (Donovan et al., 2013; Kodym et al., 2009). In contrast to recognizing consensus sequences, a recent study show that OAS1 is also activated by sequences that both stabilize and destabilize the dsRNA structure.
It has been previously established that, dsRNA bends in order to establish the necessary contacts with the allosteric activation site (Donovan et al., 2013). Therefore, short dsRNA containing mismatches would destabilize it and allow for it adopt a bent conformation. However, this does not explain why G-C base pairs, which decrease stability, would also enhance the activation of OAS1. To answer this question, Schwartz *et al*. generated short dsRNA with varying levels of G-C base

pairs as well as A-C or I-U mismatch sequences and observed how their structural changes correlates with OAS1 activation. Thermal difference spectra and molecular dynamics (MD) results suggest that the sequences with highest OAS1 activation are those that have mismatches in the bent portion of the dsRNA while remain stable at areas which make contact with OAS1 (Schwartz et al., 2022). These findings are exemplified in another recent study looking into interactions between the stem loop 1 within the 5'TR of severe acute respiratory syndrome coronavirus 2 and OAS1. MD simulations done in this study suggests that the degree of flexibility in SL1 and other dsRNA tertiary structures enables its recognition by OAS1 (Bignon, Miclot, Terenzi, Barone, & Monari, 2022). This study is particularly interesting because several other studies have shown previously that certain OAS1 variants are correlated to milder COVID-19 symptoms and better systemic response (Di Maria, Latini, Borgiani, & Novelli, 2020).

1.7 RNASE L

The next step in the OAS-RNase L pathway, after producing 2-5A chains of sufficient length, involves activation of RNase L. RNase L is very sensitive and can be activated with sub-nanomolar concentrations of 2-5A. Once activated, RNase L recognizes favorable sequences and indiscriminately degrades foreign and self ssRNA. This results in the trigger of apoptosis and inevitable cell death (B. Dong et al., 1994; Player & Torrence, 1998; Silverman, 2007a).

RNase L is a 2-5 A dependent endonuclease that mediates the interferon response and impedes viral proliferation by apoptosis (A. Zhou, Hassel, & Silverman, 1993; A. Zhou et al., 1997). X-ray crystallography studies show RNase L is a monomeric protein whose overall structure is divided into 3 major domains: Ankyrin repeat (ANK) domain, Pseudo Kinase (PK) domain and the Rnase domain (Han, Whitney, Donovan, & Korennykh, 2012; Huang et al., 2014). The 'L' in RNase L denotes that its monomeric form is latent in the cell and can only carry out its endonuclease function after dimerization (A. Zhou, Molinaro, Malathi, & Silverman, 2005). Binding of 2-5 A to the ANK domains of a pair of monomers brings about conformational change that allows RNase L to dimerize (Figure 1.8) (Han et al., 2012; Huang et al., 2014).

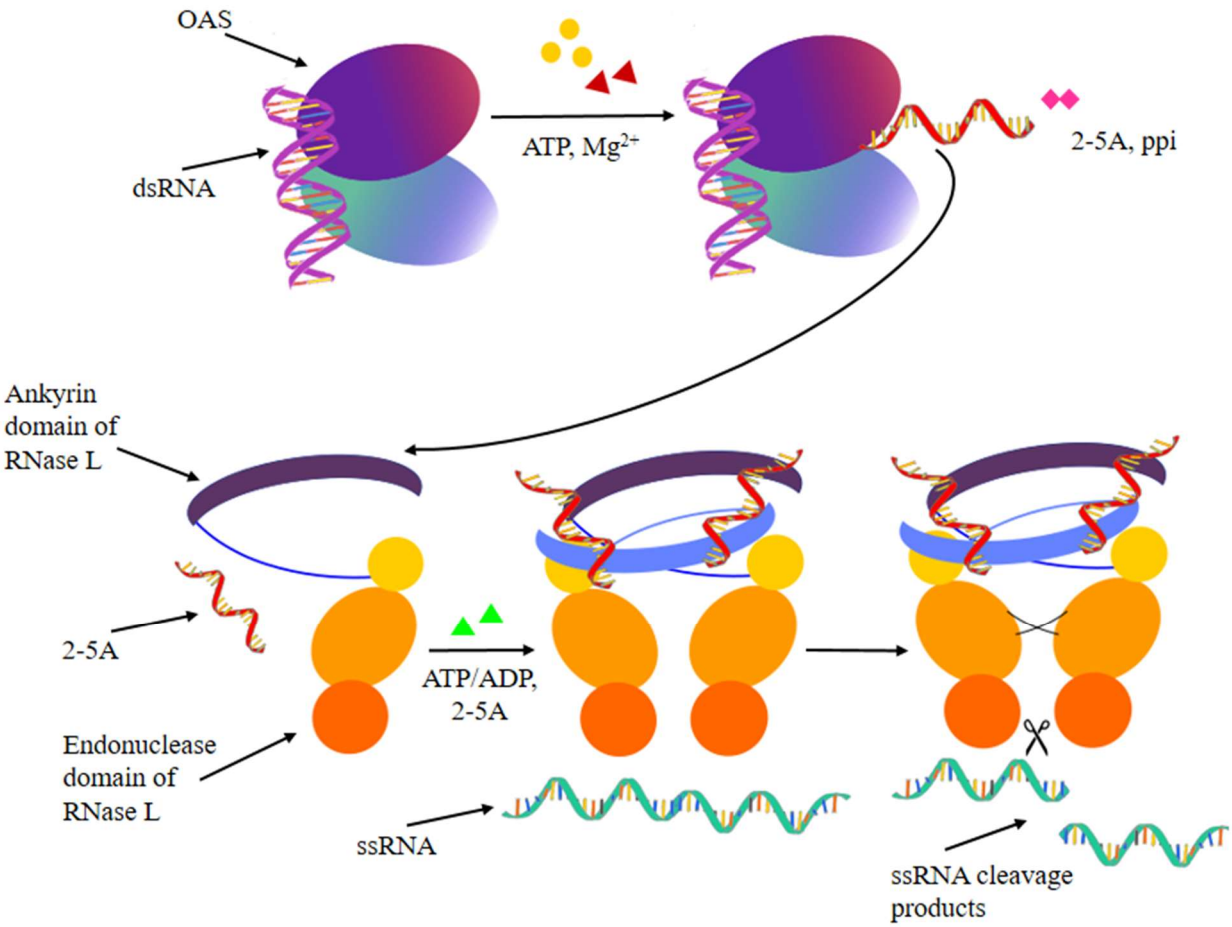

Figure 1.8. Schematic representation of OAS-RNaseL pathway.

OAS is activated by dsRNA and produces 2-5A chains. These chains bind to the ankyrin domains of two RNase L monomers and initiate its dimerization. The endonuclease domains of two RNase L monomers are brought closer together, allowing the cleavage of cellular ssRNA.

1.7.1 ANK DOMAIN AND DIMERIZATION OF RNASE L

The ANK domain consists of eight alpha helices consisting of ankyrin repeat elements and an incomplete ninth repeat which is disordered (Hassel, Zhou, Sotomayor, Maran, & Silverman, 1993). The alpha helices are connected side by side via beta-hairpin motifs which creates a curved 'cupped hand' shape (Figure 1.8). Through X-ray crystallography and mutational studies Han *et al.* has revealed two main interactions between 2-5A and ANK domain which results in activation of RNase L (Han et al., 2012). The first interaction involves the contact between 2-5A and repeats 2-4 on the concave side of the ANK domain. The phosphate and –OH groups of the adenine nucleotides bind to specific residues on repeats 2-4 via strong interactions such as salt bridges and hydrogen bonding (Torrence, Brozda, Alster, Charubala, & Pfleiderer, 1988). The second interaction involves the bound 2-5A on opposite ANK domains with Tyr312 and Arg310 residues of the R9 motif (Han et al., 2012). Simultaneous binding of two 2-5A to two RNase L monomers brings about initiation of dimerization. The process involves the pseudo kinase domain which stabilizes the interaction between RNase L monomers.

The PK domain is named because of structural deviations from a conventional kinase domain that results in the inability in carrying out kinase function. The PK domain is a bilobal structure with a smaller N-terminal lobe (N-lobe) and a larger C-terminal lobe (C-lobe) (Nolen, Taylor, & Ghosh, 2004). The C-lobe of PK contains a non-canonical appendage which is predominantly involved in recognition of ANK bound 2-5A activator and inter-domain interactions. Between the

two lobes resides a cleft containing critical invariant residues which coordinate binding of AMP or ADP as well as two molecules of Mg^{2+}. The dimeric configuration of RNase L arises from several interactions within the ANK and PK domains (Huang et al., 2014). The binding of 2-5A brings about conformational change in the ANK domain with the help of trans domain linkages within protomers of each domain. Together with AMP/ADP and two molecules of Mg^{2+} bound to the interlobe cleft of PK domain makes the full length dimeric RNase L into an overall rigid structure (Figure 1.8) (Kornev, Taylor, & Ten Eyck, 2008; Tanaka et al., 2004).

The dimerization of RNase L brings two Rnase domains closer together, which is necessary for their endonuclease activity. Within the active site of each RNase monomer, exists four amino acids of great importance known as the catalytic tetrad (Tyr663, Arg 675, Asn676, and His680). To carry out phosphodiester bond cleavage, two copies of the catalytic tetrad must be present and forms a cleft when brought close together (Huang et al., 2014). Although RNA cleavage is not dependent on nucleotide sequence, RNase L does prefer to cleave after UU or UA nucleotides and others sequences up to a lesser frequency (Chakrabarti, Jha, & Silverman, 2011; Silverman, 2007b).

1.8 OVERVIEW OF THESIS

In the introductory chapter, I have elaborated on numerous RNA-dependent PRRs including OAS involved in recognition of PAMPs. Further, I have provided our current understanding of OAS genome organization, structural features, method of

action as well as its relationship to *flavivral* terminal regions. In addition, I have included extensive research on the significance of conserved secondary sequences present in the terminal regions of numerous *flaviviridae.* Lastly, I have talked about the structural and functional aspects of RNase L as well as its relationship to OAS and *flavivirus* dsRNA.

In Chapter 2, I will present the materials and methods I have used to obtain the findings of my research. I start by stating the methods by which I obtain my proteins of interest, followed by transcription and purification of viral dsRNA. Finally I elucidate the OAS-RNase L assay I have developed in my study.

In Chapter 3, I will present and discuss the results obtained in my study. Firstly, I present data and rationalization for the purification process of my proteins and nucleic acids. This is followed by an in depth analysis of the steps involved in developing my assay. I elaborate how the parameters for each variable is selected and how each variable bring the assay into fruition. Lastly I show an example of the assay at work by comparing two different dsRNA from WNV and JEV as well as a brief explanation behind the observations.

Finally, in the concluding chapter I summarize my findings and provide possible future directions of my research. In this chapter, I attempt to rationalize the observed results from the development stages of my assay as well as through testing of viral dsRNA truncations. In addition, I highlight the contribution my study makes to the understanding of OAS enzymes.

1.9 REFERENCES

Ablasser, A., & Hur, S. (2020). Regulation of cGAS-and RLR-mediated immunity to nucleic acids. *Nature immunology, 21*(1), 17-29.

Akira, S., Uematsu, S., & Takeuchi, O. (2006). Pathogen recognition and innate immunity. *Cell, 124*(4), 783-801.

Allen, I. C., Scull, M. A., Moore, C. B., Holl, E. K., McElvania-TeKippe, E., Taxman, D. J., . . . Ting, J. P.-Y. (2009). The NLRP3 inflammasome mediates in vivo innate immunity to influenza A virus through recognition of viral RNA. *Immunity, 30*(4), 556-565.

Alvarez, D., Lodeiro, M. F., Filomatori, C., Fucito, S., Mondotte, J., & Gamarnik, A. (2006). *Structural and functional analysis of dengue virus RNA.* Paper presented at the Novartis Foundation Symposium.

Alvarez, D. E., Lodeiro, M. F., Luduena, S. J., Pietrasanta, L. I., & Gamarnik, A. V. (2005). Long-range RNA-RNA interactions circularize the dengue virus genome. *Journal of virology, 79*(11), 6631-6643.

Anderson, B. R., Muramatsu, H., Jha, B. K., Silverman, R. H., Weissman, D., & Karikó, K. (2011). Nucleoside modifications in RNA limit activation of 2′-5′-oligoadenylate synthetase and increase resistance to cleavage by RNase L. *Nucleic acids research, 39*(21), 9329-9338.

Balachandran, S., Roberts, P. C., Brown, L. E., Truong, H., Pattnaik, A. K., Archer, D. R., & Barber, G. N. (2000). Essential role for the dsRNA-dependent protein kinase PKR in innate immunity to viral infection. *Immunity, 13*(1), 129-141.

Bandyopadhyay, S., Ghosh, A., Sarkar, S. N., & Sen, G. C. (1998). Production and Purification of Recombinant 2 ‘-5 ‘Oligoadenylate Synthetase and Its Mutants Using the Baculovirus System. *Biochemistry, 37*(11), 3824-3830.

Barba-Spaeth, G., Dejnirattisai, W., Rouvinski, A., Vaney, M.-C., Medits, I., Sharma, A., . . . Haouz, A. (2016). Structural basis of potent Zika–dengue virus antibody cross-neutralization. *Nature, 536*(7614), 48-53.

Baumstark, T., & Ahlquist, P. (2001). The brome mosaic virus RNA3 intergenic replication enhancer folds to mimic a tRNA TpsiC-stem loop and is modified in vivo. *Rna, 7*(11), 1652-1670.

Becker, H. F., Motorin, Y., Florentz, C., Giegé, R., & Grosjean, H. (1998). Pseudouridine and ribothymidine formation in the tRNA-like domain of turnip yellow mosaic virus RNA. *Nucleic Acids Res, 26*(17), 3991-3997. doi: 10.1093/nar/26.17.3991

Bevilacqua, P. C., & Cech, T. R. (1996). Minor-groove recognition of double-stranded RNA by the double-stranded RNA-binding domain from the RNA-activated protein kinase PKR. *Biochemistry, 35*(31), 9983-9994.

Bignon, E., Miclot, T., Terenzi, A., Barone, G., & Monari, A. (2022). Structure of the 5′ untranslated region in SARS-CoV-2 genome and its specific recognition by innate immune system via the human oligoadenylate synthase 1. *Chemical Communications*.

Boo, S. H., & Kim, Y. K. (2020). The emerging role of RNA modifications in the regulation of mRNA stability. *Experimental & molecular medicine, 52*(3), 400-408.

Borisevich, V., Seregin, A., Nistler, R., Mutabazi, D., & Yamshchikov, V. (2006). Biological properties of chimeric West Nile viruses. *Virology, 349*(2), 371-381.

Brinton, M. A., & Dispoto, J. H. (1988). Sequence and secondary structure analysis of the 5′-terminal region of flavivirus genome RNA. *Virology, 162*(2), 290-299.

Broggi, A., Ghosh, S., Sposito, B., Spreafico, R., Balzarini, F., Lo Cascio, A., . . . Granucci, F. (2020). Type III interferons disrupt the lung epithelial barrier upon viral recognition. *Science, 369*(6504), 706-712.

Broz, P., & Dixit, V. M. (2016). Inflammasomes: mechanism of assembly, regulation and signalling. *Nature reviews immunology, 16*(7), 407-420.

Burghaus, P. A., & Holder, A. A. (1994). Expression of the 19-kilodalton carboxy-terminal fragment of the Plasmodium falciparum merozoite surface protein-1 in Escherichia coli as a correctly folded protein. *Molecular and biochemical parasitology, 64*(1), 165-169.

Calderon, B. M., & Conn, G. L. (2018). A human cellular noncoding RNA activates the antiviral protein 2'–5'-oligoadenylate synthetase 1. *Journal of Biological Chemistry, 293*(41), 16115-16124.

Carey, C. M., Govande, A. A., Cooper, J. M., Hartley, M. K., Kranzusch, P. J., & Elde, N. C. (2019). Recurrent loss-of-function mutations reveal costs to OAS1 antiviral activity in primates. *Cell host & microbe, 25*(2), 336-343. e334.

Cattaneo, R., & Billeter, M. (1992). Mutations and A/I hypermutations in measles virus persistent infections. *Genetic Diversity of RNA Viruses*, 63-74.

Chakrabarti, A., Jha, B. K., & Silverman, R. H. (2011). New insights into the role of RNase L in innate immunity. *Journal of Interferon & Cytokine Research, 31*(1), 49-57.

Chambers, T. J., Hahn, C. S., Galler, R., & Rice, C. M. (1990). Flavivirus genome organization, expression, and replication. *Annual review of microbiology, 44*(1), 649-688.

Chapman, E. G., Moon, S. L., Wilusz, J., & Kieft, J. S. (2014). RNA structures that resist degradation by Xrn1 produce a pathogenic Dengue virus RNA. *elife, 3*, e01892.

Chong, K., Feng, L., Schappert, K., Meurs, E., Donahue, T. F., Friesen, J. D., . . . Williams, B. (1992). Human p68 kinase exhibits growth suppression in yeast and homology to the translational regulator GCN2. *The EMBO journal, 11*(4), 1553-1562.

Clerzius, G., Gélinas, J.-F., Daher, A., Bonnet, M., Meurs, E. F., & Gatignol, A. (2009). ADAR1 interacts with PKR during human immunodeficiency virus infection of lymphocytes and contributes to viral replication. *Journal of virology, 83*(19), 10119-10128.

Dar, A. C., Dever, T. E., & Sicheri, F. (2005). Higher-order substrate recognition of eIF2α by the RNA-dependent protein kinase PKR. *Cell, 122*(6), 887-900.

Darnell Jr, J. E. (1997). STATs and gene regulation. *Science, 277*(5332), 1630-1635.

Darnell Jr, J. E., Kerr, I. M., & Stark, G. R. (1994). Jak-STAT pathways and transcriptional activation in response to IFNs and other extracellular signaling proteins. *Science, 264*(5164), 1415-1421.

de Borba, L., Villordo, S. M., Iglesias, N. G., Filomatori, C. V., Gebhard, L. G., & Gamarnik, A. V. (2015). Overlapping local and long-range RNA-RNA interactions modulate dengue virus genome cyclization and replication. *Journal of virology, 89*(6), 3430-3437.

Deo, S., Patel, T. R., Chojnowski, G., Koul, A., Dzananovic, E., McEleney, K., . . . McKenna, S. A. (2015). Characterization of the termini of the West Nile virus genome and their interactions with the small isoform of the 2' 5'-oligoadenylate synthetase family. *Journal of structural biology, 190*(2), 236-249.

Der, S. D., Zhou, A., Williams, B. R., & Silverman, R. H. (1998). Identification of genes differentially regulated by interferon alpha, beta, or gamma using oligonucleotide arrays. *Proc Natl Acad Sci U S A, 95*(26), 15623-15628. doi: 10.1073/pnas.95.26.15623

Di, H., Elbahesh, H., & Brinton, M. A. (2020). Characteristics of human OAS1 isoform proteins. *Viruses, 12*(2), 152.

Di Maria, E., Latini, A., Borgiani, P., & Novelli, G. (2020). Genetic variants of the human host influencing the coronavirus-associated phenotypes (SARS, MERS and COVID-19): rapid systematic review and field synopsis. *Human genomics, 14*(1), 1-19.

Dong, B., Xu, L., Zhou, A., Hassel, B. A., Lee, X., Torrence, P. F., & Silverman, R. H. (1994). Intrinsic molecular activities of the interferon-induced 2-5A-dependent RNase. *Journal of Biological Chemistry, 269*(19), 14153-14158.

Dong, H., Zhang, B., & Shi, P.-Y. (2008). Terminal structures of West Nile virus genomic RNA and their interactions with viral NS5 protein. *Virology, 381*(1), 123-135.

Donovan, Dufner, M., & Korennykh, A. (2013). Structural basis for cytosolic double-stranded RNA surveillance by human oligoadenylate synthetase 1. *Proceedings of the National Academy of Sciences, 110*(5), 1652-1657.

Donovan, J., Whitney, G., Rath, S., & Korennykh, A. (2015). Structural mechanism of sensing long dsRNA via a noncatalytic domain in human oligoadenylate synthetase 3. *Proc Natl Acad Sci U S A, 112*(13), 3949-3954. doi: 10.1073/pnas.1419409112

Engelhart, A. E., Powner, M. W., & Szostak, J. W. (2013). Functional RNAs exhibit tolerance for non-heritable 2′–5′ versus 3′–5′ backbone heterogeneity. *Nature chemistry, 5*(5), 390-394.

Filomatori, C. V., Lodeiro, M. F., Alvarez, D. E., Samsa, M. M., Pietrasanta, L., & Gamarnik, A. V. (2006). A 5′ RNA element promotes dengue virus RNA synthesis on a circular genome. *Genes & development, 20*(16), 2238-2249.

Fitzgerald, D., Meade, K., McEvoy, A., Lillis, L., Murphy, E., MacHugh, D., & Baird, A. (2007). Tumour necrosis factor-α (TNF-α) increases nuclear factor κB (NFκB) activity in and interleukin-8 (IL-8) release from bovine mammary epithelial cells. *Veterinary immunology and immunopathology, 116*(1-2), 59-68.

Fontana, W., Konings, D. A., Stadler, P. F., & Schuster, P. (1993). Statistics of RNA secondary structures. *Biopolymers: Original Research on Biomolecules, 33*(9), 1389-1404.

Friebe, P., Shi, P.-Y., & Harris, E. (2011). The 5′ and 3′ downstream AUG region elements are required for mosquito-borne flavivirus RNA replication. *J Virol, 85*(4), 1900-1905.

Gandy, S. Z., Linnstaedt, S. D., Muralidhar, S., Cashman, K. A., Rosenthal, L. J., & Casey, J. L. (2007). RNA editing of the human herpesvirus 8 kaposin transcript eliminates its transforming activity and is induced during lytic replication. *Journal of virology, 81*(24), 13544-13551.

Garcia, M., Gil, J., Ventoso, I., Guerra, S., Domingo, E., Rivas, C., & Esteban, M. (2006). Impact of protein kinase PKR in cell biology: from antiviral to antiproliferative action. *Microbiology and Molecular Biology Reviews, 70*(4), 1032-1060.

George, C. X., Gan, Z., Liu, Y., & Samuel, C. E. (2011). Adenosine deaminases acting on RNA, RNA editing, and interferon action. *Journal of Interferon & Cytokine Research, 31*(1), 99-117.

Ghosh, A., Sarkar, S. N., Rowe, T. M., & Sen, G. C. (2001). A specific isozyme of 2′-5′ oligoadenylate synthetase is a dual function proapoptotic protein of the Bcl-2 family. *Journal of Biological Chemistry, 276*(27), 25447-25455.

Giannaris, P. A., & Damha, M. J. (1993). Oligoribonucleotides containing 2′, 5′-phosphodiester linkages exhibit binding selectivity for 3′, 5′-RNA over 3′, 5′-ssDNA. *Nucleic acids research, 21*(20), 4742-4749.

Gilbert, W. (1986). Origin of life: The RNA world. *Nature, 319*(6055), 618-618.

Grandvaux, N., Servant, M. J., TenOever, B., Sen, G. C., Balachandran, S., Barber, G. N., . . . Hiscott, J. (2002). Transcriptional profiling of interferon regulatory factor 3 target genes: direct involvement in the regulation of interferon-stimulated genes. *Journal of virology, 76*(11), 5532-5539.

Gubler, D. J. (1998). Dengue and dengue hemorrhagic fever. *Clinical microbiology reviews, 11*(3), 480-496.

Hahn, C. S., Hahn, Y. S., Rice, C. M., Lee, E., Dalgarno, L., Strauss, E. G., & Strauss, J. H. (1987). Conserved elements in the 3′ untranslated region of flavivirus RNAs and potential cyclization sequences. *Journal of molecular biology, 198*(1), 33-41.

Han, Y., Whitney, G., Donovan, J., & Korennykh, A. (2012). Innate immune messenger 2-5A tethers human RNase L into active high-order complexes. *Cell reports, 2*(4), 902-913.

Hartmann, R., Justesen, J., Sarkar, S. N., Sen, G. C., & Yee, V. C. (2003). Crystal structure of the 2′-specific and double-stranded RNA-activated interferon-induced antiviral protein 2′-5′-oligoadenylate synthetase. *Molecular cell, 12*(5), 1173-1185.

Hartmann, R., Norby, P. L., Martensen, P. M., Jorgensen, P., James, M. C., Jacobsen, C., . . . Justesen, J. (1998). Activation of 2'-5' oligoadenylate synthetase by single-stranded and double-stranded RNA aptamers. *J Biol Chem, 273*(6), 3236-3246.

Hassel, B. A., Zhou, A., Sotomayor, C., Maran, A., & Silverman, R. H. (1993). A dominant negative mutant of 2-5A-dependent RNase suppresses antiproliferative and antiviral effects of interferon. *The EMBO journal, 12*(8), 3297-3304.

Hiscott, J., Lin, R., Nakhaei, P., & Paz, S. (2006). MasterCARD: a priceless link to innate immunity. *Trends in molecular medicine, 12*(2), 53-56.

Hornung, V., Hartmann, R., Ablasser, A., & Hopfner, K.-P. (2014). OAS proteins and cGAS: unifying concepts in sensing and responding to cytosolic nucleic acids. *Nature reviews immunology, 14*(8), 521-528.

Hovanessian, A. G., Brown, R. E., & Kerr, I. M. (1977). Synthesis of low molecular weight inhibitor of protein synthesis with enzyme from interferon-treated cells. *Nature, 268*(5620), 537-540.

Hovanessian, A. G., & Justesen, J. (2007). The human 2′-5′ oligoadenylate synthetase family: unique interferon-inducible enzymes catalyzing 2′-5′ instead of 3′-5′ phosphodiester bond formation. *Biochimie, 89*(6-7), 779-788.

Hovnanian, A., Rebouillat, D., Mattei, M.-G., Levy, E. R., Marie, I., Monaco, A. P., & Hovanessian, A. G. (1998). The human 2′, 5′-oligoadenylate synthetase locus is composed of three distinct genes clustered on chromosome 12q24. 2 encoding the 100-, 69-, and 40-kDa forms. *Genomics, 52*(3), 267-277.

Hu, J., Wang, X., Xing, Y., Rong, E., Ning, M., Smith, J., & Huang, Y. (2018). Origin and development of oligoadenylate synthetase immune system. *BMC evolutionary biology, 18*(1), 1-13.

Huang, H., Zeqiraj, E., Dong, B., Jha, B. K., Duffy, N. M., Orlicky, S., . . . Ceccarelli, D. F. (2014). Dimeric structure of pseudokinase RNase L bound to 2-5A reveals a basis for interferon-induced antiviral activity. *Molecular cell, 53*(2), 221-234.

Hundley, H. A., & Bass, B. L. (2010). ADAR editing in double-stranded UTRs and other noncoding RNA sequences. *Trends in biochemical sciences, 35*(7), 377-383.

Hyde, J. L., & Diamond, M. S. (2015). Innate immune restriction and antagonism of viral RNA lacking 2′-O methylation. *Virology, 479*, 66-74.

Ibsen, M. S., Gad, H. H., Andersen, L. L., Hornung, V., Julkunen, I., Sarkar, S. N., & Hartmann, R. (2015). Structural and functional analysis reveals that human OASL binds dsRNA to enhance RIG-I signaling. *Nucleic Acids Res, 43*(10), 5236-5248. doi: 10.1093/nar/gkv389

Ivanyi-Nagy, R., & Darlix, J.-L. (2012). Core protein-mediated 5′–3′ annealing of the West Nile virus genomic RNA in vitro. *Virus research, 167*(2), 226-235.

Janeway Jr, C. A., Travers, P., Walport, M., & Shlomchik, M. J. (2001). Principles of innate and adaptive immunity *Immunobiology: The Immune System in Health and Disease. 5th edition*: Garland Science.

Jiang, F., Ramanathan, A., Miller, M. T., Tang, G.-Q., Gale, M., Patel, S. S., & Marcotrigiano, J. (2011). Structural basis of RNA recognition and activation by innate immune receptor RIG-I. *Nature, 479*(7373), 423-427.

Johansson, O., & Ward, M. (2017). The human immune system's response to carcinogenic and other infectious agents transmitted by mosquito vectors. *Parasitology Research, 116*(1), 1-9.

Justesen, J., Hartmann, R., & Kjeldgaard, N. (2000). Gene structure and function of the 2′-5′-oligoadenylate synthetase family. *Cellular and Molecular Life Sciences CMLS, 57*(11), 1593-1612.

Kanneganti, T.-D., & Lamkanfi, M. (2007). Intracellular NOD-like receptors in host defense and disease. *Immunity, 27*(4), 549-559.

Kato, H., Takeuchi, O., Sato, S., Yoneyama, M., Yamamoto, M., Matsui, K., . . . Ishii, K. J. (2006). Differential roles of MDA5 and RIG-I helicases in the recognition of RNA viruses. *Nature, 441*(7089), 101-105.

Kawai, T., & Akira, S. (2011). Toll-like receptors and their crosstalk with other innate receptors in infection and immunity. *Immunity, 34*(5), 637-650.

Khromykh, A. A., Meka, H., Guyatt, K. J., & Westaway, E. G. (2001). Essential role of cyclization sequences in flavivirus RNA replication. *Journal of virology, 75*(14), 6719-6728.

Khurana, S., & George, S. P. (2008). Regulation of cell structure and function by actin-binding proteins: villin's perspective. *FEBS Lett, 582*(14), 2128-2139. doi: 10.1016/j.febslet.2008.02.040

Kieft, J. S., Rabe, J. L., & Chapman, E. G. (2015). New hypotheses derived from the structure of a flaviviral Xrn1-resistant RNA: Conservation, folding, and host adaptation. *RNA biology, 12*(11), 1169-1177.

Kjær, K. H., Pahus, J., Hansen, M. F., Poulsen, J. B., Christensen, E. I., Justesen, J., & Martensen, P. M. (2014). Mitochondrial localization of the OAS1 p46 isoform associated with a common single nucleotide polymorphism. *BMC cell biology, 15*(1), 1-14.

Kodym, R., Kodym, E., & Story, M. D. (2009). 2'-5'-Oligoadenylate synthetase is activated by a specific RNA sequence motif. *Biochemical and biophysical research communications, 388*(2), 317-322.

Komuro, A., & Horvath, C. M. (2006). RNA-and virus-independent inhibition of antiviral signaling by RNA helicase LGP2. *Journal of virology, 80*(24), 12332-12342.

Koonin, E. V., & Aravind, L. (2000). The NACHT family-a new group of predicted NTPases implicated in apoptosis and MHC transcription activation. *Trends in biochemical sciences, 25*(5), 223-224.

Kornev, A. P., Taylor, S. S., & Ten Eyck, L. F. (2008). A helix scaffold for the assembly of active protein kinases. *Proc Natl Acad Sci U S A, 105*(38), 14377-14382. doi: 10.1073/pnas.0807988105

Koul, A., Deo, S., Booy, E. P., Orriss, G. L., Genung, M., & McKenna, S. A. (2020). Impact of double-stranded RNA characteristics on the activation of human 2'–5'-oligoadenylate synthetase 2 (OAS2). *Biochemistry and Cell Biology, 98*(1), 70-82.

Koul, A., Gemmill, D., Lubna, N., Meier, M., Krahn, N., Booy, E. P., . . . McKenna, S. A. (2020). Structural and hydrodynamic characterization of dimeric human oligoadenylate synthetase 2. *Biophysical journal, 118*(11), 2726-2740.

Kranzusch, P. J., Lee, A. S.-Y., Berger, J. M., & Doudna, J. A. (2013). Structure of human cGAS reveals a conserved family of second-messenger enzymes in innate immunity. *Cell reports, 3*(5), 1362-1368.

Kristiansen, H., Gad, H. H., Eskildsen-Larsen, S., Despres, P., & Hartmann, R. (2011). The oligoadenylate synthetase family: an ancient protein family with multiple antiviral activities. *Journal of Interferon & Cytokine Research, 31*(1), 41-47.

Kumar, M., & Carmichael, G. G. (1997). Nuclear antisense RNA induces extensive adenosine modifications and nuclear retention of target transcripts. *Proceedings of the National Academy of Sciences, 94*(8), 3542-3547.

Langland, J. O., Pettiford, S., Jiang, B., & Jacobs, B. L. (1994). Products of the porcine group C rotavirus NSP3 gene bind specifically to double-stranded RNA and inhibit activation of the interferon-induced protein kinase PKR. *Journal of virology, 68*(6), 3821-3829.

Leonard, W. J., & O'Shea, J. J. (1998). Jaks and STATs: biological implications. *Annual review of immunology, 16*(1), 293-322.

Li, F., Li, S., Wang, Z., Shen, Y., Zhang, T., & Yang, X. (2013). Structure of the kinase domain of human RNA-dependent protein kinase with K296R mutation reveals a face-to-face dimer. *Chinese Science Bulletin, 58*(9), 998-1002.

Li, Y., Banerjee, S., Goldstein, S. A., Dong, B., Gaughan, C., Rath, S., . . . Weiss, S. R. (2017). Ribonuclease L mediates the cell-lethal phenotype of double-stranded RNA editing enzyme ADAR1 deficiency in a human cell line. *elife, 6*, e25687.

Lin, R., Génin, P., Mamane, Y., & Hiscott, J. (2000). Selective DNA binding and association with the CREB binding protein coactivator contribute to differential activation of alpha/beta interferon genes by interferon regulatory factors 3 and 7. *Molecular and Cellular Biology, 20*(17), 6342-6353.

Liu, L., Botos, I., Wang, Y., Leonard, J. N., Shiloach, J., Segal, D. M., & Davies, D. R. (2008). Structural basis of toll-like receptor 3 signaling with double-stranded RNA. *Science*.

Lo, M. K., Tilgner, M., Bernard, K. A., & Shi, P.-Y. (2003). Functional analysis of mosquito-borne flavivirus conserved sequence elements within 3' untranslated region of West Nile virus by use of a reporting replicon that differentiates between viral translation and RNA replication. *J Virol, 77*(18), 10004-10014.

Lodeiro, M. F., Filomatori, C. V., & Gamarnik, A. V. (2009). Structural and functional studies of the promoter element for dengue virus RNA replication. *Journal of virology, 83*(2), 993-1008.

Lohöfener, J., Steinke, N., Kay-Fedorov, P., Baruch, P., Nikulin, A., Tishchenko, S., . . . Fedorov, R. (2015). The activation mechanism of 2'-5'-oligoadenylate synthetase gives new insights into OAS/cGAS triggers of innate immunity. *Structure, 23*(5), 851-862.

Loo, Y.-M., Fornek, J., Crochet, N., Bajwa, G., Perwitasari, O., Martinez-Sobrido, L., . . . Katze, M. G. (2008). Distinct RIG-I and MDA5 signaling by RNA viruses in innate immunity. *Journal of virology, 82*(1), 335-345.

Lucas, C., Wong, P., Klein, J., Castro, T. B., Silva, J., Sundaram, M., . . . Israelow, B. (2020). Longitudinal analyses reveal immunological misfiring in severe COVID-19. *Nature, 584*(7821), 463-469.

Malathi, K., Dong, B., Gale, M., & Silverman, R. H. (2007). Small self-RNA generated by RNase L amplifies antiviral innate immunity. *Nature, 448*(7155), 816-819.

Manivannan, P., Siddiqui, M. A., & Malathi, K. (2020). RNase L amplifies interferon signaling by inducing protein kinase R-mediated antiviral stress granules. *Journal of virology, 94*(13), e00205-00220.

Manzano, M., Reichert, E. D., Polo, S., Falgout, B., Kasprzak, W., Shapiro, B. A., & Padmanabhan, R. (2011). Identification of cis-acting elements in the 3'-untranslated region of the dengue virus type 2 RNA that modulate translation and replication. *Journal of Biological Chemistry, 286*(25), 22521-22534.

Marceau, C. D., Puschnik, A. S., Majzoub, K., Ooi, Y. S., Brewer, S. M., Fuchs, G., . . . Carette, J. E. (2016). Genetic dissection of Flaviviridae host factors through genome-scale CRISPR screens. *Nature, 535*(7610), 159-163. doi: 10.1038/nature18631

Marie, I., Blanco, J., Rebouillat, D., & Hovanessian, A. G. (1997). 69-kDa and 100-kDa isoforms of interferon-induced (2'-5')oligoadenylate synthetase exhibit differential catalytic parameters. *Eur J Biochem, 248*(2), 558-566.

Marié, I., Durbin, J. E., & Levy, D. E. (1998). Differential viral induction of distinct interferon-α genes by positive feedback through interferon regulatory factor-7. *The EMBO journal, 17*(22), 6660-6669.

Marie, I., Rebouillat, D., & Hovanessian, A. G. (1999). The expression of both domains of the 69/71 kDa 2',5' oligoadenylate synthetase generates a catalytically active enzyme and mediates an anti-viral response. *Eur J Biochem, 262*(1), 155-165.

Markoff, L. (2003). 5'-and 3'-noncoding regions in flavivirus RNA. *Advances in virus research, 59*, 177.

McKenna, S. A., Lindhout, D. A., Kim, I., Liu, C. W., Gelev, V. M., Wagner, G., & Puglisi, J. D. (2007). Molecular Framework for the Activation of RNA-dependent Protein Kinase*♦. *Journal of Biological Chemistry, 282*(15), 11474-11486.

Megyeri, K., Au, W.-C., Rosztoczy, I., Raj, N., Miller, R. L., Tomai, M. A., & Pitha, P. M. (1995). Stimulation of interferon and cytokine gene expression by imiquimod and stimulation by Sendai virus utilize similar signal transduction pathways. *Molecular and Cellular Biology, 15*(4), 2207-2218.

Meng, H., Deo, S., Xiong, S., Dzananovic, E., Donald, L. J., van Dijk, C. W., & McKenna, S. A. (2012). Regulation of the interferon-inducible 2'-5'-oligoadenylate synthetases by adenovirus VA(I) RNA. *J Mol Biol, 422*(5), 635-649. doi: 10.1016/j.jmb.2012.06.017

Michel, T., Reichhart, J.-M., Hoffmann, J. A., & Royet, J. (2001). Drosophila Toll is activated by Gram-positive bacteria through a circulating peptidoglycan recognition protein. *Nature, 414*(6865), 756-759.

Minks, M. (1979). West DK, Benvin S, Baglioni C: Structural requirements of double-stranded RNA for the activation of 53. 2', 5'-oligo (A) polymerase and protein kinase of interferontreated HeLa cells. *J Biol Chem, 254*, 10180-10183.

Nachtergaele, S., & He, C. (2018). Chemical modifications in the life of an mRNA transcript. *Annual review of genetics, 52*, 349-372.

Nagul, E. A., McKelvie, I. D., Worsfold, P., & Kolev, S. D. (2015). The molybdenum blue reaction for the determination of orthophosphate revisited: Opening the black box. *Analytica chimica acta, 890*, 60-82.

Netzband, R., & Pager, C. T. (2020). Epitranscriptomic marks: Emerging modulators of RNA virus gene expression. *Wiley Interdisciplinary Reviews: RNA, 11*(3), e1576.

Nolen, B., Taylor, S., & Ghosh, G. (2004). Regulation of protein kinases; controlling activity through activation segment conformation. *Mol Cell, 15*(5), 661-675. doi: 10.1016/j.molcel.2004.08.024

Oakes, E., Anderson, A., Cohen-Gadol, A., & Hundley, H. A. (2017). Adenosine deaminase that acts on RNA 3 (ADAR3) binding to glutamate receptor subunit B pre-mRNA inhibits RNA editing in glioblastoma. *Journal of Biological Chemistry, 292*(10), 4326-4335.

Paul, W. E. (2012). *Fundamental immunology*: Lippincott Williams & Wilkins.

Pedersen, F. K., Henrichsen, J., & Schiffman, G. (1982). Antibody response to vaccination with pneumococcal capsular polysaccharides in splenectomized children. *Acta Pædiatrica, 71*(3), 451-455.

Pichlmair, A., Lassnig, C., Eberle, C.-A., Górna, M. W., Baumann, C. L., Burkard, T. R., . . . Bennett, K. L. (2011). IFIT1 is an antiviral protein that recognizes 5′-triphosphate RNA. *Nature immunology, 12*(7), 624-630.

Player, M. R., & Torrence, P. F. (1998). The 2–5 A system: Modulation of viral and cellular processes through acceleration of RNA degradation. *Pharmacology & therapeutics, 78*(2), 55-113.

Qin, H., Wilson, C. A., Lee, S. J., Zhao, X., & Benveniste, E. N. (2005). LPS induces CD40 gene expression through the activation of NF-κB and STAT-1α in macrophages and microglia. *Blood, 106*(9), 3114-3122.

Rebouillat, D., Hovnanian, A., David, G., Hovanessian, A. G., & Williams, B. R. (2000). Characterization of the gene encoding the 100-kDa form of human 2',5' oligoadenylate synthetase. *Genomics, 70*(2), 232-240. doi: 10.1006/geno.2000.6382

Rebouillat, D., Hovnanian, A., Marié, I., & Hovanessian, A. G. (1999). The 100-kDa 2′, 5′-oligoadenylate synthetase catalyzing preferentially the synthesis of dimeric pppA2′ p5′ A molecules is composed of three homologous domains. *Journal of Biological Chemistry, 274*(3), 1557-1565.

Rehwinkel, J., & Reis e Sousa, C. (2010). RIGorous detection: exposing virus through RNA sensing. *Science, 327*(5963), 284-286.

Rivas, E., & Eddy, S. R. (2000). Secondary structure alone is generally not statistically significant for the detection of noncoding RNAs. *Bioinformatics, 16*(7), 583-605.

Rosenbaum, J. N. (1986). Comparison of two theorists on care: Orem and Leininger. *Journal of advanced nursing, 11*(4), 409-419.

Rothenfusser, S., Goutagny, N., DiPerna, G., Gong, M., Monks, B. G., Schoenemeyer, A., . . . Fitzgerald, K. A. (2005). The RNA helicase Lgp2 inhibits TLR-independent sensing of viral replication by retinoic acid-inducible gene-I. *The Journal of Immunology, 175*(8), 5260-5268.

Sabbah, A., Chang, T. H., Harnack, R., Frohlich, V., Tominaga, K., Dube, P. H., . . . Bose, S. (2009). Activation of innate immune antiviral responses by Nod2. *Nature immunology, 10*(10), 1073-1080.

Sadler, A. J., & Williams, B. R. (2008). Interferon-inducible antiviral effectors. *Nature reviews immunology, 8*(7), 559-568.

Samuel, C. E. (2001). Antiviral actions of interferons. *Clinical microbiology reviews, 14*(4), 778-809.

Sarkar, S. N., Bandyopadhyay, S., Ghosh, A., & Sen, G. C. (1999). Enzymatic characteristics of recombinant medium isozyme of 2′-5′ oligoadenylate synthetase. *Journal of Biological Chemistry, 274*(3), 1848-1855.

Sarkar, S. N., Ghosh, A., Wang, H.-W., Sung, S.-S., & Sen, G. C. (1999). The nature of the catalytic domain of 2′-5′-oligoadenylate synthetases. *Journal of Biological Chemistry, 274*(36), 25535-25542.

Sarkar, S. N., Miyagi, M., Crabb, J. W., & Sen, G. C. (2002). Identification of the substrate-binding sites of 2′-5′-oligoadenylate synthetase. *Journal of Biological Chemistry, 277*(27), 24321-24330.

Sarkar, S. N., Pal, S., & Sen, G. C. (2002). Crisscross enzymatic reaction between the two molecules in the active dimeric P69 form of the 2′-5′ oligodenylate synthetase. *Journal of Biological Chemistry, 277*(47), 44760-44764.

Satoh, T., Kato, H., Kumagai, Y., Yoneyama, M., Sato, S., Matsushita, K., . . . Takeuchi, O. (2010). LGP2 is a positive regulator of RIG-I–and MDA5-mediated antiviral responses. *Proceedings of the National Academy of Sciences, 107*(4), 1512-1517.

Schierhorn, K. L., Jolmes, F., Bespalowa, J., Saenger, S., Peteranderl, C., Dzieciolowski, J., . . . Herrmann, A. (2017). Influenza A virus virulence depends on two amino acids in the N-terminal domain of its NS1 protein to facilitate inhibition of the RNA-dependent protein kinase PKR. *Journal of virology, 91*(10), e00198-00117.

Schneider, W. M., Chevillotte, M. D., & Rice, C. M. (2014). Interferon-stimulated genes: a complex web of host defenses. *Annual review of immunology, 32*, 513-545.

Schoggins, J. W., & Rice, C. M. (2011). Interferon-stimulated genes and their antiviral effector functions. *Current opinion in virology, 1*(6), 519-525.

Schoggins, J. W., Wilson, S. J., Panis, M., Murphy, M. Y., Jones, C. T., Bieniasz, P., & Rice, C. M. (2011). A diverse range of gene products are effectors of the type I interferon antiviral response. *Nature, 472*(7344), 481-485.

Schwartz, S. L., & Conn, G. L. (2019). RNA regulation of the antiviral protein 2′-5′-oligoadenylate synthetase. *Wiley Interdisciplinary Reviews: RNA, 10*(4), e1534.

Schwartz, S. L., Dey, D., Tanquary, J., Bair, C. R., Lowen, A. C., & Conn, G. L. (2022). Role of helical structure and dynamics in oligoadenylate synthetase 1 (OAS1) mismatch tolerance and activation by short dsRNAs. *Proceedings of the National Academy of Sciences, 119*(3).

Sen, G. C. (2001). Viruses and interferons. *Annual Reviews in Microbiology, 55*(1), 255-281.

Seo, H.-J., Kim, H. C., Klein, T. A., Ramey, A. M., Lee, J.-H., Kyung, S.-G., . . . Yeh, J.-Y. (2013). Molecular detection and genotyping of Japanese encephalitis virus in mosquitoes during a 2010 outbreak in the Republic of Korea. *PLoS One, 8*(2), e55165.

Shuai, K., & Liu, B. (2003). Regulation of JAK–STAT signalling in the immune system. *Nature reviews immunology, 3*(11), 900-911.

Silverman, R. H. (2007a). A scientific journey through the 2-5A/RNase L system. *Cytokine & growth factor reviews, 18*(5-6), 381-388.

Silverman, R. H. (2007b). Viral encounters with 2′, 5′-oligoadenylate synthetase and RNase L during the interferon antiviral response. *Journal of virology, 81*(23), 12720-12729.

Skrivergaard, S., Jensen, M. S., Rolander, T. B., Nguyen, T. B. N., Bundgaard, A., Nejsum, L. N., & Martensen, P. M. (2019). The cellular localization of the p42 and p46 oligoadenylate synthetase 1 isoforms and their impact on mitochondrial respiration. *Viruses, 11*(12), 1122.

Stark, G. R., Kerr, I. M., Williams, B. R., Silverman, R. H., & Schreiber, R. D. (1998). How cells respond to interferons. *Annual review of biochemistry, 67*(1), 227-264.

Stetson, D., & Medzhitov, R. (2006). Recognition of cytosolic DNA activates an IRF3-dependent innate immune response. *Immunity, 25*(3), 373–381.

Suspène, R., Petit, V., Puyraimond-Zemmour, D., Aynaud, M.-M., Henry, M., Guétard, D., . . . Vartanian, J.-P. (2011). Double-stranded RNA adenosine deaminase ADAR-1-induced hypermutated genomes

among inactivated seasonal influenza and live attenuated measles virus vaccines. *Journal of virology, 85*(5), 2458-2462.

Sztuba-Solinska, J., Teramoto, T., Rausch, J. W., Shapiro, B. A., Padmanabhan, R., & Le Grice, S. F. (2013). Structural complexity of Dengue virus untranslated regions: cis-acting RNA motifs and pseudoknot interactions modulating functionality of the viral genome. *Nucleic acids research, 41*(9), 5075-5089.

Takeda, K., Kaisho, T., & Akira, S. (2003). Toll-like receptors. *Annual review of immunology, 21*(1), 335-376.

Tan, M. H., Li, Q., Shanmugam, R., Piskol, R., Kohler, J., Young, A. N., . . . Ariyoshi, K. (2017). Dynamic landscape and regulation of RNA editing in mammals. *Nature, 550*(7675), 249-254.

Tanaka, N., Nakanishi, M., Kusakabe, Y., Goto, Y., Kitade, Y., & Nakamura, K. T. (2004). Structural basis for recognition of 2', 5'-linked oligoadenylates by human ribonuclease L. *The EMBO journal, 23*(20), 3929-3938.

Torralba, S., Sojat, J., & Hartmann, R. (2008). 2'-5'oligoadenylate synthetase shares active site architecture with the archaeal CCA-adding enzyme. *Cellular and molecular life sciences, 65*(16), 2613-2620.

Torrence, P., Brozda, D., Alster, D., Charubala, R., & Pfleiderer, W. (1988). Only one 3'-hydroxyl group of ppp5'A2'p5'A2'p5'A (2-5A) is required for activation of the 2-5A-dependent endonuclease. *Journal of Biological Chemistry, 263*(3), 1131-1139.

Vachon, V. K., Calderon, B. M., & Conn, G. L. (2015). A novel RNA molecular signature for activation of 2'-5' oligoadenylate synthetase-1. *Nucleic acids research, 43*(1), 544-552.

Vagn, B.-N., L, Shao, L., Dong-Jun, Z., Min, L., Pia, M. M., . . . Flemming, P. (2005). Variation in Antiviral 2',5'-Oligoadenylate Synthetase (2'5'AS) Enzyme Activity Is Controlled by a Single-Nucleotide Polymorphism at a Splice-Acceptor Site in the OAS1 Gene. *The American Journal of Human Genetics, 76*(4), 623-633. doi: https://doi.org/10.1086/429391

Venkataraman, T., Valdes, M., Elsby, R., Kakuta, S., Caceres, G., Saijo, S., . . . Barber, G. N. (2007). Loss of DExD/H box RNA helicase LGP2 manifests disparate antiviral responses. *The Journal of Immunology, 178*(10), 6444-6455.

Vilcek, J., & Sen, G. (1996). Interferons and other cytokines. In "Fields Virology," 3rd ed.(BN Fields, DM Knipe, PM Howley, et al., Eds.) pp. 375–399. *Lippincott-Raven, Philadelphia. Wilson, IA and Cox, NJ (1990). Structural basis of immune recognition of influenza virus hemagglutinin. Annu. Rev. Immunol, 8*, 737-771.

Villordo, S. M., Filomatori, C. V., Sánchez-Vargas, I., Blair, C. D., & Gamarnik, A. V. (2015). Dengue virus RNA structure specialization facilitates host adaptation. *PLoS Pathog, 11*(1), e1004604.

Villordo, S. M., & Gamarnik, A. V. (2009). Genome cyclization as strategy for flavivirus RNA replication. *Virus research, 139*(2), 230-239.

Wang, N., Liang, Y., Devaraj, S., Wang, J., Lemon, S. M., & Li, K. (2009). Toll-like receptor 3 mediates establishment of an antiviral state against hepatitis C virus in hepatoma cells. *Journal of virology, 83*(19), 9824-9834.

Wasner, M., Arion, D., Borkow, G., Noronha, A., Uddin, A. H., Parniak, M. A., & Damha, M. J. (1998). Physicochemical and Biochemical Properties of 2 ', 5 '-Linked RNA and 2 ', 5 '-RNA: 3 ', 5 '-RNA "Hybrid" Duplexes. *Biochemistry, 37*(20), 7478-7486.

Wipff, J., Allanore, Y., & Boileau, C. (2009). Interactions between fibrillin-1 and tgf-beta: consequences and human pathology. *Medecine Sciences: M/S, 25*(2), 161-167.

Yoneyama, M., Kikuchi, M., Matsumoto, K., Imaizumi, T., Miyagishi, M., Taira, K., . . . Akira, S. (2005). Shared and unique functions of the DExD/H-box helicases RIG-I, MDA5, and LGP2 in antiviral innate immunity. *The Journal of Immunology, 175*(5), 2851-2858.

Zhang, B., Dong, H., Stein, D. A., Iversen, P. L., & Shi, P.-Y. (2008). West Nile virus genome cyclization and RNA replication require two pairs of long-distance RNA interactions. *Virology, 373*(1), 1-13.

Zhang, B., Dong, H., Zhou, Y., & Shi, P.-Y. (2008). Genetic interactions among the West Nile virus methyltransferase, the RNA-dependent RNA polymerase, and the 5′ stem-loop of genomic RNA. *Journal of virology, 82*(14), 7047-7058.

Zhou, A., Hassel, B. A., & Silverman, R. H. (1993). Expression cloning of 2-5A-dependent RNAase: a uniquely regulated mediator of interferon action. *Cell, 72*(5), 753-765.

Zhou, A., Molinaro, R. J., Malathi, K., & Silverman, R. H. (2005). Mapping of the human RNASEL promoter and expression in cancer and normal cells. *Journal of Interferon & Cytokine Research, 25*(10), 595-603.

Zhou, A., Paranjape, J., Brown, T. L., Nie, H., Naik, S., Dong, B., . . . Colmenares, C. (1997). Interferon action and apoptosis are defective in mice devoid of 2′, 5′-oligoadenylate-dependent RNase L. *The EMBO journal, 16*(21), 6355-6363.

Zhou, Z., Ren, L., Zhang, L., Zhong, J., Xiao, Y., Jia, Z., . . . Jiang, S. (2020). Heightened innate immune responses in the respiratory tract of COVID-19 patients. *Cell host & microbe, 27*(6), 883-890. e882.

CHAPTER 2: MATERIALS AND METHODS

2.1 OVERVIEW

Understanding the effects of OAS activation on downstream RNase L activity *in vitro* is the focus of this thesis. Since the colorimetric assay previously described (Putnins & Yamada, 1975) measures only OAS catalytic activity, I developed a combined one-pot assay that measures RNase L activity under conditions that enable OAS activation. For my work I studied two different OAS isoforms; OAS1 transcript variant p42 and OAS2 transcript variant p69. These specific variants were chosen as the majority of studies, including those from my research group, have used these variants and we wanted to corroborate previous results with our assay. We also used *Sus scrofa* RNase L for this experiment, the plasmid of which was generously provided to us by the Sicheri lab at the University of Toronto.

In addition to protein expression and purification, I carried out *in vitro* transcription and purification of various *flavivirus* TRs to investigate their ability to activate OAS enzymes and RNase L downstream. 5' and 3' TRs from various *flaviviral* genomes were used in order to measure OAS1 and subsequently, RNase L activation. OAS1 and viral TRs was purified using affinity and size exclusion chromatography (SEC) whereas RNase L and OAS2 were only purified using affinity chromatography.

After the individual components of the assay were purified, we focused on establishing the parameters for the 'one pot' assay. To measure enzyme activation in our

‘one pot’ assay, I used an RNase L specific ssRNA probe that was attached to a 5’ fluorophore (6-Carboxyfluorescein or 6-FAM) and a 3’ black hole quencher. When the RNA was cleaved by active RNase L, the fluorophore can escape the immediate vicinity of the quencher via diffusion, thereby increasing the fluorescence measured. The sequence for this probe was also provided by the Sicheri lab and is outlined in their publication (Daou et al., 2020). Since buffer compositions for individual enzymes were different, it was imperative to find a middle ground if we were to perform both enzymatic reactions simultaneously. Likewise, it was also important to establish the order in which to add the reaction components to measure initial rates and minimize activation during the mixing process. After preliminary optimization of the assay, I decided to further optimize the assay using the fluorescence detection ability of the StepOnePlus quantitative real- time PCR (qPCR) system (Thermo-Fisher Scientific, Ottawa, Canada). While qPCR instrumentation is lower sensitivity than a state-of-the art fluorimeter, my research group has direct access to a qPCR instrument, multiwell plates allow for medium throughput assays, and qPCR systems are widely available in research and commercial labs allowing the methods developed to be widely adopted if successful.

To validate our fluorescence data I also performed gel electrophoresis of the cleaved fluorescent probe on a denaturing Tris-Borate-EDTA (TBE) RNA gel to confirm cleavage by RNase L. I carried out the previously established colorimetric assay to correlate with the one-pot assay results.

2.2. PLASMID VECTORS AND REAGENTS

Respective protein and RNA expression vectors were produced in *E.coli* DH5α cells for plasmid purification and linearization purposes (detailed below). OAS1 and RNase L expression was performed in the *E.coli* strain BL21(DE3) (Invitrogen, USA) as it is adapted to produce large amounts of foreign proteins without misfolding or aggregating into inclusion bodies. Attempts to purify a functionally active OAS2 from bacterial cells and yeast has been unsuccessful due to improperly folded protein. Therefore, this thesis outlines OAS2 expression and purification protocol using the HEK293T cell line which has been generously donated by Dr. Thomas Klonisch (University of Manitoba) (Koul, Deo, et al., 2020). HEK293T cells are efficient at protein production and easily accessible for transfection.

The human OAS1 (NCBI Reference Sequence: NP_002525.2) transcript variant 2 (tv2) is inserted in a modified pET30a vector with a GNSHT fusion tag (N- to C-Terminus: GB1, NusA, Streptavidin, 8xHis (Histidine) and tobacco etch virus (TEV) protease site). The purpose of this tag is several fold; GB1 is an immunoglobulin binding domain from *Streptococcus* (Huth et al., 1997)and NusA from *E. Coli*, is an anti-termination factor that stops transcription termination. These are proteins are part of the fusion tag not because of their function, but because they are very soluble proteins that encourage OAS1 solubility and prevent inclusion body formation (Hammarström, Hellgren, van Den Berg, Berglund, & Härd, 2002). It is hypothesized that GB1 and NusA prevent protein aggregation by acting as chaperone proteins, but the exact mechanism has not been investigated. (Costa, Almeida, Castro, & Domingues, 2014). The streptavidin and 8XHis

tags are part of the expressed fusion tag for affinity purification by a Biotin- or nickel affinity chromatography. The TEV protease recognition site is used for cleavage by in-house purified TEV protease to release the GNSHT fusion tag after OAS1 purification (Waugh, 2011). The affinity chromatography method we used was Nickel- Nitrilotriacetic acid (Ni-NTA) chromatography (GE Healthcare)(Waugh, 2005).

Recombinant human OAS2 p69 tv2 (transcript variant 2) was contained within a modified pCDNA3 vector with an N-terminal DYKDDDDK (FLAG) tag and an N-terminal His tag.

pCDNA3 is a vector which is often used for mammalian protein expression as it provides high-level, constitutive expression. The FLAG tag has dual function as it is used for purification in anti-FLAG affinity chromatography as well as being used for western blotting and immunoprecipitation.

Sus scrofa RNase L was inserted into a pGEX – 2T vector with an N-terminal Glutathione S-transferases (GST) expression vector for bacterial cells. The pGEX vector is designed with a tac promotor that allows high-level expression of protein in *E. coli* BL21 cells. Contained between the protein expression gene and GST tag is the thrombin recognition site Leu-Val-Pro-Arg-Gly-Ser- sequence and cleaved at the Arg-Gly bond. The pGEX-GST vector allows for very mild elution conditions when eluting from an affinity column. This allows for minimized effects on antigenicity and functional activity.

We have conducted our assay optimization using the 5’ TR of WNV contained within pUC119 vector, and 3’ TR of JEV contained within the pUC57 vector. pUC57 is designed for the cloning of DNA insert and is able to produce high copy number of the

insert. The multiple cloning site of this vector contains restriction sites that produce blunt 3'-ends specifically designed to avoid digestion from the *E. coli* exonuclease III.

2.3 EXPRESSION AND PURIFICATION OF OAS ENZYMES

2.3.1. EXPRESSION OF OAS1 IN BACTERIA

Human OAS1 pET30a(+)-GNSHT vector was inserted into *E. coli BL21*(DE3) cells via heat shock transformation described previously (Green & Sambrook, 2021). Starter cultures were then prepared by inoculating a small volume of Lysogeny Broth (LB) (Sigma-Aldrich) with the transformed bacteria. This starter culture was then used to inoculate 1 to 2 liters of LB for large scale protein production. To ensure selective pressure is maintained, all media were treated with 50ug/uL of kanamycin. The large-scale cultures were then induced with final concentration of 1 mM isopropyl-β-D-thio-galactopyranoside (IPTG) as soon as an optical density (OD) of 0.6 was reached at the absorbance of 600nm. (200rpm).

2.3.2. PURIFICATION OF OAS1

Overnight bacterial cultures were sedimented by centrifuging (Thermo Scientific TM Sorvall TM) at 6,000g for 15 min (4°C) and the resulting pellet was resuspended using cold resuspension/lysis buffer (50 mM Tris, 1M NaCl, 20 mM imidazole, 5% glycerol, 1mM phenylmethylsulfonyl fluoride (PMSF) and 1 mM Dithiothreitol (DTT), pH 7.5).

Resuspended cells were then mechanically perforated (Branson Sonic dismembrator) by sonicating at 50% amplitude, 20s pulses at 30s intervals for 10 cycles before centrifuging again at 40,000 g for 40 min (4°C) (Thermo Scientific TM Sorvall TM) to sediment cellular debris and to suspend proteins in the supernatant. The protein suspension was then filtered (0.22 µm) and applied to a 5ml prepacked Nickel Sepharose (Cytiva His-Trap^{TM} HP, Fisher Scientific) column which had been pre-equilibrated by lysis/resuspension buffer (4°C). The affinity column was then washed with 25 CV of wash buffer (50 mM Tris, 1 M NaCl, 25 mM imidazole, 5% glycerol and 1 mM DTT, pH 7.5) to detach nonspecific protein interactions. Following the wash procedure, elution buffer (50 mM Tris, 300 mM NaCl, 200 mM imidazole, 5% glycerol and 1 mM DTT, pH 7.5) was added to the column following a linear gradient while 1 mL aliquots were collected until fractions no longer produced a visible blue color when reacted with Bradford reagent.

Aliquots collected were then dialyzed into TEV buffer (50 mM Tris, 50 mM NaCl, 1 mM EDTA, 5% glycerol and 1 mM DTT, pH 7.5) for 2h at 4°C before the addition of TEV protease to proteolyze the GNSHT fusion tag (overnight at 4°C). Overnight cleavage was confirmed by analyzing a 10% SDS-PAGE gel of the sample before dialyzing cleaved protein into FPLC buffer (50mM Tris pH 7.4, 100 mM NaCl, 1mM DTT) for 2 hours (4°C).

Next, it is imperative to separate the GNSHT tag and TEV protease from OAS1 and this is done using SEC. Following dialysis, protein sample was loaded on to a pre-equilibrated HiLoad Superdex 200 (26/60, GE Healthcare) column to be separated based on hydrodynamic size The column was connected to an AKTA Purifier 10 system was housed within refrigerated conditions (4°C) and aliquots were collected using the same buffer that was used to equilibrate the SEC column. Fractions collected were then

analyzed for purity using spectrophotometer (A280 nm, extinction coefficient of OAS1 is 63360 mol^{-1} cm^{-1}) and Bradford assay before running on a SDS-PAGE gel. Protein was then dialyzed into storage buffer (50 mM Tris, 100 mM NaCl, 50% glycerol and 1 mM DTT, pH 7.4) for long term storage at -20°C. Standard curve for Bradford assay was determined using bovine serum albumin (BSA). Extinction coefficients were determined using ProtParam tool on ExPASy servers (Gasteiger et al., 2005)

2.3.3. EXPRESSION OF OAS2 IN MAMMALIAN CELLS

HEK293T cells were cultured in Dulbecco's Modified Eagle's Medium (DMEM) (Thermo-Fisher Scientific) supplemented with 10% fetal bovine serum (FBS). When the cells reached 80% confluency, they were transfected with recombinant FLAG-OAS2 pCDNA3 vector as described previously (Koul, Gemmill, et al., 2020). After 48 hours of growth at 37°C, the cells were harvested by using phosphate buffered saline (137 mM NaCl, 2.7 mM KCl, 8 mM Na_2HPO_4, and 2 mM KH_2PO_4) and centrifuged at 1000xg for 5 minutes (4°C).

2.3.4. PURIFICATION OF OAS2 IN MAMMALIAN CELLS

The following steps were carried out at 4°C. The pelleted cells were re-suspended in lysis buffer (50 mM Tris Base pH 7.4, 400 mM NaCl, 1% octylphenoxy

poly(ethyleneoxy) ethanol (IGEPAL), 1 mM DTT supplemented with 1X halt protease cocktail inhibitor (Thermo-Fisher Scientific). To release the contents of the cell, the lysate was sonicated at 35% amplitude for 6 pulses of 10 seconds (Branson Sonic dismembrator). The lysate was then centrifuged at 20,000g for 20 minutes to pellet cell debris and filtered through s 0.2 µm filter. The filtered lysate was then loaded onto a pre-equilibrated a 2 CV gravity column with anti-FLAG affinity resin (Genescript). The equilibration buffer was the lysis buffer with 0.1% IGEPAL as any higher concentration would disrupt the affinity function of the resin. The resin was then washed twice with at least 15 CVs of wash buffer-1 (50 mM Tris base pH 7.4, 400 mM NaCl, 0.1% IGPAL, 1 mM DTT) and 30 CVs of wash buffer-2 (50 mM Tris Base pH 7.4, 100 mM NaCl, 0.1% IGEPAL, 1 mM DTT). Following washing procedure, the resin was incubated in elution buffer (50 mM Tris base pH 7.4, 100 mM NaCl, 1 mM DTT, 10% Glycerol and 0.1 mg/mL FLAG peptide) for 15 minutes before collecting 1mL aliquots of eluent. The fractions were then assayed for purity by SDS-PAGE gel before dialyzing at 4°C overnight in storage buffer (50 mM Tris Base pH 7.4, 100 mM NaCl, 1 mM DTT, 10% glycerol) to remove any residual FLAG peptide. Finally, protein purity was checked by SDS-PAGE and protein concentration was determined by Bradford assay (standard curve produced using BSA) and spectroscopic measurement at 280nm (extinction coefficient of OAS2 is 129830 mol^{-1} cm^{-1}). Extinction coefficients were determined using ProtParam tool on ExPASy servers (Gasteiger et al., 2005)

2.3.5 EXPRESSION OF RNASE L IN BACTERIA

Sus scrofa RNase L pGEX-2T-GST was inserted into *E. coli* BL21(DE_3) cells via heat shock transformation described previously (Green & Sambrook, 2021). Starter cultures were then prepared by inoculating a small volume of LB (Sigma-Aldrich) with the transformed bacteria. This starter culture was then used to inoculate 1 to 2 liters of LB medium for large scale protein production. To ensure selective pressure is maintained, all media were treated with 100ug/µl of Ampicillin. The large-scale cultures were then induced with final concentration of 1 mM IPTG at A280 (OD 0.6) and grown overnight at 20°C.

2.3.6 PURIFICATION OF RNASE L

Overnight bacterial culture was sedimented by centrifuging (Thermo Scientific TM Sorvall TM) at 5,000g for 15 min (4 °C) and the resulting pellet was resuspended using cold lysis buffer (30 mM HEPES, 500 mM NaCl, 5 mM ethylenediaminetetraacetic acid (EDTA), 2 mM PMSF and 2 mM DTT, pH 7.5). Resuspended cells were then mechanically perforated by sonication (Branson Sonic dismembrator) (50% amplitude, 20s pulses at 45s intervals for 12 cycles) before centrifuging again (30,000 g for 30 minus at 4°C) (Thermo Scientific TM Sorvall TM) to sediment cellular debris and to suspend proteins in the supernatant. The protein suspension was then filtered (0.22 µm) and applied to a 2ml column filled with anti-GST affinity resin (Fisher Scientific) which has been pre-

equilibrated by lysis buffer (4°C). The affinity column was then washed with 30 CV wash buffer (30 mM HEPES, 50 mM NaCl, 0.5 mM EDTA, 2 mM PMSF and 2 mM DTT, pH 7.5) to detach nonspecific protein interactions. Following the wash procedure, 10 CV of elution buffer (30 mM HEPES, 50 mM NaCl, 0.5 mM EDTA, 2 mM PMSF, 2 mM DTT, and 10 mM glutathione pH 7.5) was added to the column while 1 ml aliquots were collected until fractions no longer produced blue color when reacted with Bradford reagent. Protein concentration was determined by Bradford assay (standard curve produced using BSA) and measuring absorbance at 280nm (extinction coefficient of RNase L is 77810 mol^{-1} cm^{-1}). Extinction coefficients were determined using ProtParam tool on ExPASy servers (Gasteiger et al., 2005)

2.4 *IN VITRO* TRANSCRIPTION AND PURIFICATION OF RNA

To enzymatically activate OAS enzymes, dsRNA of sufficient length are necessary. To this end, I transcribed WNV 5'TR and JEV 3'TR *in vitro* for initial testing a following previously published protocol for *in vitro* transcription (Booy, Meng, & McKenna, 2013). T7 RNA polymerase directed *in vitro* transcription was carried from linearized plasmid DNA templates as described previously (McKenna et al., 2007). Following large scale transcriptions, the RNA truncations were loaded onto a Superdex 200 26/60 SEC column (GE Healthcare) pre-equilibrated with buffer (50 mM Tris, 100 mM NaCl, pH 7.0). The SEC eluents were then tested for purity by performing denaturing TBE (Tris-Borate-EDTA)-PAGE where samples were mixed with 2X denaturing loading buffer (95% deionized formamide, 0.5 mM EDTA, 0.025% Xylene Cyanol, 0.025% Bromophenol Blue,

0.025% SDS) and heated to 95°C for 5 minutes prior to gel loading. The gel was run in 1X TBE buffer (89 mM Tris Base, 89 mM Boric acid, 2 mM EDTA, pH 8.0) and visualized by staining with toluidine blue solution (0.1% toluidine blue, 1% glacial acetic acid). Finally, the concentration of RNA was determined by obtaining their absorbance at 260 nm and using extinction coefficients for the RNA obtained using predicted values from IDT online tool Oligo Analyzer 3.1. The extinction coefficient used for WNV 5'-TR is 166000 mol^{-1} cm^{-1} and JEV 3'-TR is 1247500 mol^{-1} cm^{-1}. The purified RNA were stored in -20°C for long term storage.

2.5 *IN-VITRO* FUNCTIONAL ASSAYS

2.5.1 OAS COLORIMETRIC ACTIVITY ASSAY

The assay for measuring OAS activity was carried out according to established method described previously (Meng *et. al.* 2012). The assay consisted of OAS1 (400 nM) in FPLC buffer (see above), dsRNA TR of various *flaviviruses* (300 nM) and activation buffer (20 mM Tris, 5mM MgCl2, 1 mM DTT and 2 mM ATP) in a reaction volume of 100 µl. The mixture was then incubated at 37°C for 30 min to an hour. A 20µl aliquot was then taken for pyrophosphate (PPi) assay and 10 µl aliquot was added to RNase L activity assay.

Prior to the PPi assay, the OAS activation mixture (20µl aliquot) was quenched using 50 mM EDTA. It was then mixed with 20 µL of molybdate reagent (2.5% ammonium molybdate in 2.5 M H_2SO_4), 20 µL β-mercaptoethanol (0.5M) and 8 µL of Eikonogen

reagent (0.125 g of 1-amino-2- naphthol-4-sulfonic acid, 0.125 g of sodium sulfite, and 7.325 g of sodium bisulfite to 100 mL of ddH_2O) in that order in a 96 well reading plate. Color formation was detected using Epoch plate reader (BioTek, VT, USA) at an absorbance of 580 nm. PPi formed is calculated by comparing with standard curve created using PPi standards as described previously (Meng et al., 2012). EDTA was not added to RNase L assay as it would inhibit the reaction.

2.5.2 OAS/RNASE L FLUORESCENCE ASSAY

2.5.2.1 RNASE L CONCENTRATION OPTIMIZATION FOR 'TWO POT ASSAY'

Initially, the endonuclease cleavage assay was performed as two separate reactions which were later combined to one reaction. OAS activation assay was performed as described in the previous section and its contents were mixed with RNase L activation assay such that 2-5A produced from the first reaction would be diluted ten-fold in the second reaction. The RNase L activity assay contained RNase L buffer (25 mM Tris pH 7.4, 100 mM KCl, 10 mM $MgCl_2$, 0.01% IGEPAL, and 50 µM Adenosine diphosphate (ADP)), various concentrations of RNase L ranging from 2-20 nM, and 200 nM ssRNA probe (Thakur et al., 2007). The ssRNA substrate (5'-UUA-UCA-AAU-UCU-UAU-UUG-CCC-CAU-UUUUUU-GGU-UUA-3'), labelled on the 5' and 3' termini with 6-FAM (6-Carboxyfluorescein) and black hole quencher, respectively (IDT Technologies). Immediately after the addition of 2-5A from OAS activation (last component to be added) the mixture was transferred to a qPCR system (Bio-Rad) in order to detect fluorescence. The qPCR was programmed to detect the 6-FAM fluorophore and run for 30 minutes at

37 °C while taking measurements at 10 second intervals (optimization results presented in the next chapter).

2.5.2.2 OAS1/RNASE L CONCENTRATION OPTIMIZATION FOR 'ONE POT ASSAY'

The reaction proceeded too quickly for us to discern initial rate as the 2-5A concentration was too high, even after tenfold dilution. Therefore, we proceeded to combine both reactions into one and carried out several iterations of the same reaction in order to capture the initial rate. In order to make both reactions happen simultaneously, all the components for the OAS activation assay and all the components for the RNase L assay were mixed into one tube except for ATP. The ATP was added last, just before measurements were collected because it was the limiting factor for the entire reaction. The cleavage of ssRNA probe was further confirmed by running it on a denaturing TBE gel according to the method described above (results discussed in the next chapter). The time interval data was exported from qPCR software and data points were plotted for visual representation. Poly I:C was used as positive control and negative controls were mixtures with various key components missing such as omission of ATP, dsRNA or OAS enzyme. We decided to keep OAS1 concentration the same as the colorimetric assay in order to compare the results of the two assays.

2.5.2.3 TEMPERATURE OPTIMIZATION FOR ‘ONE POT ASSAY’

Previously, the colorimetric assay was performed at 37°C in order to simulate *in-vivo* conditions. However, we wanted the reaction to proceed slow enough to discern the initial rate from the data. Therefore, we conducted a few assays at 27°C, 30°C and 37°C to find the optimum temperature. Once we found the optimum temperature (mentioned in the next chapter) we proceeded to do all other assays at that temperature.

2.5.2.4 SSRNA PROBE CONCENTRATION OPTIMIZATION FOR ‘ONE POT ASSAY’

In order to detect RNase L activity we used a 36 nucleotide ssRNA probe (IDT Technologies) that absorbs light at nm and emits light at nm. A range of probe concentrations tested before choosing the concentration based on the intensity of fluorescence and appearance of cleavage when run on a denaturing RNA gel. The fluorescence was measured on a StepOnePlus real- time PCR system (Thermo-Fisher Scientific, Ottawa, Canada) using the existing FAM spectral settings. Data was recorded at approximately 10 second intervals (shown in the following chapter).

2.6 REFERENCES

Booy, E. P., Meng, H., & McKenna, S. A. (2013). Native RNA purification by gel filtration chromatography *Recombinant and In Vitro RNA Synthesis* (pp. 69-81): Springer.

Costa, S., Almeida, A., Castro, A., & Domingues, L. (2014). Fusion tags for protein solubility, purification and immunogenicity in Escherichia coli: the novel Fh8 system. *Frontiers in microbiology, 5*, 63.

Daou, S., Talukdar, M., Tang, J., Dong, B., Banerjee, S., Li, Y., . . . Jha, B. K. (2020). A phenolic small molecule inhibitor of RNase L prevents cell death from ADAR1 deficiency. *Proceedings of the National Academy of Sciences, 117*(40), 24802-24812.

Gasteiger, E., Hoogland, C., Gattiker, A., Wilkins, M. R., Appel, R. D., & Bairoch, A. (2005). Protein identification and analysis tools on the ExPASy server. *The proteomics protocols handbook*, 571-607.

Green, M. R., & Sambrook, J. (2021). Cloning and transformation with plasmid vectors. *Cold Spring Harbor Protocols, 2021*(11), pdb. top101170.

Hammarström, M., Hellgren, N., van Den Berg, S., Berglund, H., & Härd, T. (2002). Rapid screening for improved solubility of small human proteins produced as fusion proteins in Escherichia coli. *Protein Science, 11*(2), 313-321.

Huth, J. R., Bewley, C. A., Clore, G. M., Gronenborn, A. M., Jackson, B. M., & Hinnebusch, A. G. (1997). Design of an expression system for detecting folded protein domains and mapping macromolecular interactions by NMR. *Protein science, 6*(11), 2359-2364.

Koul, A., Deo, S., Booy, E. P., Orriss, G. L., Genung, M., & McKenna, S. A. (2020). Impact of double-stranded RNA characteristics on the activation of human 2′–5′-oligoadenylate synthetase 2 (OAS2). *Biochemistry and Cell Biology, 98*(1), 70-82.

Koul, A., Gemmill, D., Lubna, N., Meier, M., Krahn, N., Booy, E. P., . . . McKenna, S. A. (2020). Structural and hydrodynamic characterization of dimeric human oligoadenylate synthetase 2. *Biophysical journal, 118*(11), 2726-2740.

McKenna, S. A., Kim, I., Puglisi, E. V., Lindhout, D. A., Aitken, C. E., Marshall, R. A., & Puglisi, J. D. (2007). Purification and characterization of transcribed RNAs using gel filtration chromatography. *Nature protocols, 2*(12), 3270-3277.

Meng, H., Deo, S., Xiong, S., Dzananovic, E., Donald, L. J., van Dijk, C. W., & McKenna, S. A. (2012). Regulation of the interferon-inducible 2'-5'-oligoadenylate synthetases by adenovirus VA(I) RNA. *J Mol Biol, 422*(5), 635-649. doi: 10.1016/j.jmb.2012.06.017

Putnins, R. F., & Yamada, E. W. (1975). Colorimetric determination of inorganic pyrophosphate by a manual or automated method. *Analytical Biochemistry, 68*(1), 185-195.

Thakur, C. S., Jha, B. K., Dong, B., Das Gupta, J., Silverman, K. M., Mao, H., . . . Gudkov, A. (2007). Small-molecule activators of RNase L with broad-spectrum antiviral activity. *Proceedings of the National Academy of Sciences, 104*(23), 9585-9590.

Waugh, D. S. (2005). Making the most of affinity tags. *Trends in biotechnology, 23*(6), 316-320.
Waugh, D. S. (2011). An overview of enzymatic reagents for the removal of affinity tags. *Protein expression and purification, 80*(2), 283-293.

3.1 RESULTS AND DISCUSSION

3.1.1 RATIONALE FOR ASSAY

There are several previously established cell-based methods to detect single stranded RNA (ssRNA) cleavage by RNase L (Ibsen et al., 2014; Johnston, Preble, Imai, Jacobsen, & Torrence, 1983; Kristiansen et al., 2010; Mullan et al., 2005; Revel et al., 1981; Tong, Zhang, Feng, & Tao, 1998; Uno et al., 1998). These methods usually involve inducing RNase L activation by treating the cells with interferon, followed by an analysis of whole cell RNA cleavage products. Although this approach is useful to better understand signaling processes in a cellular context, it does not enable the study of the *in vitro* mechanism of the OAS-RNase L pathway by specific RNA activators. To this end, cell-free assays begun to be developed that are much more helpful in understanding the *in vitro* features of this pathway (Anderson et al., 2011; Thakur, Xu, Wang, Novince, & Silverman, 2005). In these assays, RNase L activity is measured by cleavage of a fluorescent or radiolabelled substrate in the presence of synthesized 2-5A. Signal from the radiolabel can be detected via gel electrophoresis while fluorescence is detected by a fluorometer. The RNA cleavage products can also be visualized by gel electrophoresis as done with the cell-based systems. My objective was to establish a cell-free system which would give me unfettered access to observe both OAS and RNase L activity while having control over all other variables such as buffer conditions, substrate concentration, and enzyme concentration.

To activate RNase L, OAS must produce 2-5A chains that are at least three or four adenosines long. Without means to monitor exact length of 2-5A being produced, it is difficult to predict whether a specific dsRNA activates both OAS and RNase L at the same

time. To this end, I have set out to combine the activation of OAS and the activation of RNase L into a single experimental workflow where all components of the assay are able to be manipulated. While this approach seems straightforward, it requires the *in vitro* transcription/purification of segments of viral RNA genomes, expression purification of OAS isoforms, and expression/purification of RNase L. These components then need to be calibrated so that they can work in concert to effectively probe OAS and RNase L activity. From the assay, I was attempting to learn whether there was a difference in RNase L activation as a result of OAS1 activation via various RNA substrates. I wanted to answer questions such as how does different dsRNA substrates affect the activation of RNase L? Are there any instances where OAS1 produced 2-5A that are of insufficient length to activate RNase L? Following the optimization of the assays outlined below, I set out to answer these questions.

3.2 RESULTS

In this study, I sought to develop a relatively facile method to determine enzymatic ssRNA cleavage measured by relative fluorescence units (RFU). Outlined in this chapter are first, the purification of individual assay components, followed by the chronological steps taken to optimize several parameters of our assay.

3.2.1 PROTEIN PURIFICATION AND QUALITY CONTROL

3.2.1.2 OAS1 PURIFICATION AND QUALITY CONTROL

I expressed GNSHT-tagged OAS1 in *Escherichia coli* (*E.coli)* BL21 bacteria cells and purified protein using various chromatography methods as explained in depth in Chapter 2. Fractions were collected at every step of the purification process and run on an SDS-PAGE gel shown below (Fig 3.1 A). After cell lysis a significant amount of protein is observed in the lysate (Lysate lane). Lysate containing GNSHT-tagged OAS1 was loaded onto a nickel affinity column, with the flow through showing that most of the soluble protein was not His-tagged (Flow through lane). Extensive washing (20 column volumes) removed excess contaminants (Wash lane). Subsequent lanes show a series of 2 mL fractions collected during the elution from the nickel affinity column (Ni-NTA elution fractions 1-10). Two prominent bands were observed at 100 kDa and 70 kDa, .Based on molecular weight these bands likely correspond to the GNSHT-fusion protein and free GNSHT tag respectively (Fig 3.1A). The presence of free tag without protein before protease digest can be explained by nonspecific proteolytic cleavage by *E.coli* intrinsic proteases. A series of lower molecular weight species are also observed at very low concentration, including a negligible amount of OAS1 where the GNSHT tag has been cleaved by intrinsic proteases (~42 kDa). After near-complete digestion of the pooled Ni-NTA elution fractions using our in-house purified Tobacco Etch Virus (TEV) protease (TEV digest lane), the dominant bands observed are the cleaved GNSHT affinity tag (~70 kDa) and OAS1 (~42 kDa). To remove contaminants from OAS1 including the cleaved GNSHT size-exclusion chromatography was performed (Fig. 3.1B). Fig 3.1B shows the chromatograph collected from SEC where the blue line represents absorbance at 280 nm and the red line represents absorbance at 260nm. Monitoring both wavelengths and observing the 280/260 ratio ensures that purified proteins are not RNA bound, a common

problem in the purification of RNA-binding proteins like OAS1. Since larger sized species have lower retention volumes, the contents of the eluents can be roughly determined by observing the order of peaks and confirmed by SDS-PAGE.

The first peak eluting at approximately 120 ml is consistent with high molecular weight material at the void volume of the column (Fig 3.1B). The 280/260 ratio also shows the clear presence of nucleic acid. Therefore, this peak is likely protein bound to *E.* coli RNA and was not investigated further. The second peak at approximately 155mL corresponds to the undigested fusion protein. The third peak at approximately 170 ml corresponds to the GNSHT tag while the last peak at around 230 ml corresponds to the OAS1 protein. The OAS1 peak has a 280/260 ratio consistent with pure protein and indicates that the protein was unbound to RNA. To determine the purity of OAS1 obtained from SEC, aliquots of the fractions were run on an SDS-PAGE gel (Fig 3.1A). The amount of purified OAS1 from SEC is significantly less than expected from the Ni-NTA elution and suggests loss occurred through various factors, such as aggregation of protein and uncleaved GNSHT-fusion protein.

To verify if OAS1 was enzymatically active, I carried out our previously established colorimetric assay to detect pyrophosphate production as a result of 2-5A catalysis (Fig 3.1C). Fig 3.1C shows time course plots of pyrophosphate (ppi). These are produced as a result of OAS1 and OAS2 activation using poly I:C. 2µg/ml of poly I:C is mixed with 300 mM of OAS1 or OAS2 and incubated at 37°C for an hour. Every 10 minutes, 20µl aliquots of quenched OAS activity assay was taken and mixed with colorimetric assay reagents (details in Chapter 2). The presence of ppi produces a vivid blue color and its concentration is determined by measuring absorbance at 580nm using colorimeter.

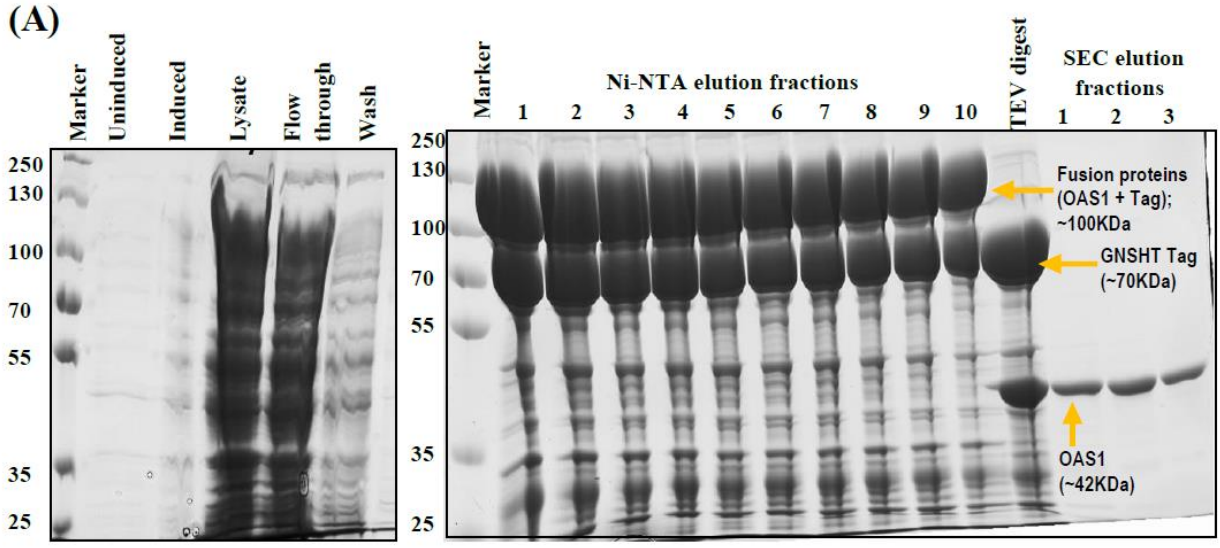
(A)
Marker
Uninduced
Induced
Lysate
Flow through
Wash
250
130
100
70
55
35
25
Marker
Ni-NTA elution fractions
1 2 3 4 5 6 7 8 9 10
TEV digest
SEC elution fractions
1 2 3
Fusion proteins (OAS1 + Tag); ~100KDa
GNSHT Tag (~70KDa)
OAS1 (~42KDa)

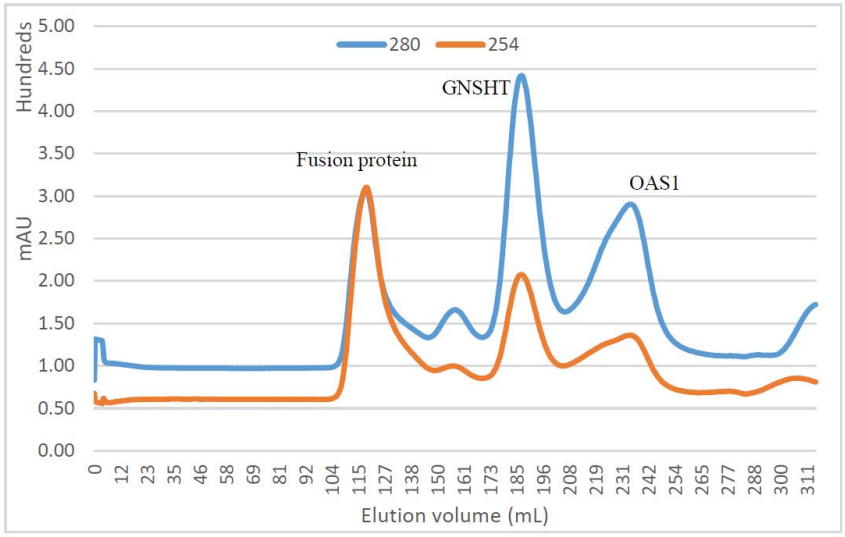
(B)
Hundreds
mAU
280
254
GNSHT
Fusion protein
OAS1
Elution volume (mL)

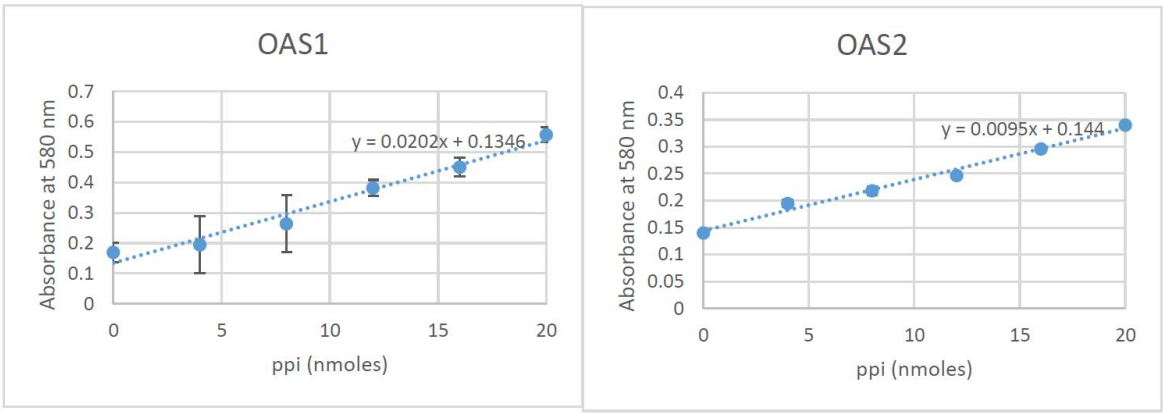
(C)
OAS1
Absorbance at 580 nm
y = 0.0202x + 0.1346
ppi (nmoles)
OAS2
Absorbance at 580 nm
y = 0.0095x + 0.144
ppi (nmoles)

Figure 3.1. Purification of recombinant human oligoadenylate synthetase 1 (OAS1).

(A). Denaturing SDS-PAGE (10%) analysis of human OAS1 purification from *E.coli* BL21 cells. Lanes (left to right) molecular weight marker, uninduced cell lysate, cell lysate after induction with 1 mM IPTG, overnight cell lysate, lysate flow through the nickel affinity column, nickel column wash, elution fractions from nickel affinity column, fusion protein digestion by TEV protease and pure OAS1 fractions from size exclusion chromatography. (B). Elution profile of OAS1 from SEC showing protein purity. A_{260} (red line) and A_{280} (blue line). (C) OAS1 and OAS2 pyrophosphate assay results. 300 nM OAS proteins were incubated with 20µg/ml poly I:C at 37°C for 1 hour. Aliquots were taken every 15 minutes and absorbance at A_{580} is measured (aliquots were quenched with EDTA before performing molybdate/pyrophosphate assay). Pyrophosphate concentration was determined using standard curve generated using known concentrations of sodium pyrophosphate.

In figure 3.1C, it is apparent that there is a linear relationship between ppi produced and time. Error bars represent linear regression analysis from assay performed in triplicate.

3.2.1.3 OAS2 PURIFICATION AND ACTIVATION

Given the different substrate specificities of OAS2 relative to OAS1 the original goal was to optimize the RNase L assay for both OAS isoforms. Therefore, I purified OAS2 in human cells according to the experimental approach outlined in Chapter 2. After

each step in the multi-step purification a small aliquot was saved for analysis. Figure 3.2A shows the SDS-PAGE gel data of fractions collected during OAS2 purification. The ‘untransfected’ lane represents lysate before transfection and ‘transfected’ represents lysate after overnight induction. At approximately 70 kDa, which is the approximate size of OAS2 monomer, I observed a slight increase in band intensity comparing untransfected to transfected lanes. The lysate lane, which has been passed through the Flag-affinity column, shows a slight reduction of bands at around 70 kDa. The subsequent lanes (wash lane and elution lanes from 1 through 6) show the sample after 20 column volumes of wash and elution fractions with pure OAS2. Fig. 3.2C shows western blot analysis using anti-FLAG antibody in order to verify whether the protein purified is indeed OAS2. Fig. 3.2B demonstrates a time course assay of ppi produced at five minutes time intervals in response to poly I:C that shows the OAS2 purified is catalytically active. Error bars represent linear regression analysis from assay performed in triplicate.

Although we planned to use OAS2 in our analysis, due to time constraints we were only able to carry out assay optimization using OAS1. Therefore, only its purification and activation via the colorimetric assay will be discussed in this chapter.

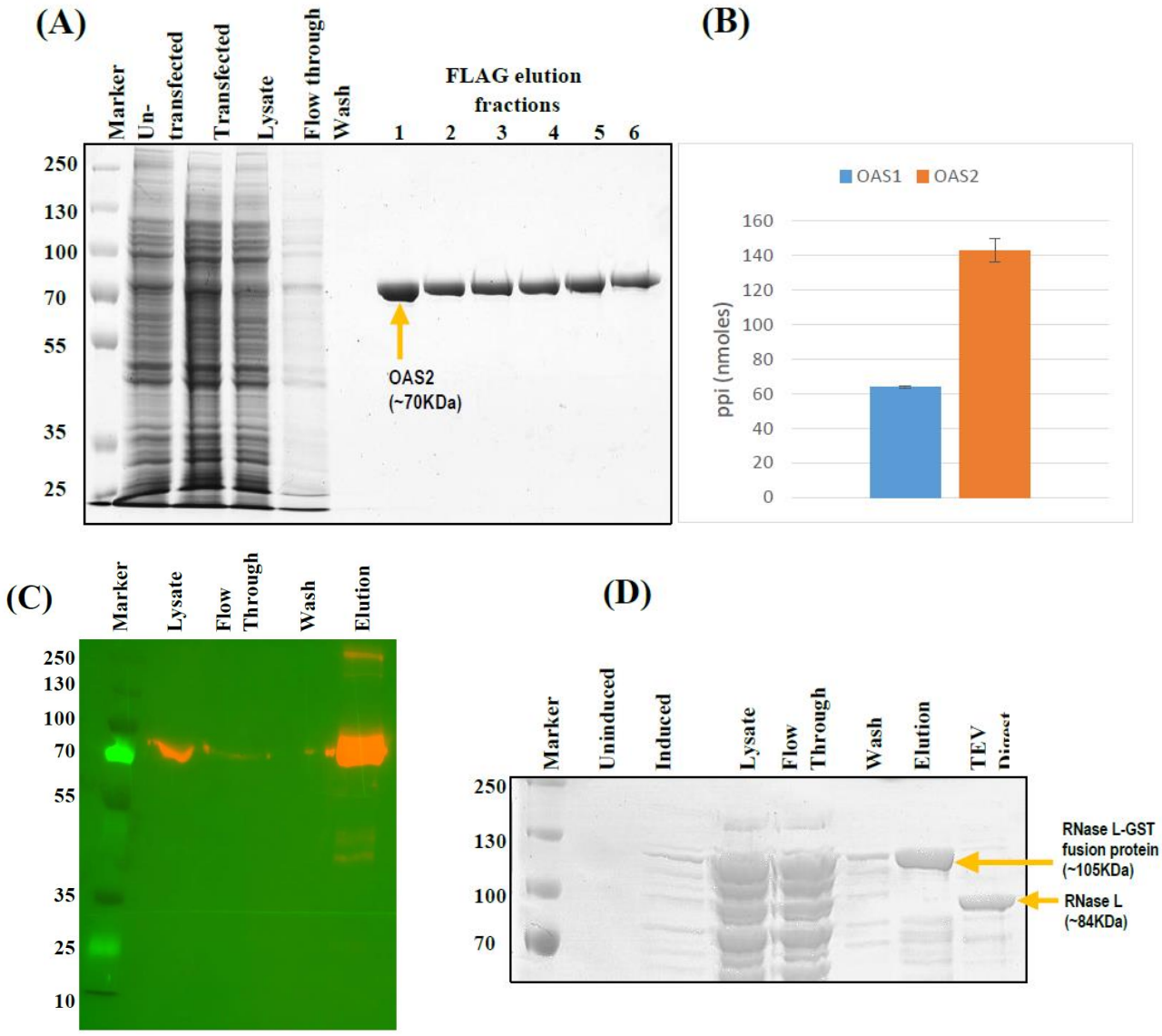

Figure 3.2. OAS2 and RNase L purification

(A). Denaturing SDS-PAGE (10%) analysis of human OAS2 purification from HEK293T cells. Lanes (left to right) molecular weight marker, untransfected cell lysate, cell lysate after transfection with PEG, overnight cell lysate, lysate flow through the FLAG affinity column, FLAG column wash, elution fractions from FLAG affinity column. (B). Catalytic activity of OAS1 and OAS2 protein (300 nM) incubated with poly I:C (20 µg/mL) in

buffered solution with ATP and MgCl2 at 37°C. Reactions were quenched with 1/10th volume EDTA after 1 hour. (C) Western blot analysis of OAS2. Equal volume of sample was loaded on 10% SDS-PAGE gel and run for 30 min at 100V. Protein was transferred to blotting membrane incubated with Anti-FLAG antibody and imaged at 428 nm. (D). Denaturing SDS-PAGE (10%) analysis of porcine RNase L purification from E.coli BL21 cells. Lanes (left to right) molecular weight marker, uninduced cell lysate, cell lysate after induction with 1 mM IPTG, overnight cell lysate, lysate flow through the GST affinity column, GST column wash, elution fractions from GST affinity column and fusion protein digestion by TEV protease.

3.2.1.4 RNASE L PURIFICATION AND ACTIVATION

I expressed RNase L in *E.coli* BL21 cells and purified using GST affinity chromatography. At every step of the purification process fractions were collected and loaded onto an SDS-PAGE gel as shown in Fig. 3.2D. The expressed RNase L-GST fusion protein migrates at 105 kDa and can be observed in the cell lysate lane (after sonication) and in the column flow through to a lesser extent. After several column volumes of washing, only background protein is observed. After washing, the fusion protein was eluted from the affinity column. GST was subsequently removed from RNase L using the TEV protease. The cleaved RNase L (84 kDa) (Fig. 3.2D) was run on GST and His affinity columns after protease digestion in order to remove residual GST tag and TEV protease, respectively. The final elution product is of sufficient purity for the purpose of the assay to be developed. To verify whether the purified RNase L was active, I carried

out an activation assay detailed later in this chapter. It must be noted that I was unable to get high yields of RNase L (approximately 5 µM/ml concentration of 2.5ml total volume). However, experiments to increase protein yield were not carried out due to the fact that the concentration obtained was enough for the preliminary assay optimization.

3.2.2 WNV 5'-TR AND JEV 3'-TR RNA PURIFICATION

It has been previously established that both 5'-terminal regions (5'-TR; nucleotides 1 to 146) and 3'-terminal regions (3'-TR; nucleotides -1 to -111) of WNV are potent activators of OAS1 (Deo et al., 2015). Therefore, I decided to use one of the WNV terminal regions (5'-TR) to benchmark our assay and compare it to our novel 'one-pot' assay. Previous studies have also suggested that OAS1 is activated by various *Flaviviral* terminal regions that are rich in secondary structures. Therefore, in addition to WNV 5'-TR, I also included the 3'-TR (nucleotides 10758 to 10976) of JEV in our analysis which has not been established previously using the colorimetric assay or our 'one-pot' assay.

I *in-vitro* transcribed and purified WNV 5'-TR and JEV-3'-TR from *E.coli* DH5α using previously published methodology (Booy, Meng, & McKenna, 2013). Denaturing TBE-PAGE was performed on transcribed RNA fractions obtained from SEC to assess purity (Fig. 3.3A & C). Both RNAs are of similar length and, therefore, elute at similar volumes relative to the elution volume of linearized plasmid (Fig. 3.3B & D). Although we had access to more *Flaviviral* TRs, I decided not to include them in the analysis due to time constraints.

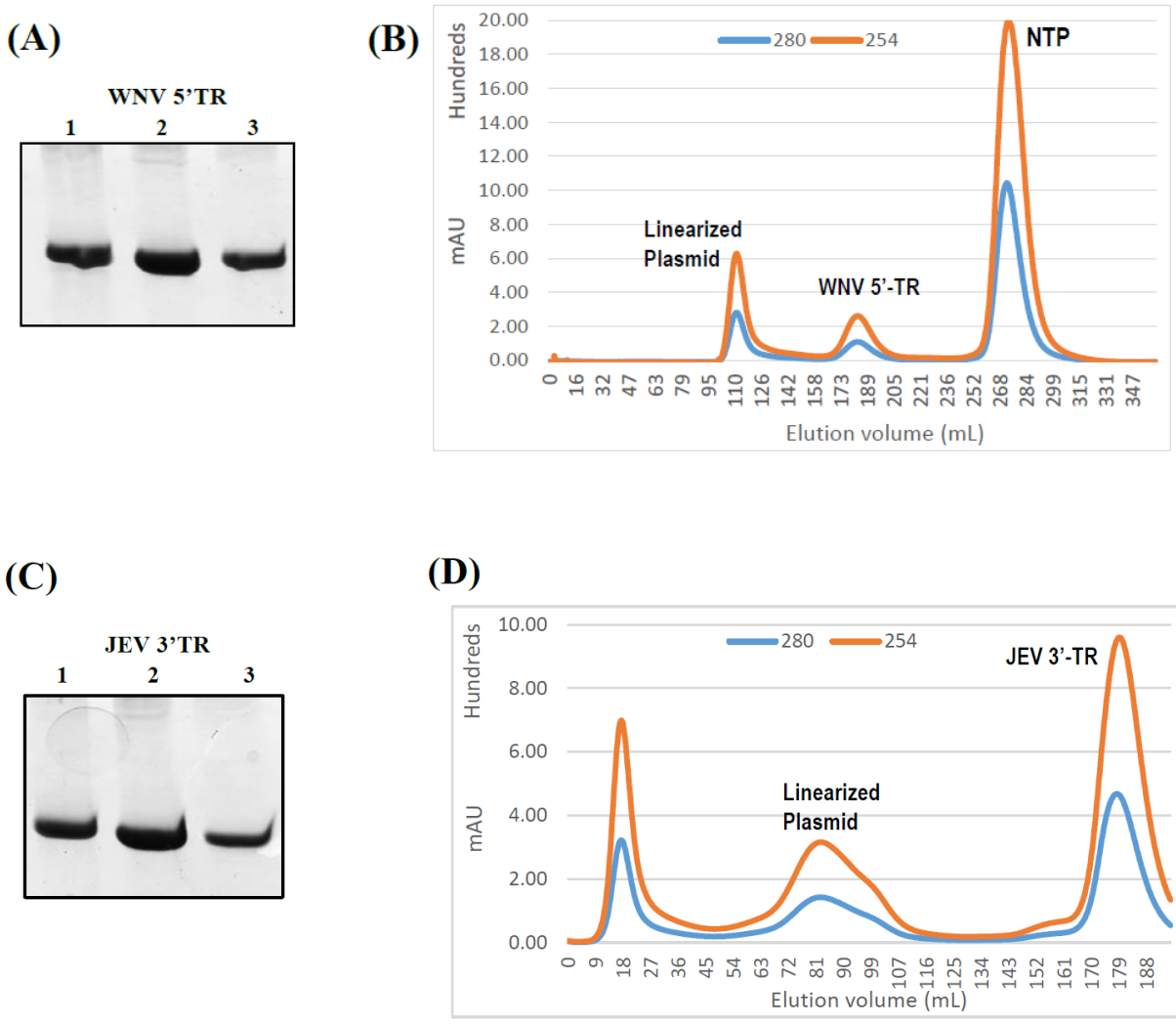

Figure 3.3. Purification *flaviviral* terminal regions.

(A) Denaturing TBE gel (10%) showing pure viral dsRNA fractions collected from SEC. 2 µg of sample was loaded onto a denaturing TBE gel and run for 30min at 120V before staining with toluidine blue stain. (B). Elution profile of WNV 5'-TR from SEC showing protein purity. A260 (red line) and A280 (blue line). (C). same as (A). (D). Elution profile of JEV 3'-TR from SEC showing protein purity. A260 (red line) and A280 (blue line).

3.2.3 'ONE POT' ASSAY COMBINING OAS AND RNASE L ACTIVITY ASSAYS

As mentioned in materials and methods chapter, the one pot assay involves mixing all components in one tube including enzymes (*i.e.* OAS1, RNase L), RNA activators (*i.e.* poly I:C, WNV 5'-TR and JEV-3'-TR), fluorescent RNA probes and reagents for activation. The ssRNA probe is attached to a 6-carboxyflurescein (6-FAM) on the 5'-end and black hole quencher 1 (BHQ1). 6-FAM is a fluorophore which absorbs light at 495nm and emits light at 517nm. When in proximity to BHQ1, 6-FAM cannot emit light. Only after RNA cleavage by RNase L, can the fluorophore diffuse away from the quencher to be able to emit light. The sequence of this ssRNA probe has been optimized to RNase L specific cleavage pattern and includes multiple cleavage sites.

The assay began as a sequential 'two pot' system involving an hour long *in-vitro* OAS1 activation by dsRNA, followed by *in-vitro* RNase L activation. The RNase L activation is carried out by adding a small volume (equal to 10% of RNase L assay volume) of the hour-long OAS1 activation mixture containing a large amount of 2-5A. The results of this method are shown in Fig 3.4. This initial method involved only activation by poly I:C (2µg/ml) and incubated with OAS1 at 37°C for an hour. A small amount of this activation mixture (equal to 10% of total volume of RNase L fluorescence assay) is added to RNase L mixture, and fluorescence is measured when ssRNA probe is released due to degradation. Due to the fact that poly I:C is a potent activator of OAS1, an extremely large amount of 2-5A is produced in the initial one hour incubation before RNase L activation. Therefore, even just a small amount of this 2-5A brings RNase L to saturation, which is the point at which enzyme reaction rate reaches the maximum point represented

by a plateau in the fluorescence graph, within the first 10 seconds. Fig. 3.4 shows the result of two pot assay with three different 2-5A dilutions, where ‘10x’ represents 10 times dilution, ‘100x’ represents 100 times dilution, and ‘1000x’ represents 1000 times dilution. The one hour OAS1 activation was diluted with OAS1 FPLC buffer (50 mM Tris pH 7.4, 100 mM NaCl, 1 mM DTT) before adding to RNase L assay. It is apparent that no dilution results in immediate saturation of RNase L as the initial initial phase is missing. The 10x dilution curve does show a linear phase followed by a plateau phase. However, the reaction had already started and the initial data from 0 RFU to approximately 20000 RFU was absent. Although the 100x dilution sample did show an initial linear phase, it resulted in a very slow reaction rate.

It was immediately apparent that our detection method was not fast enough to detect early data points in the reaction which are essential for any downstream quantitative kinetics measurements or comparisons. Additionally, a two pot assay did not allow for simultaneous activation of OAS1 and RNase L. After some iterations of the two pot assay it became clear that optimizing reaction components would be much easier with a single assay instead of two separate ones. I would also need to determine the timing of RNase L activation after OAS1 activation, such as whether it is instantaneous or if there is a delay. To this end I decided to combine all the components of both assays into a single assay and focus on its optimization. Ultimately the advantages outweighed the disadvantages.

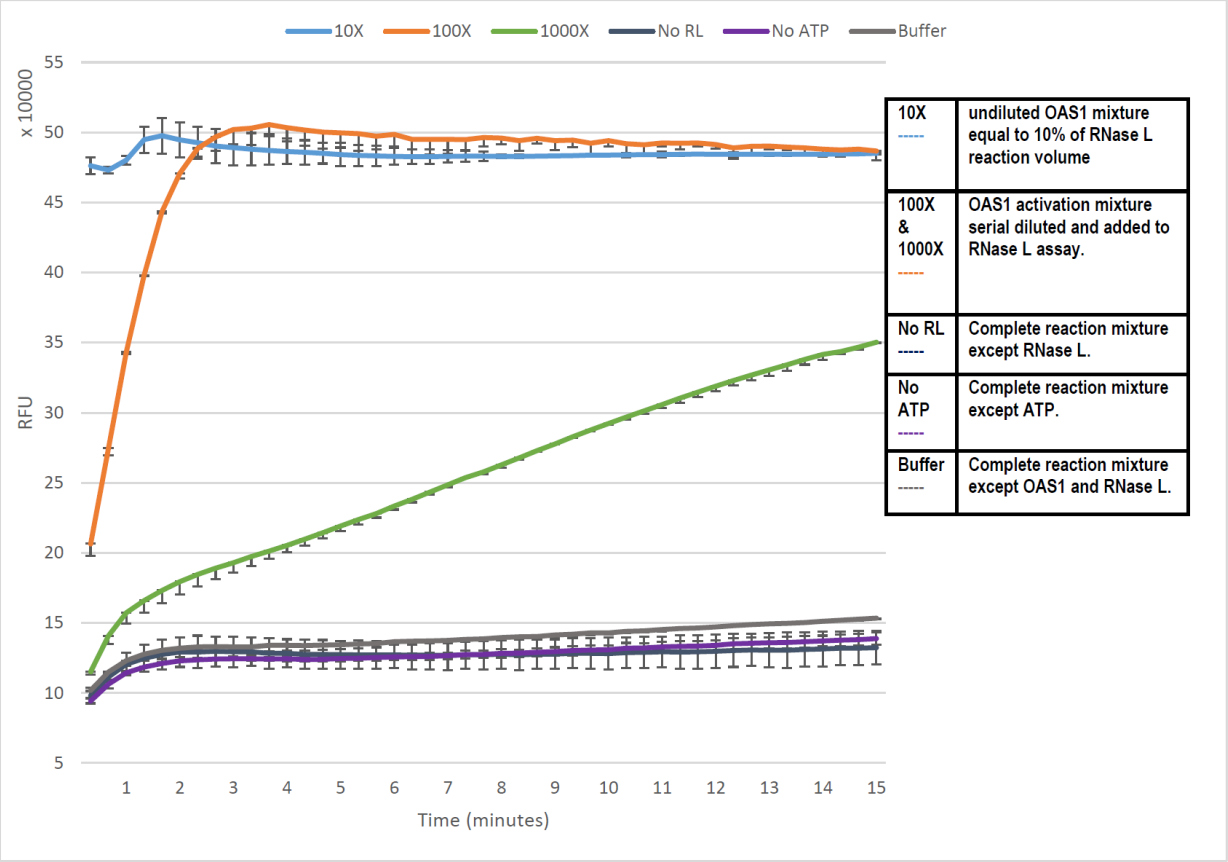

Figure 3.4. Two pot assay showing RNase L activity from different dilutions of OAS1 activation.

OAS1 (300 nM) was mixed with poly I:C (20 µg/mL) and incubated at 37°C water bath. Incubated OAS1 mixture (including activation components and 2-5A produced) was then added to RNase L assay (10% of RNase L reaction volume) according to the following proportions: 10X (undiluted OAS1 mixture equal to 10% of RNase L reaction volume), 100X (OAS1 mixture serial diluted and added to RNase L assay, making it 100X) and 1000X (OAS1 mixture serial diluted and added to RNase L assay, making it 1000X). OAS serial diluted using OAS elution buffer before adding to RNase L assay.

3.2.3.1 OPTIMIZATION OF NEGATIVE AND POSITIVE CONTROLS

As shown previously, the final purification of RNase L contains some contamination with a small concentration of nonspecific proteins (Fig. 3.2 D). I determined that it was not necessary to further purify this protein for multiple reasons. Firstly, it has been previously established that only a small amount (1.6 nM) of RNase L (Thakur et al., 2005) is necessary to achieve ssRNA cleavage. Therefore only a small amount of RNase L was necessary for my assay. Secondly, if the final sample contained any ribonuclease enzymes other than RNase L, proper positive and negative controls would rule out as many non-specific results as possible. Figure 3.5A shows a one pot FRET-based analysis of all the positive and negative controls that are used in all of our assays from here onwards. Our only positive control included poly I:C as a substrate for OAS1 activation (Putnins & Yamada, 1975). Poly I:C is a long, heterogenous dsRNA that is often used in cellular studies to examine the impact of dsRNA on cells and in *in vitro* studies for proteins that bind dsRNA. My negative controls had one or more components missing in order to rule out non-specific ssRNA cleavage as explained above. A detailed outline of all the controls is given in Fig 3.5. To determine if OAS1 and by proxy RNase L was not constitutively active, I omitted ATP in the sample named ‘no ATP’. Since OAS1 should not be able to activate without ATP, there should not be any 2-5A to activate RNase L, thus no ssRNA cleavage. This negative control also provides evidence of any other RNase contaminant in the assay. Next, I omitted RNase L enzyme from one of the negative controls named ‘no RL’, which is a failsafe in case the previous control failed as it helps me determine whether the contamination is coming from the OAS1 or RNase L

preparation. The third and final negative control contains no proteins and it is only the ssRNA probe with viral dsRNA activator in buffer. This control, named ‘only RNA’, is put in place to ensure that both the RNAs are intact (*i.e*. not degraded and in its native conformation) before the assay.

I expected to see no fluorescence signal from the negative controls. However, I observed that all negative controls emitted some level of background signal (Fig. 3.5A). This small amount of fluorescence from negative controls is negligible compared to positive controls and does not necessarily indicate RNA degradation. Presence of this small amount of fluorescence may originate from the components themselves. Nevertheless in the ultimate analysis, background signal would be subtracted from positive control and samples of interest. However, it must be noted that this background signal was not subtracted for the optimization experiments to visualize the consistency or the controls and the impact of specific reagent omission. Although fluorescence measurements initiated when the reaction had already reached approximately 30,000 RFU for the positive control, I decided to move on to other parameter optimizations. At this point poly I:C proved to be an acceptable positive control (Fig. 3.5A) as it is sufficiently distinguishable from the negative control.

Additionally, all the samples were run on a 10% denaturing RNA gel in order to determine ssRNA probe cleavage (Fig. 3.5B). This gel is not stained as the probe emits its own fluorescence that can be detected by our fluorimeter. However, it is apparent that the cleaved ssRNA probe in this gel is represented by the absence or diminishing fluorescence whereas the uncleaved probe emits fluorescence. It is unclear why there is

this dichotomy between the qPCR results and observation from the gel.

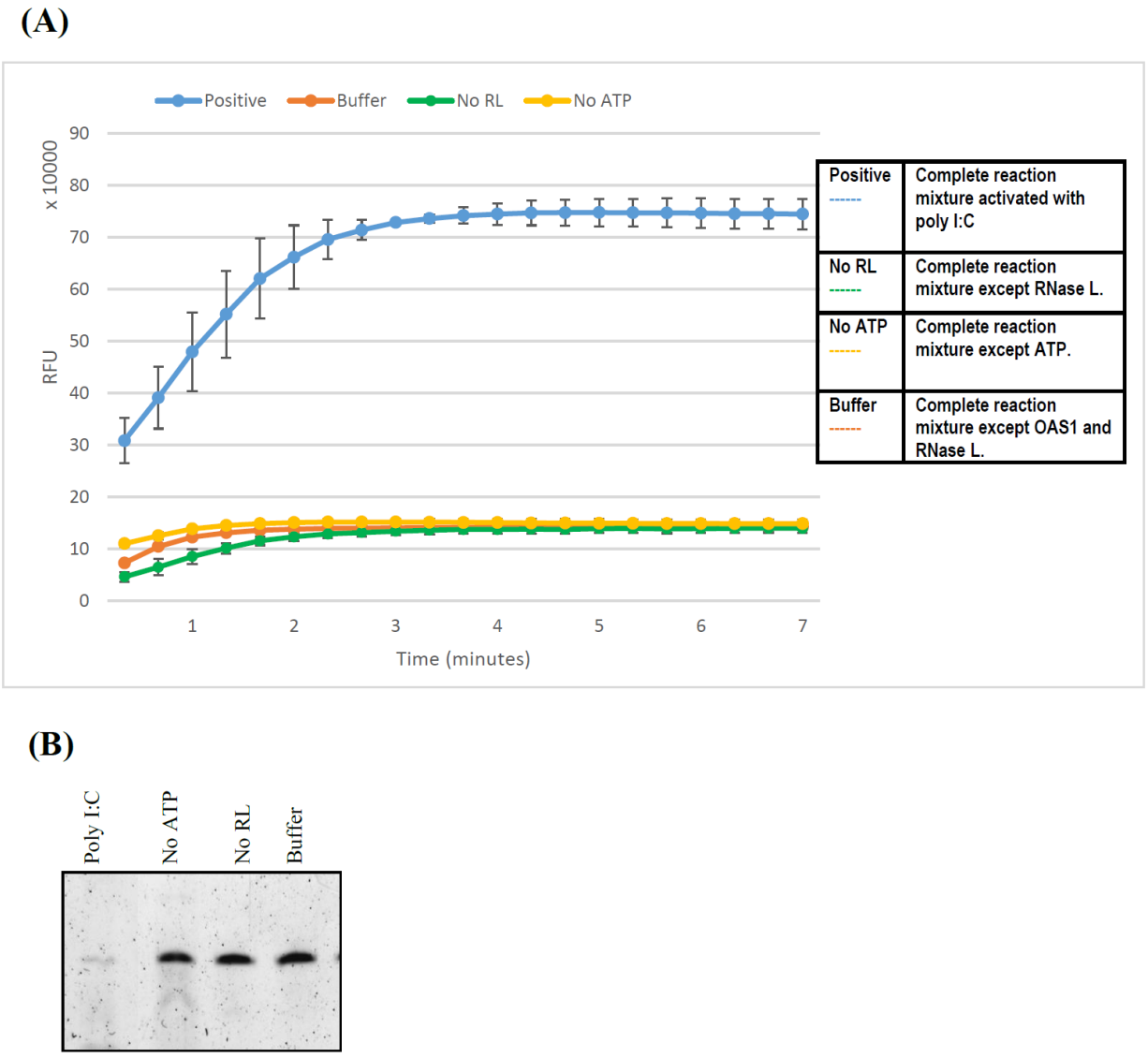

Figure 3.5. RNase L-OAS1 'one-pot' activity assay positive and negative control

(A). First 7 minutes of assay containing OAS1 (300nM) mixed with poly I:C (20 µg/mL), RNase L (20 nM), and ssRNA probe (100nM) as positive control and run in qPCR apparatus for 20 to 30 minutes at 35°C. Negative controls were as follows: reaction mixture with no RNase L (no RL), reaction mixture with no ATP (no ATP) and reaction

mixture with only buffer (FRET+Buffer) ie no proteins or viral RNA substrates. All assay samples conducted in RNase L activation buffer (Tris 25 mM pH 7.4, KCl 100 mM, MgCl2 10 mM, β-mercaptoethanol 10.5 mM, IGEPAL 0.015%, ADP 10 µM) and OAS1 activation buffer (NaCl 40 mM, 5% glycerol, 2 mM ATP). Error bars represent the standard deviation from two replicates of every assay.

(B). Denaturing TBE gel (10%) showing activation mixture collected immediately after assay completion (30 minutes). 15 µl of each sample was mixed with RNA denaturing dye (Materials and Methods) before heating up to 95°C for five minutes. The samples were then loaded onto a denaturing TBE gel and run for 30 minutes at 120V before imaging with our fluorescence imager at excitation λ 492 nm and emission λ 508 nm.

3.2.3.2 OPTIMIZATION OF ASSAY TEMPERATURE

Next, I wanted to determine the optimum temperature to run the assay. Although previous studies have carried out cell-free RNase L activation assays at various temperatures ranging from 21°C to 37°C, not all temperatures are suitable for OAS1 activation (typically performed at 37°C). Therefore, I needed to find a suitable temperature for both. Initially, I successfully carried out the assay at 37°C (positive and negative control optimization, Fig. 3.5A). However, the reaction proceeded too rapidly to be able to determine initial rates. From this point onwards, I decided to carry out optimization using WNV 5'-TR as an activator instead of only poly I:C. This is because, if all parameters were optimized based on a potent activator like poly I:C, the sensitivity of the assay may

be too low. This means that all the parameters will be primed to detect only the potent activator and not dsRNA with lower activity.

I was constrained by the limitations of our instrument, so I decided to lower the temperature in an effort to slow down and measure the initial reaction rate. Fig. 3.6A shows OAS1-RNase L activation at five different temperatures. At the lowest temperature (25°C) the reaction is extremely slow and difficult to distinguish from negative controls. At 27°C and 30°C the RFU measured is distinctly different from negative controls, but they are still not ideal. If the reaction progresses too slowly due to a low temperature, false negatives would be more frequent (*i.e*. dsRNA that produce lower OAS1 activity will be indistinguishable from negative controls).

I found that between 35°C and 37°C the reaction progressed at a reasonable pace while below 30°C the reaction proceeded too slowly. Therefore, any temperature between 35°C and 37°C would be reasonable I conducted all subsequent reactions at 37°C. Again these results are corroborated by the RNA denaturing gel (Fig 3.6B) where the top dark band gradually disappears as the temperature increases.

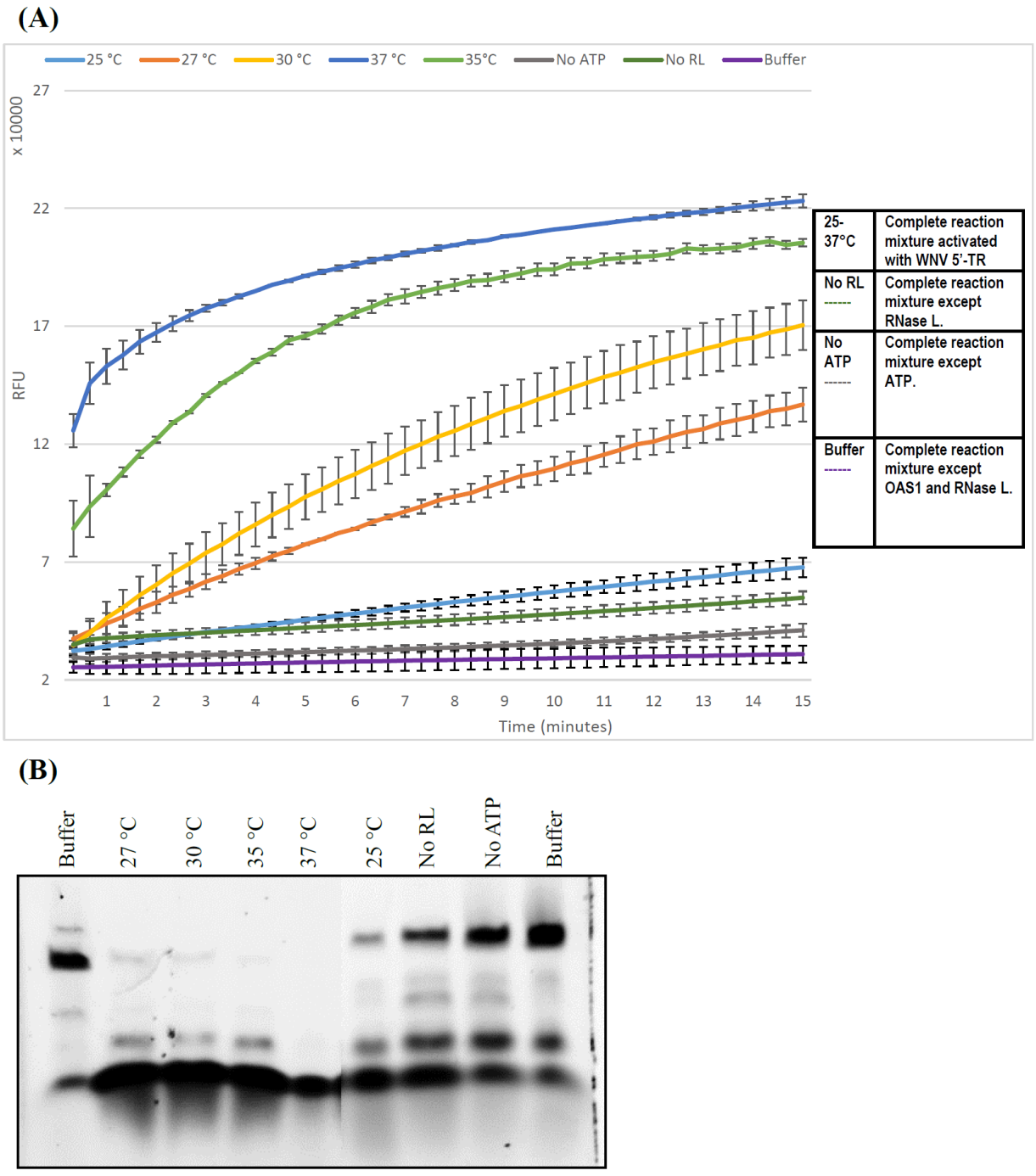

Figure 3.6. RNase L-OAS1 'one-pot' activity assay for temperature optimization

(A). Showing temperature and duration optimization. Assay containing OAS1 (300 nM) mixed with poly I:C (20 µg/mL), RNase L (20 nM), and ssRNA probe (100 nM) as positive

control and run in qPCR apparatus for 20 to 30 minutes at 35°C. Negative controls were as follows: reaction mixture with no RNase L (no RL), reaction mixture with no ATP (no ATP) and reaction mixture with no protein. All assay samples conducted in RNase L activation buffer (Tris 25 mM pH 7.4, KCl 100 mM, MgCl2 10 mM, β-mercaptoethanol 10.5 mM, IGEPAL 0.015%, ADP 10 µM) and OAS1 activation buffer (NaCl 40 mM, 5% glycerol, 2 mM ATP). Error bars represent the standard deviation from two replicates of every assay.

(B). Denaturing TBE gel (10%) showing activation mixture collected immediately after assay completion (30 minutes). 15 µl of each sample was mixed with RNA denaturing dye (Materials and Methods) before heating up to 95°C for 5 minutes. The samples were then loaded onto a denaturing TBE gel and run for 30 minutes at 120V before imaging with our fluorescence imager at excitation λ 492 nm and emission λ 508 nm.

3.2.3.3 OPTIMIZATION OF RNASE L CONCENTRATION

Once the controls, temperature, and duration were determined, I moved on to determine optimal concentrations of key components in the assay. As stated previously, I decided not to change the concentration of OAS1 activation components as these have been optimized by (Meng et al., 2012) . Instead, I focused on RNase L-specific reaction components. It is important to note that RNase L contained background impurities and, therefore the concentrations used are only an approximation -assuming all proteins detected are RNase L. I initially tested RNase L at picomolar concentrations in the reaction mixture but fluorescence results were very inconsistent even with identical

replicates (data not shown). This may be due to the fact that there is always a small amount of protein that adheres to the plastic tubes or pipette tips during reaction preparation. Therefore, I decided to test concentrations of purified RNase L ranging from 2 nM to 20 nM (Fig. 3.7). Fig. 3.7A presents the first five minutes of the one pot assay where the reaction for poly I:C (labelled as positive in green; 20 nM RNase L) proceeds much faster, whereas reactions with WNV 5'-TR (with varying RNase L concentrations) are clustered together. Since RFU that is too close to the negative controls is not ideal, I chose the highest RNase L concentration (20 nM). These findings are consistent with the denaturing RNA gel (Fig. 3.7B) showing diminished ssRNA probe cleavage with higher RNase L concentrations (top dark line lightest at 20 nM and poly I:C while darkest at 4 nM RNase L).

(A)

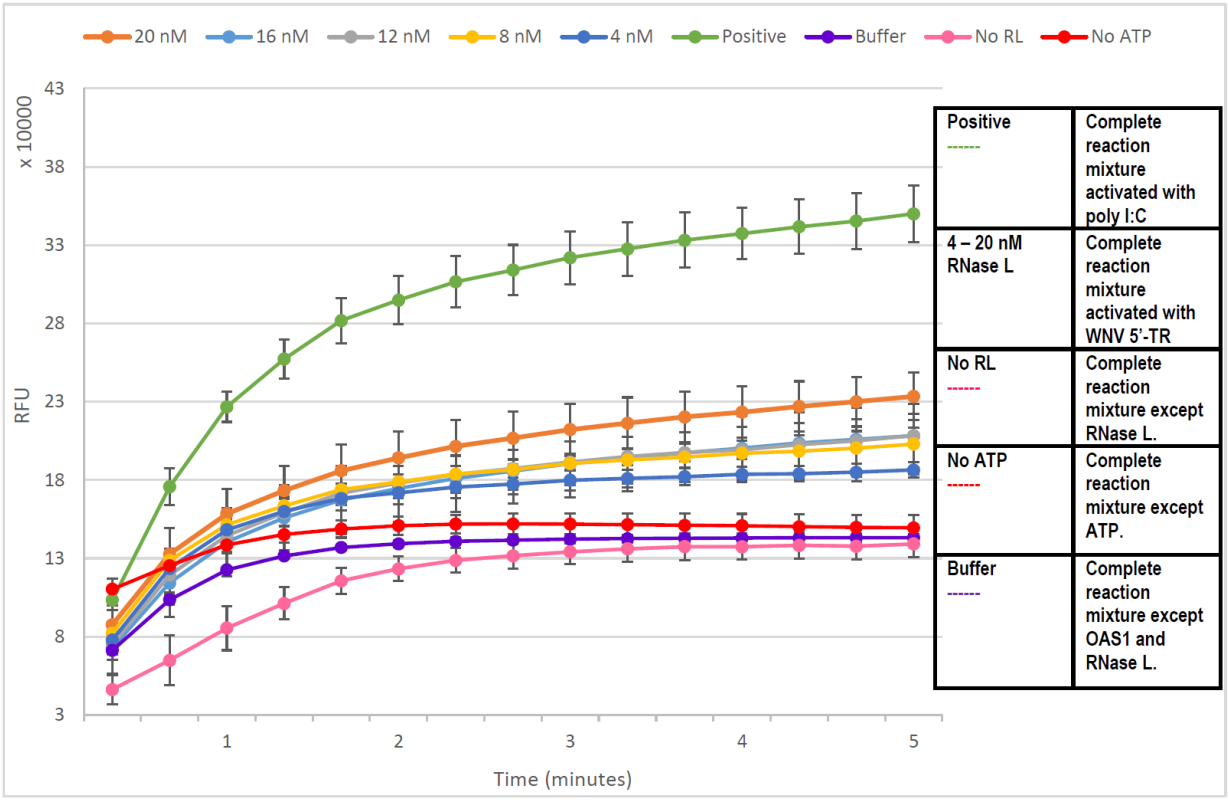
20 nM
16 nM
12 nM
8 nM
4 nM
Positive
Buffer
No RL
No ATP
x 10000
RFU
43
38
33
28
23
18
13
8
3
1
2
3
4
5
Time (minutes)
Positive ------ Complete reaction mixture activated with poly I:C
4 – 20 nM RNase L Complete reaction mixture activated with WNV 5'-TR
No RL ------ Complete reaction mixture except RNase L.
No ATP ------ Complete reaction mixture except ATP.
Buffer ------ Complete reaction mixture except OAS1 and RNase L.

(B)

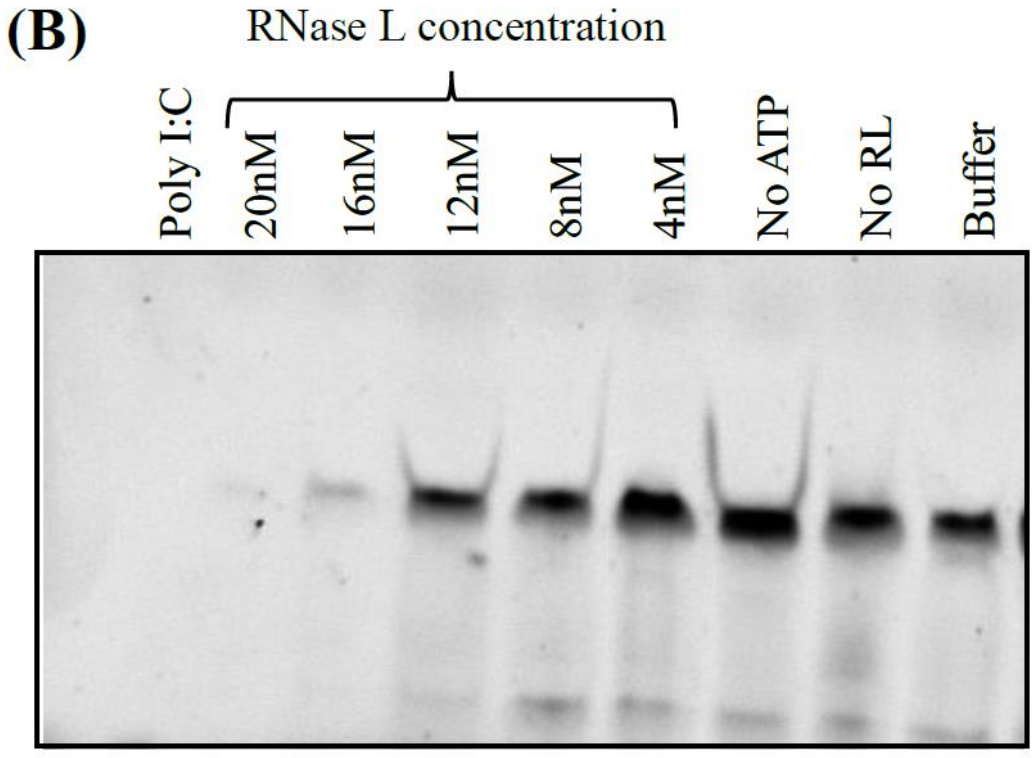
RNase L concentration
Poly I:C
20nM
16nM
12nM
8nM
4nM
No ATP
No RL
Buffer

Figure 3.7. RNase L-OAS1 'one-pot' activity assay for RNase L concentration optimization

(A). Assays containing OAS1 (300 nM) mixed with poly I:C (20 µg/mL) (positive control) or WNV 5'TR (300 nM), RNase L (20 nM), and ssRNA probe (100 nM) as positive control and run in qPCR apparatus for 20 to 30 minutes at 35°C. Negative controls were added as previously mentioned: reaction mixture with no RNase L (no RL), no ATP (no ATP) and only buffer (FRET+Buffer). All assay samples conducted in RNase L activation buffer and OAS1 activation buffer. RNase L concentrations were determined using WNV 5'-TR. Error bars represent the standard deviation from two replicates of every assay.

(B). Denaturing TBE gel (10%) showing assay mixture collected immediately after assay completion (30 minutes). 15 µl of each sample was mixed with RNA denaturing dye (Materials and Methods chapter) before heating up to 95°C for 5 minutes. The samples were then loaded onto a denaturing TBE gel and run for 30 minutes at 120V before imaging with our fluorescence imager at excitation λ 492 nm and emission λ 508 nm.

3.2.3.4 COMPARISON BETWEEN WNV 5'-TR AND JEV 3'-TR

Following optimization of key parameters, I examined two different *flaviviral* terminal regions using our 'one-pot' assay. I selected WNV 5'-TR as its ability to activate OAS1 has been well established (Deo et al., 2015). I also wanted to investigate another structured RNA in addition to WNV 5'-TR for several reasons. First, I wanted to observe if the 'one-pot' assay would be capable of detecting subtle variations (or if variations existed at all) in activation levels between our established WNV 5'-TR and other *flaviviral*

terminal regions. Although the binding affinity of WNV 5'-TR has been previously reported (Deo et al., 2015), I did not carry out such analysis for JEV 3'-TR. Nevertheless, the advantages of keeping both concentrations the same for our assay is that it would tell us how the OAS-RNase L pathway would react to the same viral loads but from different viruses.

It was not surprising that both terminal regions managed to activate RNase L in only 60 seconds and reached a reaction plateau within 280 seconds (Fig. 3.8A). However, what was more intriguing was what transpired within that first few minutes. In the first seven minutes, it is apparent that the FRET signal from WNV 5'-TR climbs faster than the signal from JEV 3'-TR. This observation could be explained by various factors. Computational analysis show that JEV 3'-TR contains one short 3'DB and one longer 3'SL structure (Mrozowich et al., 2022). This is in contrast to WNV 5'-TR which is made up of three short stem loop regions (Deo et al., 2015). Comparison of different lengths of dsRNA and their effect on OAS proteins show that longer RNAs are slightly better at activating OAS1 (Koul, Gemmill, et al., 2020). Therefore it is possible that the longer JEV 3'-TR activator was able to activate OAS1 with a higher RFU before the reaction plateaued (Fig. 3.8A orange line). However, characteristics of both dsRNA activator sequences tell a different story. As mentioned in chapter 1, cytosine rich sequences are able to activate OAS1 better and presence of stabilizing GC pairs in the immediate vicinity of the critical AUG region results in higher OAS1 activation (Schwartz et al., 2022). Comparison of both JEV 3'-TR and WNV 5'-TR sequences revealed that they have similar cytosine content. Moreover, WNV 5'-TR has more GC pairs flanking its AUG region than JEV 3'-TR with the latter having more destabilizing AU pairs flanking AUG than GC pairs.

This may explain why RFU increase was faster (represented by a steeper rise in the initial 7 minutes) for WNV 5'-TR but does not explain why overall RFU was lower than JEV 3'-TR. It has been reported previously that WNV 5'-TR has a low stimulatory potential to activate OAS1 (Koul, Deo, et al., 2020) which may explain why overall signal was lower than JEV. Further studies are necessary to fully explain my results.

(A)

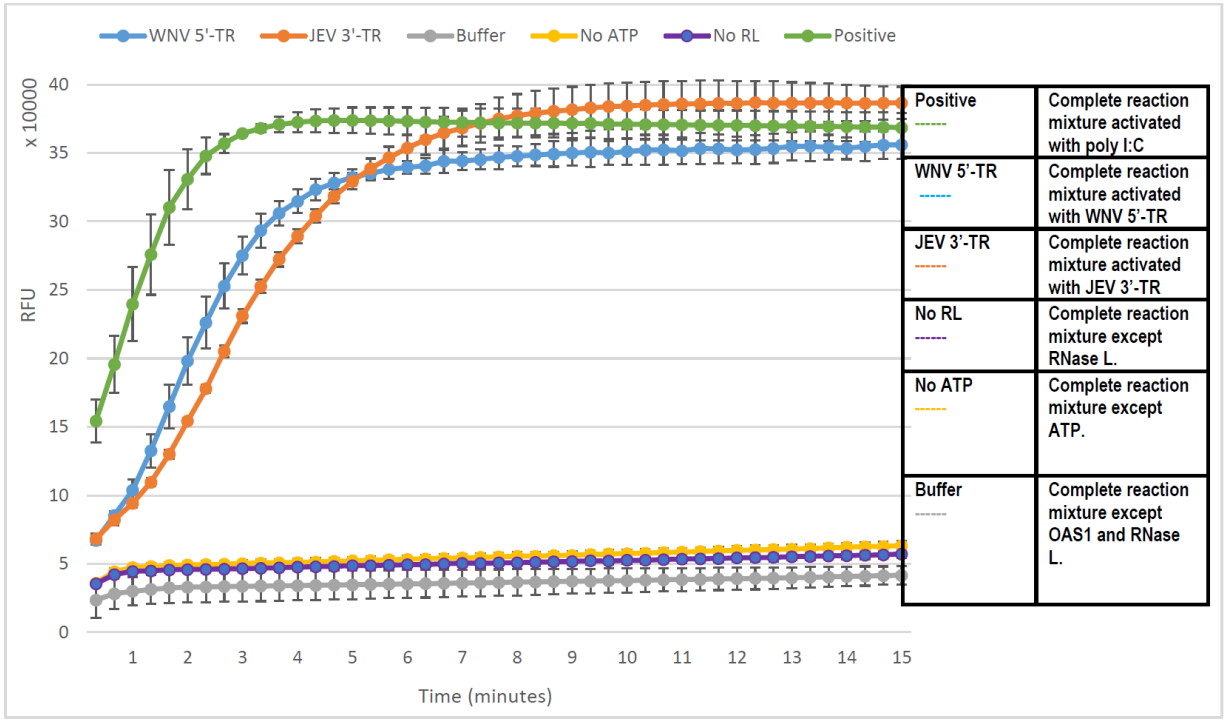

(B)

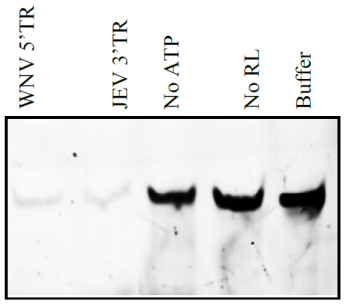

Figure 3.8. RNase L-OAS1 'one-pot' activity assay for WNV 5'-TR (orange lines) JEV 3'-TR (blue lines)

(A). Assays containing OAS1 (300 nM) mixed with poly I:C (20 µg/mL) (positive control) or, WNV 5'-TR (300 nM) or JEV (300 nM), RNase L (20 nM), and ssRNA probe (100 nM) as positive control and run in qPCR apparatus for 20 to 30 minutes at 35°C. Negative controls were added as previously mentioned: reaction mixture with no RNase L (no RL), no ATP (no ATP) and only buffer (FRET+Buffer). All assay samples conducted in RNase L activation buffer and OAS1 activation buffer. RNase L concentrations were determined using WNV 5'-TR. Error bars represent the standard deviation from two replicates of every assay.

(B). Denaturing TBE gel (10%) showing assay mixture collected immediately after assay completion (30 minutes). 15 µl of each sample was mixed with RNA denaturing dye (Materials and Methods) before heating up to 95°C for 5 minutes. The samples were then loaded onto a denaturing TBE gel and run for 30 minutes at 120V before imaging with our fluorescence imager at excitation λ 492 nm and emission λ 508 nm.

3.3 REFERENCES

Anderson, B. R., Muramatsu, H., Jha, B. K., Silverman, R. H., Weissman, D., & Karikó, K. (2011). Nucleoside modifications in RNA limit activation of 2′-5′-oligoadenylate synthetase and increase resistance to cleavage by RNase L. *Nucleic Acids Res, 39*(21), 9329-9338.

Booy, E. P., Meng, H., & McKenna, S. A. (2013). Native RNA purification by gel filtration chromatography *Recombinant and In Vitro RNA Synthesis* (pp. 69-81): Springer.

Deo, S., Patel, T. R., Chojnowski, G., Koul, A., Dzananovic, E., McEleney, K., . . . McKenna, S. A. (2015). Characterization of the termini of the West Nile virus genome and their interactions with the small isoform of the 2′ 5′-oligoadenylate synthetase family. *Journal of structural biology, 190*(2), 236-249.

Ibsen, M. S., Gad, H. H., Thavachelvam, K., Boesen, T., Desprès, P., & Hartmann, R. (2014). The 2′-5′-oligoadenylate synthetase 3 enzyme potently synthesizes the 2′-5′-oligoadenylates required for RNase L activation. *J Virol, 88*(24), 14222-14231.

Johnston, M. I., Preble, O. T., Imai, J., Jacobsen, H., & Torrence, P. F. (1983). A sensitive immunoenzymometric assay for 2',5'-oligoadenylate. Detection of elevated 2',5'-oligoadenylate synthetase in human peripheral mononuclear cells. *J Immunol Methods, 65*(1-2), 123-135.

Koul, A., Deo, S., Booy, E. P., Orriss, G. L., Genung, M., & McKenna, S. A. (2020). Impact of double-stranded RNA characteristics on the activation of human 2′–5′-oligoadenylate synthetase 2 (OAS2). *Biochemistry and Cell Biology, 98*(1), 70-82.

Koul, A., Gemmill, D., Lubna, N., Meier, M., Krahn, N., Booy, E. P., . . . McKenna, S. A. (2020). Structural and hydrodynamic characterization of dimeric human oligoadenylate synthetase 2. *Biophysical journal, 118*(11), 2726-2740.

Kristiansen, H., Scherer, C. A., McVean, M., Iadonato, S. P., Vends, S., Thavachelvam, K., . . . Weber, F. (2010). Extracellular 2′-5′ oligoadenylate synthetase stimulates RNase L-independent antiviral activity: a novel mechanism of virus-induced innate immunity. *J Virol, 84*(22), 11898-11904.

Meng, H., Deo, S., Xiong, S., Dzananovic, E., Donald, L. J., van Dijk, C. W., & McKenna, S. A. (2012). Regulation of the Interferon-Inducible 2′–5′-Oligoadenylate Synthetases by Adenovirus VAI RNA. *Journal of molecular biology, 422*(5), 635-649.

Mrozowich, T., Park, S. M., Waldl, M., Henrickson, A., Nelson, C. R., Demeler, B., . . . Patel, T. R. (2022). Cyclization studies of Japanese encephalitis virus non-coding RNA terminal regions. *bioRxiv*.

Mullan, P. B., Hosey, A. M., Buckley, N. E., Quinn, J. E., Kennedy, R. D., Johnston, P. G., & Harkin, D. P. (2005). The 2, 5 oligoadenylate synthetase/RNaseL pathway is a novel effector of BRCA1-and interferon-γ-mediated apoptosis. *Oncogene, 24*(35), 5492-5501.

Putnins, R. F., & Yamada, E. W. (1975). Colorimetric determination of inorganic pyrophosphate by a manual or automated method. *Analytical Biochemistry, 68*(1), 185-195.

Revel, M., Wallach, D., Merlin, G., Schattner, A., Schmidt, A., Wolf, D., . . . Kimchi, A. (1981). [20] Interferon-induced enzymes: Microassays and their applications; purification and assay of (2′-5′)-oligoadenylate synthetase and assay of 2′-phosphodiesterase *Methods Enzymol* (Vol. 79, pp. 149-161): Elsevier.

Schwartz, S. L., Dey, D., Tanquary, J., Bair, C. R., Lowen, A. C., & Conn, G. L. (2022). Role of helical structure and dynamics in oligoadenylate synthetase 1 (OAS1) mismatch tolerance and activation by short dsRNAs. *Proc Natl Acad Sci U S A, 119*(3). doi: 10.1073/pnas.2107111119

Thakur, C. S., Xu, Z., Wang, Z., Novince, Z., & Silverman, R. H. (2005). A convenient and sensitive fluorescence resonance energy transfer assay for RNase L and 2′, 5′ oligoadenylates *Interferon Methods and Protocols* (pp. 103-113): Springer.

Tong, W. B., Zhang, C. Y., Feng, B. F., & Tao, Q. M. (1998). Establishment of a nonradioactive assay for 2'-5' oligoadenylate synthetase and its application in chronic hepatitis C patients receiving interferon-alpha. *World J Gastroenterol, 4*(1), 70-73.

Uno, K., Sato, T., Takada, Y., Fujioka, K., Suginoshita, Y., Kakimi, K., . . . Kishida, T. (1998). A bioassay for serum interferon based on induction of 2'5'-oligoadenylate synthetase activity. *J Interferon Cytokine Res, 18*(12), 1011-1018. doi: 10.1089/jir.1998.18.1011

CHAPTER 4: SUMMARY AND FUTURE DIRECTIONS

4.1 OVERVIEW

In the introductory chapter I discussed the significance of OAS enzymes in the immune system and the network of pathways that depends on it. In the second chapter, I provided the detailed methodologies used throughout my research and the materials used to perform experiments. In the results and discussion chapter (Chapter 3), I demonstrated the outcome of various optimization trials of my assay as well as putting the assay into practice. In this final chapter, I will present a summary of my research findings and recommendations for future directions for the utilization of the 'one-pot' assay.

4.2 RESEARCH SUMMARY

In my thesis, I have presented an accessible method to study the kinetic behavior of OAS enzymes. Despite being implicated in various diseases such as cancer (Zhou, Molinaro, Malathi, & Silverman, 2005), autoimmune disorders (Choi et al., 2016) and even susceptibility to SARS-CoV2 (Bignon, Miclot, Terenzi, Barone, & Monari, 2022), little is known about the modus operandi of this polymerase. Therefore it is important to establish an enzymatic activity assay that addresses this issue. Previously, our lab has developed a colorimetric method to study the interaction between OAS enzymes and dsRNAs. Although this assay can be used to measure OAS activity, it is limited when it comes to sensitivity and quantitative analysis of 2-5A species produced. Most importantly the

colorimetric assay cannot ascertain if RNase L is activated as an outcome of OAS activation. Therefore, I have developed an assay that addresses these issues as well using a detection method that is relatively facile.

To standardize this assay, I started with optimizing several parameters such as temperature, protein concentration and type of controls. I first started with optimization of the positive and negative controls. I first chose poly I:C as the OAS activator as it is known to be the most potent substrate, however later on I changed it to WNV 5'-TR. I found that poly I:C activates OAS1 too quickly and it requires very low concentration to initiate reaction. Therefore if it were used to optimize all the parameters, the assay would be primed to detect substrates of high potency and not viral terminal regions with lower potency. Since WNV 5'-TR interaction with OAS1 is well established, I decided to use it as a positive control in later experiments. For the negative controls, it was important to determine that the RNA probe was not being cleaved by anything other than RNase L or that OAS1 was only activated by the substrate provided. To this end, I came up with three negative controls: 'No RL' which contains no RNase L to ensure ssRNA probe is only cleaved by one ribonuclease, 'No OAS' which ensures RNase L is not constitutively active, and lastly 'Buffer+RNA' contains no protein to show that nothing in the buffer performs cleavage of RNA probe. Surprisingly, despite having no mechanism available for RNA cleavage in the negative controls, they exhibited some background fluorescence. Nevertheless this fluorescence is negligible and simply has to be subtracted from the final result.

The next parameter involves the temperature and time interval for detection. Although, the colorimetric assay is performed at 37°C, the fluorescence-based assay

proceeds far too quickly at that temperature. Therefore, I tested several temperatures ranging from 25°C to 37°C with the intention to pick a temperature at which the assay was neither too fast nor too slow. The temperatures below 30 °C produced fluorescence that was far too close to the baseline fluorescence of the negative control. Therefore 35 °C was chosen as the optimum temperature. Next, I focused on the time interval between fluorescence detection and total run time of the assay. Since I was only interested in the initial rate of this assay I found that most reactions reached the plateau point within 15 to 30 minutes. The qPCR instrumentation used is capable of taking measurements every 20 seconds and therefore there is a limit to the amount of data points possible for my analysis.

The final parameter left to optimize was the RNase L concentration. Although RNase L has been reported to demonstrate activity at as low a concentration as 0.3 nM, apparently at a concentration below 1 nM RNase L enters a 1 minute lag phase (Carroll et al., 1997). Most studies have used 1.6 nM to 10 nM concentrations (Anderson et al., 2011; Daou et al., 2020), however our initial reaction at these concentrations resulted in the fluorescence being too close to the background signal. Therefore, I decided to test concentrations from 2 nM to 20 nM. I found that at 20 nM RNase L concentration, the reaction ramped up enough to be far away from the background signals of the negative controls but slow enough to determine initial velocity. After all parameters were optimized, I proceeded to test WNV 5'-TR against JEV 3'-TR where WNV worked as a positive control and a comparison partner to JEV.

4.3 FUTURE DIRECTIONS

In my thesis, I presented an experimental approach to study the OAS1-RNase L pathway in the presence of various dsRNA activators. This method not only helps us better understand OAS response to various infectious agents but also cross examine previous findings in the context on RNase L activation. This assay gives us the opportunity to study OAS1 without the complication of numerous other reactions in a living cell. It is also relatively cost-effective compared to existing *in vivo* assays. However the biggest advantage of this assay is our ability to control numerous variables and observe the outcomes of these changes on OAS.

Although there are many possibilities with this assay, below are a few of my recommendations for further research;

1. With the established protocol, testing various other *flaviviral* TRs would be the most promising next direction. Our lab possesses several plasmids for transcribing 5' and 3' TR RNAs from other *flaviviruses* such as MVEV (Murray Valley encephalitis virus), Zika and PoWV (Powassan virus). This can be followed by various kinetic experiments to establish the initial velocity for each viral TR. This will answer questions such as whether all *flaviviral* TRs activate OAS enzymes or is it just a feature of WNV? Do all flaviviral TRs activate OAS enzymes to the same extent or are there differences?
2. To better understand the mechanism of action of OAS enzymes, it is important to obtain kinetic information. Our lab has previously established initial velocity and dissociation constants for OAS1 where the dsRNA substrate was WNV 5'-TR (Deo

et al., 2015; Deo et al., 2014). Therefore the next logical step should be determine the kinetic parameters for all the *flaviviral* TRs we have available. This would likely require collaboration with a research group with expertise in modelling complex enzymatic assays.

3. There needs to be established protocols for OAS2 and OAS3 as well. It would be interesting to see how different *flaviviral* TRs behave with OAS2 and OAS3 as well as its effects on RNase L. OAS3 has also been reported to have the ability to sense the difference between longer and shorter dsRNAs (Donovan, Whitney, Rath, & Korennykh, 2015). How this effects RNase L activation downstream processes would be highly interesting.
4. The final direction I would suggest is to cross examine findings which only focused on OAS and not its effects on downstream RNase L activation. Our lab has previously established the dsRNA length dependence on OAS2 activation and its production of long 2-5A molecules (Koul et al., 2020). It would therefore be of great interest to test this in the context of RNase L. Many other findings like this can be tested easily using the assay outlined in this thesis.

4.4 REFERENCES

Anderson, B. R., Muramatsu, H., Jha, B. K., Silverman, R. H., Weissman, D., & Karikó, K. (2011). Nucleoside modifications in RNA limit activation of 2′-5′-oligoadenylate synthetase and increase resistance to cleavage by RNase L. *Nucleic Acids Res, 39*(21), 9329-9338.

Bignon, E., Miclot, T., Terenzi, A., Barone, G., & Monari, A. (2022). Structure of the 5′ untranslated region in SARS-CoV-2 genome and its specific recognition by innate immune system via the human oligoadenylate synthase 1. *Chemical Communications*.

Carroll, S. S., Cole, J. L., Viscount, T., Geib, J., Gehman, J., & Kuo, L. C. (1997). Activation of RNase L by 2′, 5′-oligoadenylates: kinetic characterization. *Journal of Biological Chemistry, 272*(31), 19193-19198.

Choi, B. Y., Sim, C. K., Cho, Y. S., Sohn, M., Kim, Y. J., Lee, M. S., & Suh, S. W. (2016). 2'-5' oligoadenylate synthetase-like 1 (OASL1) deficiency suppresses central nervous system damage in a murine MOG-induced multiple sclerosis model. *Neurosci Lett, 628*, 78-84. doi: 10.1016/j.neulet.2016.06.026

Daou, S., Talukdar, M., Tang, J., Dong, B., Banerjee, S., Li, Y., . . . Jha, B. K. (2020). A phenolic small molecule inhibitor of RNase L prevents cell death from ADAR1 deficiency. *Proceedings of the National Academy of Sciences, 117*(40), 24802-24812.

Deo, S., Patel, T. R., Chojnowski, G., Koul, A., Dzananovic, E., McEleney, K., . . . McKenna, S. A. (2015). Characterization of the termini of the West Nile virus genome and their interactions with the small isoform of the 2' 5'-oligoadenylate synthetase family. *J Struct Biol, 190*(2), 236-249. doi: 10.1016/j.jsb.2015.04.005

Deo, S., Patel, T. R., Dzananovic, E., Booy, E. P., Zeid, K., McEleney, K., . . . McKenna, S. A. (2014). Activation of 2' 5'-oligoadenylate synthetase by stem loops at the 5'-end of the West Nile virus genome. *PLoS One, 9*(3), e92545. doi: 10.1371/journal.pone.0092545

Donovan, J., Whitney, G., Rath, S., & Korennykh, A. (2015). Structural mechanism of sensing long dsRNA via a noncatalytic domain in human oligoadenylate synthetase 3. *Proc Natl Acad Sci U S A, 112*(13), 3949-3954. doi: 10.1073/pnas.1419409112

Koul, A., Deo, S., Booy, E. P., Orriss, G. L., Genung, M., & McKenna, S. A. (2020). Impact of double-stranded RNA characteristics on the activation of human 2′–5′-oligoadenylate synthetase 2 (OAS2). *Biochemistry and Cell Biology, 98*(1), 70-82.

Zhou, A., Molinaro, R. J., Malathi, K., & Silverman, R. H. (2005). Mapping of the human RNASEL promoter and expression in cancer and normal cells. *Journal of interferon & cytokine research, 25*(10), 595-603.